

A dedicated hypothalamic oxytocin circuit controls aversive social learning



<https://doi.org/10.1038/s41586-023-06958-w>

Received: 11 September 2022

Accepted: 8 December 2023

Published online: 24 January 2024

 Check for updates

Takuya Osakada^{1,4}, Rongzhen Yan^{1,4}, Yiwen Jiang^{1,4}, Dongyu Wei¹, Rina Tabuchi¹, Bing Dai¹, Xiaohan Wang¹, Gavin Zhao¹, Clara Xi Wang¹, Jing-Jing Liu¹, Richard W. Tsien^{1,2}, Adam C. Mar^{1,3} & Dayu Lin^{1,2,3}

To survive in a complex social group, one needs to know who to approach and, more importantly, who to avoid. In mice, a single defeat causes the losing mouse to stay away from the winner for weeks¹. Here through a series of functional manipulation and recording experiments, we identify oxytocin neurons in the retrochiasmatic supraoptic nucleus (SOR^{OXT}) and oxytocin-receptor-expressing cells in the anterior subdivision of the ventromedial hypothalamus, ventrolateral part (aVMHvl^{OXT^R}) as a key circuit motif for defeat-induced social avoidance. Before defeat, aVMHvl^{OXT^R} cells minimally respond to aggressor cues. During defeat, aVMHvl^{OXT^R} cells are highly activated and, with the help of an exclusive oxytocin supply from the SOR, potentiate their responses to aggressor cues. After defeat, strong aggressor-induced aVMHvl^{OXT^R} cell activation drives the animal to avoid the aggressor and minimizes future defeat. Our study uncovers a neural process that supports rapid social learning caused by defeat and highlights the importance of the brain oxytocin system in social plasticity.

Fighting is a major means to compete for limited resources in the wild. After the fight ends, typically through the retreat of the loser, the traumatic defeat experience is clearly remembered. The loser continuously avoids close interaction with the winner and readily flees when confronted². In male mice, a single 10-min defeat bout can induce avoidance of the winner for 15 days¹. Defeat-induced avoidance is observed across species, including humans³. For example, in the United States, a quarter of teenagers reportedly experience bullying and show increased social isolation and school avoidance⁴.

The neural mechanisms that underlie the rapid and long-lasting behavioural changes induced by defeat remain incompletely understood. Early studies focused on conditioned defeat⁵ in male hamsters and concluded that defeat and non-social aversive experiences, for example, foot shock, utilize the same brain circuit for associative fear learning. This circuit includes the prefrontal cortex, the basolateral amygdala and the hippocampus^{6–8}. Recently, several studies have suggested a potential role for the VMHvl in social defence and avoidance^{9–13}. The VMHvl is a part of the social behaviour network and is highly activated by conspecific cues^{14,15}. VMHvl cells are activated during defeat, and their reactivation elicits fear responses towards a benign conspecific⁹. Conversely, inactivating the VMHvl and its surrounding area reduces social avoidance of the aggressor 1 day after defeat¹⁰. Our previous study further revealed functional heterogeneity within the VMHvl, whereby the aVMHvl is preferentially activated during defeat, whereas the posterior VMHvl (pVMHvl) is most activated during attack¹¹. Optogenetic activation of aVMHvl cells elicits freezing, upright postures and avoidance of a conspecific, whereas activation of pVMHvl cells elicits approach, social


investigation and attack^{11,15}. These studies provide support for a role of the aVMHvl in social avoidance and fear. However, whether the aVMHvl mediates defeat-induced behaviour changes and, if so, how remains unknown. Here we investigated this question using a series of recording, functional and molecular tools. We show that aVMHvl^{OXT^R} cells undergo substantial changes during defeat with the help of an exclusive source of oxytocin to mediate defeat-induced social avoidance and fear.

One-day defeat induces avoidance and fear

We used the social interaction (SI) test¹⁶ to characterize the behaviour changes induced by defeat. During the SI test, an aggressive Swiss Webster (SW) male mouse or a lactating female mouse was placed under a metal wire cup ('constrained aggressor'). A C57BL/6 (C57) male or female mouse was then allowed to freely interact with the constrained aggressor for 10 min (Extended Data Fig. 1a,b). We performed the SI tests 1 day before and after a 10-min resident–intruder (RI) test, during which the C57 test mouse was introduced into the home cage (HC) of the aggressor, the same one used for the SI tests, for 10 min (Extended Data Fig. 1c). During the RI test, SW aggressors attacked and defeated the C57 intruders rapidly and repeatedly (Extended Data Fig. 1d,e). After several bouts of defeat, C57 intruders spent more time immobile (body centre velocity of <1 pixel per frame) in the corner (Extended Data Fig. 1f,g). During the pre-defeat SI test, C57 males repeatedly approached and investigated the constrained aggressor and spent approximately half the time around the cup (Extended Data Fig. 1h–m). After defeat, the animal spent most of the time staying at the

¹Neuroscience Institute, New York University Langone Medical Center, New York, NY, USA. ²Department of Psychiatry, New York University Langone Medical Center, New York, NY, USA.

³Department of Neuroscience and Physiology, New York University Langone Medical Center, New York, NY, USA. ⁴These authors contributed equally: Takuya Osakada, Rongzhen Yan, Yiwen Jiang.

 e-mail: takuya.osakada@nyulangone.org; dayu.lin@nyulangone.org

end far from the aggressor and less time investigating the aggressor. This behaviour was reflected in the combined reduced approach frequency and investigation duration per visit of the mouse (Extended Data Fig. 1n,o). Additionally, when the C57 mouse was far from the aggressor, it significantly reduced its movement velocity (that is, freezing more) (Extended Data Fig. 1p,q). Thus, a single 10-min defeat was sufficient to induce both social avoidance (as measured by the reduced interaction time with the SW mouse) and social fear (as measured by the reduced movement velocity when the aggressor is far away). The defeat-induced behaviour change was qualitatively similar between males and females, although the extent of avoidance was lower in females than in males (Extended Data Fig. 1k–q).

To address whether the avoidance behaviour of a test mouse is specific to the SW aggressor mouse that defeated it, we examined its behaviour towards a different SW aggressor (Extended Data Fig. 1r). The defeated animal also reduced the time it spent around the new SW aggressor and it decreased its movement velocity when away from the aggressor. However, the decrease was lower than when encountering the original SW aggressor (Extended Data Fig. 1s–x). To understand whether defeat-induced avoidance is generalizable to mice with different genetic backgrounds to that of the aggressor mice, we used a multi-animal social interaction (MSI) test and compared the behaviours of the test C57 mice towards SW aggressor mice, Balb/C (BC) non-aggressor mice and unfamiliar C57 mice (Extended Data Fig. 2a,b). One day after defeat, the C57 test males spent significantly less time investigating or around the constrained SW aggressor and approached the aggressor fewer times (Extended Data Fig. 2c,e–g). By contrast, interactions between the defeated C57 mouse and an unfamiliar C57 mouse or a previously encountered BC mouse remained unchanged (Extended Data Fig. 2c, e–g). We observed qualitatively similar results in C57 female mice during the MSI test (Extended Data Fig. 2d,h–j). Thus, a 10-min defeat bout induced avoidance of winner-like conspecifics.

Winner cues drive loser aVMHvl^{OxTR} cells

We have previously shown that Fos expression is higher in the aVMHvl after defeat than winning¹¹. Moreover, defeat-induced Fos expression overlaps with OXTR at the VMHvl¹⁷. We therefore examined defeat-induced Fos expression in *Oxtr^{Cre};Ai6 (Oxtr^{ZsGreen})* mice and found that defeat induced the expression of more cells positive for both OXTR and Fos (OXTR⁺Fos⁺) in the aVMHvl (Bregma: –1.34 mm to –1.50 mm) than attack. Conversely, these two behaviours induced a similar number of OXTR⁺Fos⁺ cells in the pVMHvl (Bregma: –1.66 mm to –1.82 mm) (Extended Data Fig. 3a,b). Compared with oestrogen receptor- α (*Esr1*), a gene marker for aggression-related VMHvl cells^{18,19}, OXTR was expressed more in the aVMHvl (Extended Data Fig. 3c,d). Approximately 10% of aVMHvl^{OxTR} cells expressed *Esr1*, whereas the overlap increased to 30% in the pVMHvl (Extended Data Fig. 3e,f).

Fibre photometry recording of GCaMP6f-expressing aVMHvl^{OxTR} cells (OXTR^{GCaMP6}) in male mice further revealed low cell activity during investigating or attacking a non-aggressive BC male intruder despite a large response following introduction (Extended Data Fig. 4a–c,f–j). By contrast, when the test mouse fought and was defeated by a SW aggressor, in the cage of either the test mouse or the SW aggressor, aVMHvl^{OxTR} cells showed strong increases in activity (Extended Data Fig. 4d,e,h–j). Overall, aVMHvl^{OxTR} cells responded strongly during defeat but not during winning or social investigation (Extended Data Fig. 4h–j). Female aVMHvl^{OxTR} cells were also highly excited during defeat by a lactating SW female, but showed no activity change during non-agonistic interactions with naive C57 females (Extended Data Fig. 5a–j).

After defeat, as expected, male mice expressing OXTR^{GCaMP6} cells showed decreased interaction with the constrained aggressor during

the SI test (Extended Data Fig. 4k–o). Notably, aVMHvl^{OxTR} cells showed a large increase in response to the constrained aggressor (Extended Data Fig. 4p–r). Furthermore, the avoidance level and the post-defeat response increase were significantly and positively correlated (Extended Data Fig. 4s). During the post-defeat SI test, the test animal often rapidly retreated from the constrained aggressor after investigation. At the onset of retreat, the Ca²⁺ signal reached the maximum and gradually decreased during retreat (Extended Data Fig. 4t–v). By contrast, when the animal stayed immobile far from the aggressor, Ca²⁺ activity remained low (Extended Data Fig. 4w–y). Similar response patterns were observed in female mice (Extended Data Fig. 5k–v). These results suggest that aVMHvl^{OxTR} cells may drive social avoidance but probably not immobility.

This defeat-induced response increase was winner-specific, as responses to a previously encountered BC or unfamiliar C57 male mouse did not change in the post-defeat MSI test (Fig. 1a–h and Supplementary Video 1). Again, there was a significant correlation between post-defeat avoidance levels and changes in cell responses (Fig. 1i). Similarly, female mice strongly avoided the lactating SW females in the post-defeat MSI test, whereas interaction time with the C57 females increased (Extended Data Fig. 6a–e). The response towards the SW mothers, but not C57 females, increased after defeat, and the increased response and decreased social investigation time were significantly correlated (Extended Data Fig. 6f–i).

Our *in vivo* recording results were consistent with the Fos expression pattern. In male mice that the aggressor defeated over 2 days, aVMHvl^{OxTR} cells, but not pVMHvl^{OxTR} cells, expressed more Fos after interaction with the constrained aggressor for 10 min compared with mice that interacted with the constrained aggressor for 2 days (Extended Data Fig. 7).

To understand the physiological and synaptic changes underlying the *in vivo* changes in response, we performed patch-clamp recordings of aVMHvl^{OxTR} cells in brain slices from *Oxtr^{Cre};Ai6* male mice that experienced a 10-min defeat bout, a non-agonistic SI or no interaction (single housing (SH)) 1 day before the recording (Fig. 1j,k). The amplitude of spontaneous excitatory postsynaptic currents (sEPSCs) of aVMHvl^{OxTR} cells in the defeated males was significantly higher than that in SH males, whereas SI animals showed the opposite change (Fig. 1l,m). The sEPSC frequency did not differ across groups (Fig. 1n). Spontaneous inhibitory postsynaptic currents (sIPSCs) also increased slightly but significantly in amplitude, but not frequency, in defeated animals compared with other groups (Fig. 1o–q). Parameters reflecting intrinsic cell properties, including current–frequency curve, resting membrane potential, rheobase and input resistance, did not differ significantly between defeated and SH males (Extended Data Fig. 8). However, cells in defeated males appeared more excitable than those in SI animals, owing to their opposite trends in changes from SH mice (Extended Data Fig. 8b). These data suggest that potentiation of the excitatory synapses onto aVMHvl^{OxTR} cells is probably the main contributor of increased *in vivo* cell responses to the aggressor after defeat.

The aVMHvl^{OxTR} response is specific to social contexts

We next asked whether aVMHvl^{OxTR} cells are activated only by aversive social cues or by aversive cues in general. First, we recorded aVMHvl^{OxTR} cell Ca²⁺ activity during investigation of 1% 2-methyl-2-thiazoline (2MT), an analogue of the predator odour component 2,4,5-trimethyl-3-thiazoline that is highly aversive to mice²⁰ (Extended Data Fig. 9a–j). For comparison, male test mice were subjected to defeat 1 day before the test and the response to the constrained aggressor was recorded in the same session. The Ca²⁺ signal consistently and strongly increased during investigation of the aggressor mouse. By contrast, there was no increase in Ca²⁺ activity during investigation of 2MT, even though 2MT elicited strong avoidance and fear-like behaviours

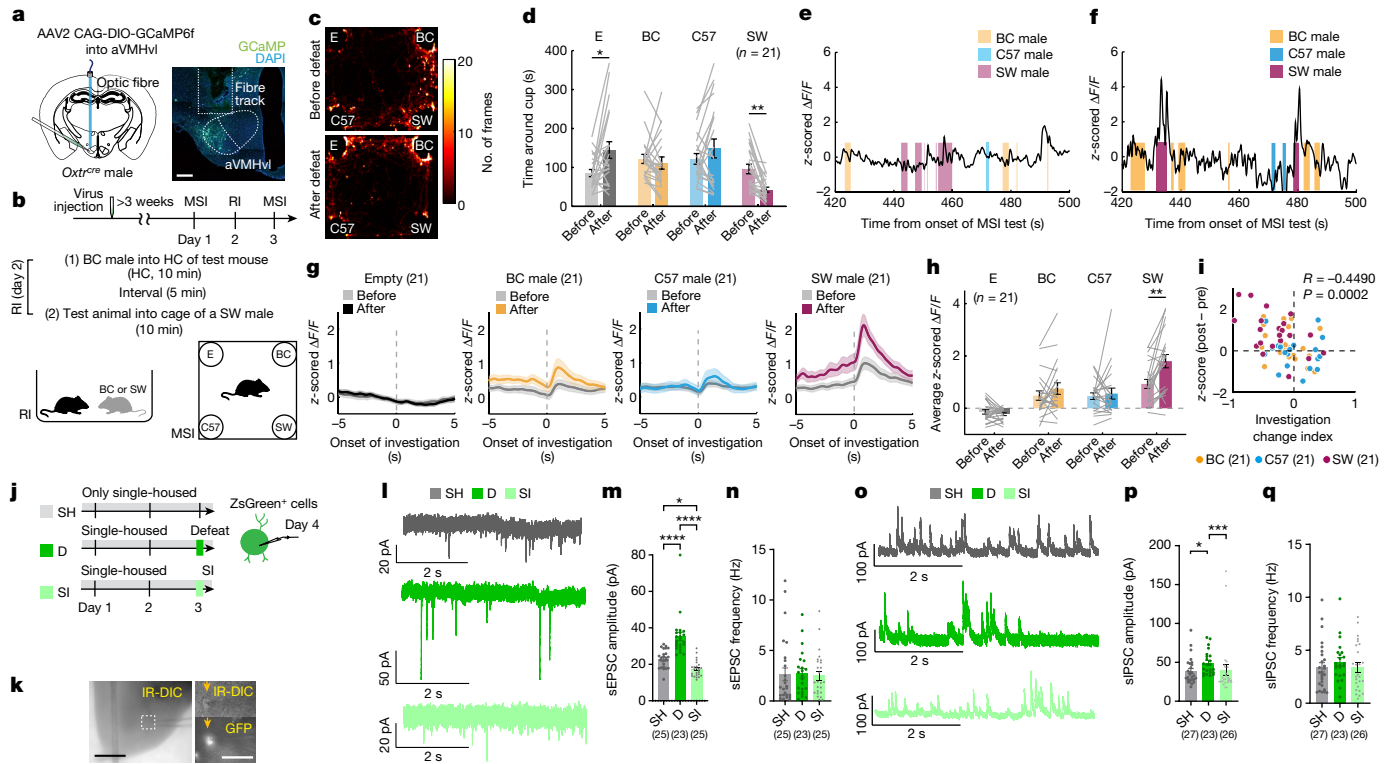


Fig. 1 | **aVMHvl^{OXTR} cells in male mice show increased responses to aggressors after defeat.** **a**, Schematics (left) and representative histology (right). Scale bar, 200 μm . **b**, Experimental timeline and illustrations of behaviour tests. C57, unfamiliar C57 male; E, empty. **c**, A recording of the body centre distribution of a mouse in pre-defeat and post-defeat MSI tests. **d**, Time spent around each cup during pre-defeat and post-defeat MSI tests. **e, f**, Representative GCaMP6f traces during pre-defeat (**e**) and post-defeat (**f**) MSI tests. $\Delta F/F$, change in fluorescence. **g**, Peri-event histograms (PETHs) of GCaMP6f signals aligned to different investigations of the cup during pre-defeat and post-defeat MSI tests. **h**, Average GCaMP6f signal during investigations of the cup in the pre-defeat and post-defeat MSI tests. **i**, Changes in z-scored GCaMP6f signals (post-defeat – pre-defeat) and investigation time of all stimuli are significantly correlated. **j, k**, Experiments were performed using *Oxtr^{ZsGreen}* male mice. **j**, Slice recording timeline. D, defeated by a SW male resident for 10 min. **k**, Recording site and a recorded aVMHvl *OXTR*–ZsGreen cell. IR-DIC, infrared differential interference

contrast. Right image shows the enlarged boxed area. Scale bars, 500 μm (left) and 50 μm (right). **l**, Representative sEPSCs from various groups. **m, n**, Amplitude (**m**) and frequency (**n**) of sEPSCs from various groups. Cells are from $n = 3$ –4 mice per group. **o–q**, sIPSC results, following plotting conventions in **l–n**. Plots with shades and error bars represent mean \pm s.e.m. Circles and lines in **d, h** and **i** represent individual animals. Circles in **m, n, p** and **q** represent individual cells. Numbers on the plots (in parentheses) indicate the number of animals (**d, g–i**) or cells (**m, n, p, q**). Statistics: Kruskal–Wallis test with Dunn’s multiple comparisons (**m, n, p, q**); one-way analysis of variance (ANOVA) with Tukey’s multiple comparisons (**q**); two-way repeated-measure ANOVA with Sidak’s multiple comparisons (**d, h**); or Pearson cross-correlation (**i**). All statistical tests are two-tailed. * $P < 0.05$, ** $P < 0.01$, *** $P < 0.001$ and **** $P < 0.0001$. See Supplementary Table 1 for detailed statistics. Brain illustration in **a** is adapted from the Allen Brain Reference Atlas (<https://atlas.brain-map.org>).

at least comparable to those induced by the aggressor (Extended Data Fig. 9h–j).

Next, we used an olfactory fear-conditioning paradigm to pair a neutral odour (pentyl acetate or (*R*)-(+)-limonene) with 1 mA foot shock (Extended Data Fig. 9k, l). Control odour was delivered with no shock. One day after training, the animals showed effective aversive learning as they reduced movement velocity when the paired odour but not the unpaired odour was delivered (Extended Data Fig. 9m, n). Throughout the post-conditioning odour test, aVMHvl^{OXTR} cells showed little Ca²⁺ activity fluctuation, and the average GCaMP6 signal did not differ among pre-odour, shock-unpaired and shock-paired odour delivery periods (Extended Data Fig. 9o, p).

As it was difficult to determine the exact moment when the odour reached the test animal, we also recorded aVMHvl^{OXTR} cell responses to shock-unpaired and shock-paired odours, as well as to 2MT, delivered directly to the animal on a cotton swab using a head-fixed preparation (Extended Data Fig. 10a). We again found no change or suppressed aVMHvl^{OXTR} cell Ca²⁺ activity during all non-social aversive odour presentations (Extended Data Fig. 10b–d). In particular, 2MT caused a decrease in cell activity for at least 30 s beyond odour delivery

(Extended Data Fig. 10b3, c3). By contrast, urine from SW aggressor mice significantly increased aVMHvl^{OXTR} cell activity in 1-day defeated test mice (Extended Data Fig. 10b2, c2). These results suggest that aVMHvl^{OXTR} cells are activated by aversive social, but not non-social, olfactory cues.

Avoidance expression requires aVMHvl^{OXTR} cells

We next examined the functional relevance of the increased aVMHvl^{OXTR} cell response after defeat. We optogenetically activated aVMHvl^{OXTR} cells in naive animals (ChR2^{OXTR} mice) during SI tests (Fig. 2a, b). Control animals expressed GFP in aVMHvl^{OXTR} cells (GFP^{OXTR} mice). After delivery of light, ChR2^{OXTR} mice, but not GFP^{OXTR} mice, strongly avoided the constrained animal, as indicated by the significantly increased distance from the cup, reduced investigation time and approach frequency (Fig. 2c–e and Supplementary Video 2). aVMHvl^{OXTR} cell activation also elicited social fear, as indicated by significantly decreased movement velocity (Fig. 2f). The stimulation-induced avoidance and fear response were not specific to the aggressor mouse, as similar behaviours were induced when the constrained animal was a non-aggressive BC male (Extended Data Fig. 11a–f). In the absence of any target, the

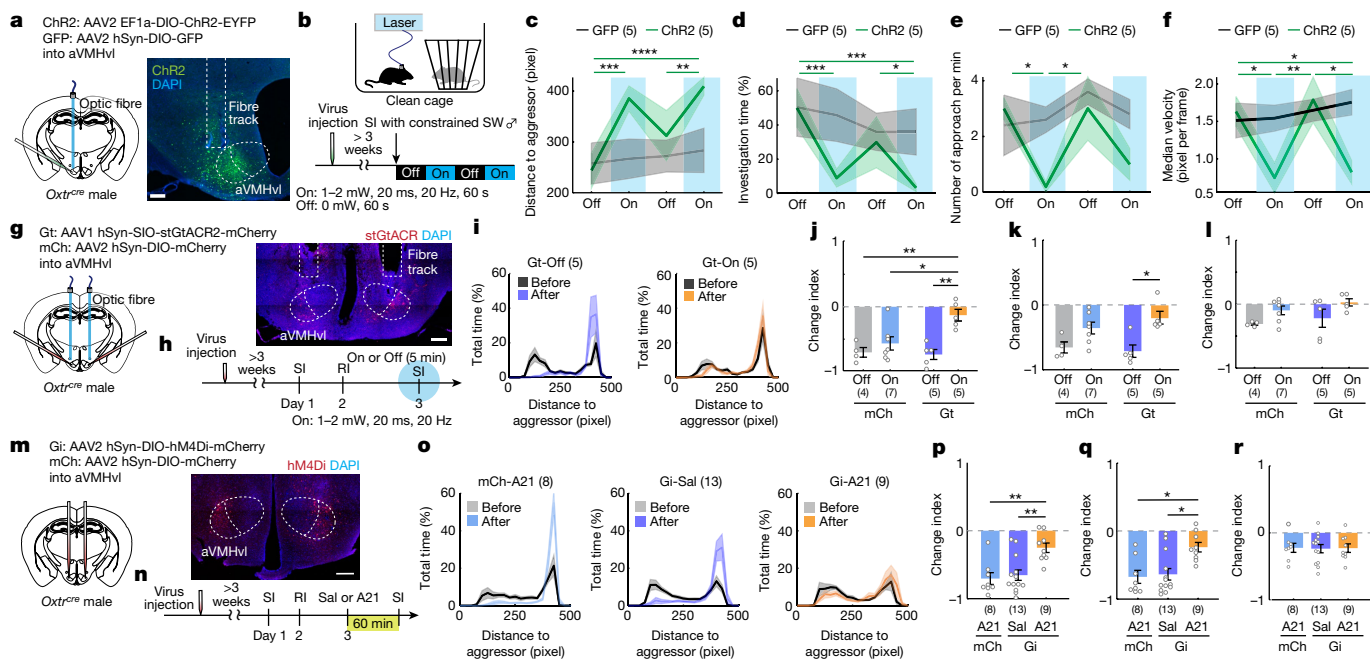


Fig. 2 | aVMHvl^{OXTR} cells bidirectionally modulate social avoidance. **a**, Virus schematics (left) and representative histology (right). **b**, Timeline and illustration of the behaviour assay. **c–f**, Average distance to the constrained aggressor (**c**), percentage of time spent investigating the aggressor (**d**), approach frequency (**e**) and median body centre velocity (**f**) during on (blue shaded area) and off periods in GFP and ChR2 groups. Statistical results are for the ChR2 group. All $P > 0.05$ for the GFP group. **g**, Schematics (left) and representative histology (right). **h**, Timeline and light delivery protocol. **i**, Distribution of the distance between the body centre of the test animal and the constrained aggressor during pre-defeat and post-defeat SI tests for Gt-Off and Gt-On groups. **j–l**, Change index of the investigation time percentage (**j**), time around cup percentage (**k**) and the median velocity when far from the aggressor (**l**) during SI tests for various groups. Change index: $(P_{\text{after}} - P_{\text{before}}) / (P_{\text{after}} + P_{\text{before}})$. P_{before} and P_{after} behaviour

performance during pre-defeat and post-defeat SI tests, respectively. **m–r**, Behaviour changes in post-defeat SI tests after chemogenetic inhibition of aVMHvl^{OXTR} cells. Plots follow conventions in **g–l**. A21, agonist 21; Sal, saline. Plots with shades and error bars represent mean \pm s.e.m. Circles represent individual animals. Numbers on the plots in parentheses indicate the number of animals. Statistics: two-way repeated-measure ANOVA with Sidak's multiple comparisons (**c–f**); Kruskal–Wallis test with Dunn's multiple comparisons (**k, q**); or one-way ANOVA with Tukey's multiple comparisons (**j, l, p, r**). All statistical tests are two-tailed. * $P < 0.05$, ** $P < 0.01$, *** $P < 0.001$ and **** $P < 0.0001$. See Supplementary Table 1 for detailed statistics. Brain illustrations in **a, g** and **m** are adapted from the Allen Brain Reference Atlas (<https://atlas.brain-map.org>). Scale bars, 200 μm (**a, g, m**).

stimulated animals showed interleaved freeze and flight, as indicated by the increased time spent staying immobile (velocity of <1 pixel per frame) and rapid movement (velocity of >20 pixels per frame) (Extended Data Fig. 11g–k). In the real-time place preference (RTPP) test, the animal spent significantly less time in the light-paired chamber, which indicated the aversive nature of aVMHvl^{OXTR} cell activation (Extended Data Fig. 11l–n). These results suggest that the increased aVMHvl^{OXTR} cell response to the winner after defeat is functionally relevant, as high activity of these cells drives social avoidance and fear and induces a negative emotional state.

To understand whether the increased activity of aVMHvl^{OXTR} cells after defeat is necessary for the change in behaviour, we optogenetically inhibited aVMHvl^{OXTR} cells in male mice using stGtACR²¹ (Gt^{OXTR}-On mice) during the post-defeat SI test (Fig. 2g,h). Three control groups of animals were also tested, including mice expressing stGtACR2 and receiving no light (Gt^{OXTR}-Off mice), mice expressing mCherry and receiving light (mCh^{OXTR}-On mice) and mice expressing mCherry and receiving no light (mCh^{OXTR}-Off mice) (Fig. 2g). Compared with control animals, Gt^{OXTR}-On mice spent more time surrounding and investigating the constrained aggressor. This result indicated that aVMHvl^{OXTR} cells have a necessary role in inducing post-defeat social avoidance (Fig. 2i–k). However, the effect of aVMHvl^{OXTR} optogenetic inhibition on post-defeat social fear could not be determined, as delivery of the light itself affected immobility. Although control mCh^{OXTR}-Off or Gt^{OXTR}-Off mice showed decreased movement velocity during the post-defeat SI test, control mCh^{OXTR}-On mice or test Gt^{OXTR}-On animals did not (Fig. 2l).

As a complementary strategy to inhibit aVMHvl^{OXTR} cells without light, we chemogenetically inhibited aVMHvl^{OXTR} cells using hM4Di and agonist 21, a hM4Di-specific ligand (Gi^{OXTR}-A21 mice)²² during the post-defeat SI test (Fig. 2m,n). Two control groups were also tested, including mice expressing hM4Di and injected with saline (Gi^{OXTR}-Sal mice) and mice expressing mCherry and injected with agonist 21 (mCh^{OXTR}-A21 mice)²³ (Fig. 2m). Compared with Gi^{OXTR}-Sal and mCh^{OXTR}-A21 groups, Gi^{OXTR}-A21 mice spent more time surrounding and investigating the constrained aggressor during the post-defeat SI test (Fig. 2o–q). However, Gi^{OXTR}-A21 mice showed reduced movement velocity, comparable to that of control animals, which suggested that this manipulation did not reduce social fear (Fig. 2r). Thus, the activity of aVMHvl^{OXTR} cells is necessary for social avoidance but not social fear expression.

Social avoidance learning requires OXTR

We next questioned whether aVMHvl oxytocin–OXTR signalling is essential for defeat-induced social avoidance and fear learning and/or expression. We knocked out OXTR in the aVMHvl by bilaterally injecting Cre-GFP virus into *Oxtr*^{lox/lox} male mice (*Oxtr*^{aVMHvl-KO}) (Fig. 3a). Control animals were injected with GFP virus (*Oxtr*^{aVMHvl-GFP}) (Fig. 3a). To confirm successful *Oxtr* knockout (KO), we injected Cre-GFP and GFP viruses each into one side of the aVMHvl in *Oxtr*^{lox/lox} male mice and performed in vitro patch-clamp recording of GFP⁺ cells (Extended Data Fig. 12a). Seven out of 16 (44%) GFP⁺ cells in the GFP-expressing side were depolarized by TGOT, a highly specific OXTR agonist, whereas

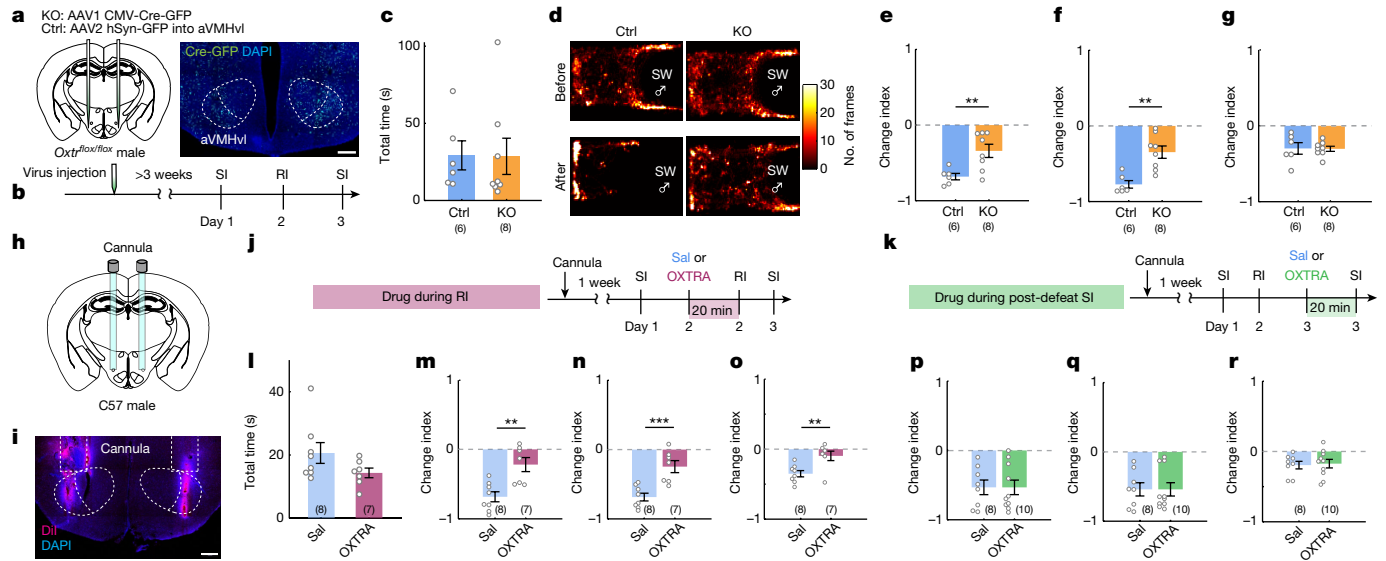


Fig. 3 | OXTRs in the aVMHvl are essential for defeat-induced social avoidance learning. **a**, Schematics (left) and representative histology (right). Ctrl, control. **b**, Experimental timeline and behaviour assay. **c**, Total defeat duration of the *Oxtr* KO and control mice in RI tests. **d**, Body centre distributions of representative *Oxtr* KO and control mice during pre-defeat and post-defeat SI tests. **e–g**, Change index of aggressor investigation time percentage (**e**), time around cup percentage (**f**) and median velocity when far from the aggressor (**g**) during SI tests for various groups. **h**, Cannula implantation schematics. **i**, Representative histology. **j, k**, Timelines for antagonizing OXTR during defeat (**j**) or post-defeat SI test (**k**). **l**, Total defeat time of saline-injected and

OXTRA-injected animals during RI tests. **m–r**, Change index of aggressor investigation time percentage (**m, p**), time around cup percentage (**n, q**) and median velocity when far from the aggressor (**o, r**) during SI tests of animals injected defeat RI (**m–o**) or post-defeat SI tests (**p–r**). Plots with error bars represent mean \pm s.e.m. Circles represent individual animals. Numbers in parentheses on the plots indicate the number of animals. Statistics: Mann–Whitney test (**c, o, q**) or unpaired *t*-test (**e–g, l–n, p, r**). All statistical tests are two-tailed. *******P* < 0.01 and ********P* < 0.001. See Supplementary Table 1 for detailed statistics. Brain illustrations in **a** and **h** are adapted from the Allen Brain Reference Atlas (<https://atlas.brain-map.org>). Scale bars, 200 μ m (**a, i**).

no GFP⁺ cells responded to TGOT in the Cre-GFP-expressing side. This result indicated that OXTR was effectively knocked out by Cre-GFP (Extended Data Fig. 12b,c).

We then asked whether *Oxtr* KO at the aVMHvl affects defeat-induced social avoidance and fear (Fig. 3b). During RI tests with SW aggressors, *Oxtr*^{aVMHvl-KO} and *Oxtr*^{aVMHvl-GFP} male mice were defeated for a similar amount of time (Fig. 3c). In the post-defeat SI test, *Oxtr*^{aVMHvl-KO} males spent significantly more time surrounding and investigating the constrained aggressor than *Oxtr*^{aVMHvl-GFP} males, which suggested that aVMHvl OXTR has an essential role in defeat-induced social avoidance (Fig. 3d–f). By contrast, both test and control groups showed decreased velocity after defeat when far away from the constrained aggressor. This result indicates that aVMHvl OXTR has a less crucial role in social fear (Fig. 3g). However, we noted that the absolute movement velocity of *Oxtr*^{aVMHvl-KO} males was higher than that of *Oxtr*^{aVMHvl-GFP} males during pre-defeat SI tests. This result suggests that there are tonic changes in the aVMHvl^{OXTR} cell output after *Oxtr* KO, which may lead to circuit compensation (Supplementary Note 1).

To avoid potential circuit compensation that may mask endogenous OXTR functions and to address whether OXTR signalling is required for acquiring or expressing defeat-induced social avoidance, we injected L-368,899 hydrochloride (100 μ M, 250 nl per side), a potent OXTR antagonist (OXTRA), into the aVMHvl of wild-type male mice either 20 min before the RI test (OXTRA-RI mice) or 20 min before the post-defeat SI test (OXTRA-SI mice) (Fig. 3h–k). Control males were injected with saline (Sal-RI and Sal-SI, respectively). OXTRA-injected and saline-injected animals were defeated for a similar amount of time during the RI tests (Fig. 3l). During post-defeat SI test, OXTRA-RI male mice spent more time surrounding and investigating the constrained aggressor and showed less reductions in movement velocity when far away from the aggressor in comparison to Sal-RI mice (Fig. 3m–o). By contrast, injecting the OXTRA before the post-defeat SI test did not affect social avoidance or fear (Fig. 3p–r). These results suggest that

OXTR signalling at the aVMHvl is necessary for social avoidance and fear learning during defeat but not their expression during post-defeat social encounters.

The SOR provides oxytocin to aVMHvl^{OXTR} cells

Next, we aimed to identify the source of oxytocin for aVMHvl^{OXTR} cells. Given that OXTR signalling in the aVMHvl is required during defeat for social avoidance learning, we reasoned that relevant release of oxytocin should occur during defeat. Defeat-induced cells positive for both Fos and oxytocin were present in the paraventricular hypothalamic nucleus (PVN), the supraoptic nucleus (SON) and the SOR²⁴, a small region caudal to the SON (and sometimes considered a subdivision of the SON^{25,26}) (Extended Data Fig. 13a,b). The SOR was particularly interesting as it contained the highest percentage (around 50%) of oxytocin cells expressing defeat-induced Fos (Extended Data Fig. 13c). Anatomically, the SOR is located immediately next to aVMHvl^{OXTR} cells (Fig. 4a), which makes it well positioned to provide oxytocin to aVMHvl cells through somatodendritic release^{27,28}.

To understand the influence of oxytocin input on aVMHvl cell activity, we virally expressed Chr2 in SOR^{OXTR} or PVN^{OXTR} cells in *Oxtr*^{Cre} male mice and performed current-clamp recording of aVMHvl cells on brain slices while delivering light pulses (1 ms, 20 Hz) for 5 min to activate SOR^{OXTR} or PVN^{OXTR} input (Fig. 4b–d). After activation of SOR^{OXTR} input, 11 out of 22 aVMHvl cells showed >4 mV increase in the resting membrane potential, consistent with the reported effect of oxytocin on VMHvl cells²⁹, and we considered those cells as putatively OXTR⁺ (Fig. 4e,f(left),g,i). By comparison, only 2 out of 24 aVMHvl cells were depolarized through activation of PVN^{OXTR} terminals (Fig. 4h,i). For aVMHvl cells that were not depolarized by PVN^{OXTR} or SOR^{OXTR} activation, we applied TGOT to functionally determine OXTR expression (Fig. 4e). A total of 3 out of 11 cells unresponsive to SOR^{OXTR} activation were depolarized by TGOT compared with 11 out of 22 cells unresponsive to PVN^{OXTR}

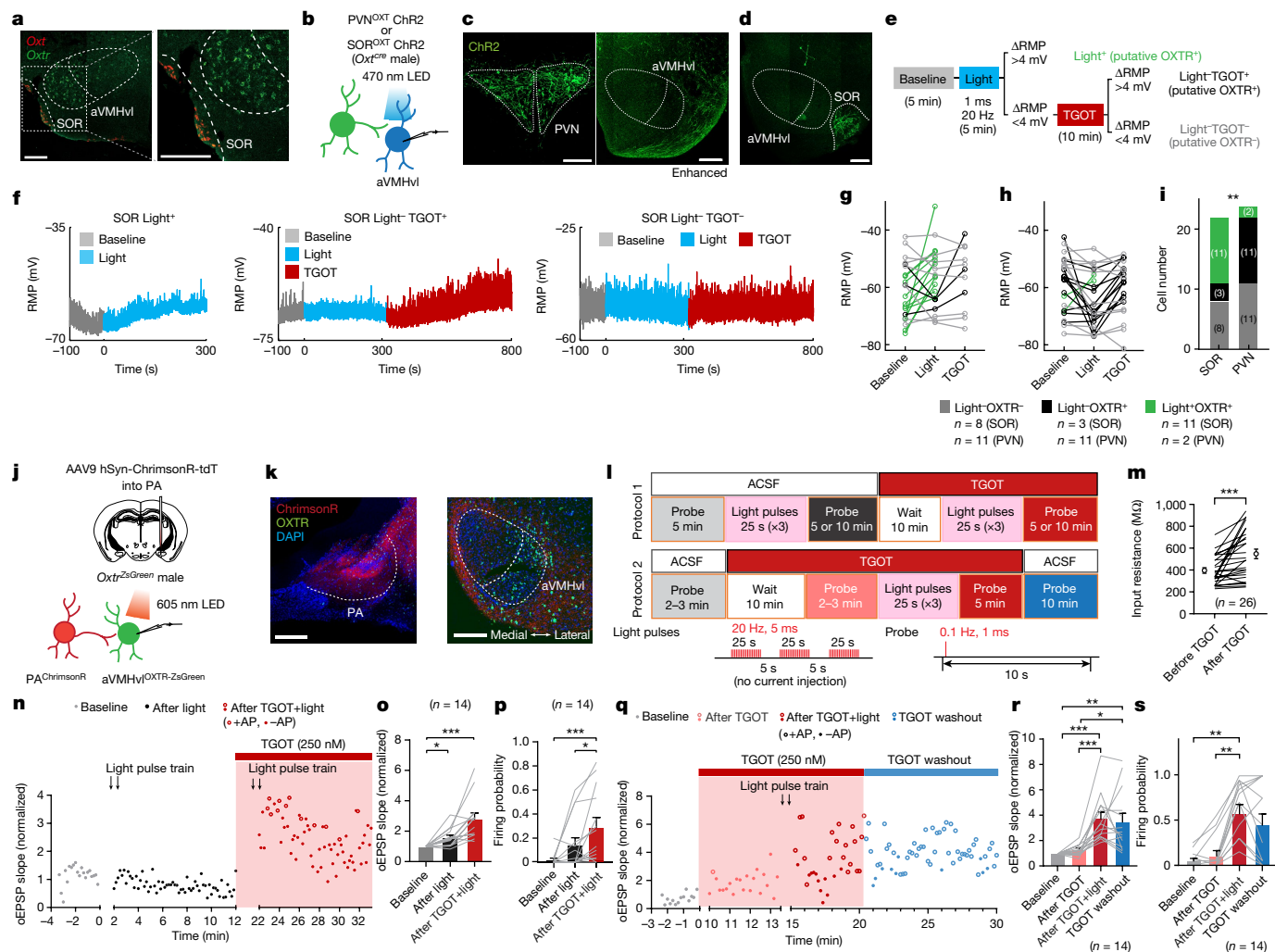


Fig. 4 | The SOR is the primary source of oxytocin for aVMHvl^{OXTR} cells. **a**, *Oxt* and *OxtR* mRNA expression in the SOR and aVMHvl of a male mouse. **b**, Slice recordings of aVMHvl cell responses to PVN or SOR OXT inputs. **c, d**, ChR2 expression in PVN^{OXTR} (**c**) and SOR^{OXTR} (**d**) cells and their axons surrounding the aVMH. The aVMH image on the right in **c** was digitally enhanced. **e**, Schematic of the strategy used to examine aVMHvl cell responses to oxytocin input. RMP, resting membrane potential. **f**, Representative recording traces of aVMHvl cells responsive to SOR^{OXTR} stimulation (SOR Light⁺), unresponsive to SOR^{OXTR} stimulation but depolarized by TGOT (SOR Light⁻ TGOT⁺) or unresponsive to SOR^{OXTR} activation and TGOT (SOR Light⁻ TGOT⁻). **g, h**, RMP change of aVMHvl cells after SOR^{OXTR} (**g**) or PVN^{OXTR} (**h**) light activation and TGOT. **i**, Distribution of response types. Cells in **g–i** are from *n* = 4 male mice per group. **j**, Slice recording schematics. **k**, ChrimsonR-expressing PA cells (left) and their axons in the aVMHvl (right). **l**, Recording and light delivery protocols to examine the role of oxytocin in synaptic potentiation. ACSF, artificial cerebrospinal fluid.

m, aVMHvl^{OXTR} cell input resistance before and after 10 min of TGOT. **n, q**, Normalized slopes of oEPSPs of aVMHvl^{OXTR} cells before and after TGOT and PA-VMHvl stimulation. Open and filled circles indicate oEPSPs with and without action potential (AP), respectively. **o, p, r, s**, Normalized oEPSP slope (**o, r**) and light-evoked firing probability (**p, s**) at different recording periods. Cells are from *n* = 5 (**o, p**) and *n* = 4 (**r, s**) male mice. Plots with error bars represent mean ± s.e.m. Lines in **g, h, j, o, p, r** and **s** represent individual cells. Numbers in parentheses on the plots indicate the number of cells (**g–i, m, o, p, r, s**). Statistics: one-way repeated measure ANOVA with Tukey's multiple comparisons (**r**); Chi-square test (**i**); Friedman test with Dunn's multiple comparisons (**o, p, s**); or paired *t*-test (**m**). All statistical tests are two-tailed. **P* < 0.05, ****P* < 0.01 and *****P* < 0.001. See Supplementary Table 1 for detailed statistics. Brain illustration in **j** is adapted from the Allen Brain Reference Atlas (<https://atlas.brain-map.org>). Scale bars, 200 μm (**a, c, d, k**).

stimulation (Fig. 4e, f (middle and right), g–i). Altogether, SOR^{OXTR} and PVN^{OXTR} inputs influenced 79% (11 out of 14 cells) and 15% (2 out of 13 cells) of aVMHvl^{OXTR} cells, respectively. The impact of SOR^{OXTR} on aVMHvl^{OXTR} cells depended on OXTR. Pre-application of an OXTRA prevented SOR^{OXTR}-activation-induced depolarization in all recorded aVMHvl cells (Extended Data Fig. 12d, e).

Most oxytocin cells express vesicular glutamate transporter 2 (VGLUT2), which suggests that oxytocin cells may also release glutamate (Extended Data Fig. 12f–i). However, we did not observe optogenetically induced EPSCs (oEPSCs) with light delivery to activate SOR^{OXTR} or PVN^{OXTR} inputs (Extended Data Fig. 12j–m). These results suggest that SOR^{OXTR} cells are the primary source of oxytocin for aVMHvl cells and they probably do not form glutamatergic synapses with aVMHvl cells.

Oxytocin facilitates synaptic potentiation

We next asked whether oxytocin–OXTR signalling at the aVMHvl can facilitate synaptic potentiation as observed in defeated animals (Fig. 1m). To control the excitatory input to aVMHvl^{OXTR} cells, we virally expressed ChrimsonR³⁰ in posterior amygdala (PA) cells and performed current-clamp recording of aVMHvl^{OXTR} cells in *Oxtr^{Cre}:Ai6* male mice (Fig. 4j, k). The PA is the primary extrahypothalamic glutamatergic input to the VMHvl and induces strong monosynaptic EPSCs from VMHvl cells^{31–33}. For each recorded aVMHvl^{OXTR} cell, we probed its postsynaptic responses to PA inputs with 1 ms, 0.1 Hz, 605 nm light pulses for 5 min (Fig. 4l). Then, we delivered 20 Hz, 5 ms, 25 s light pulses 3 times to mimic the strong PA input that could occur naturally

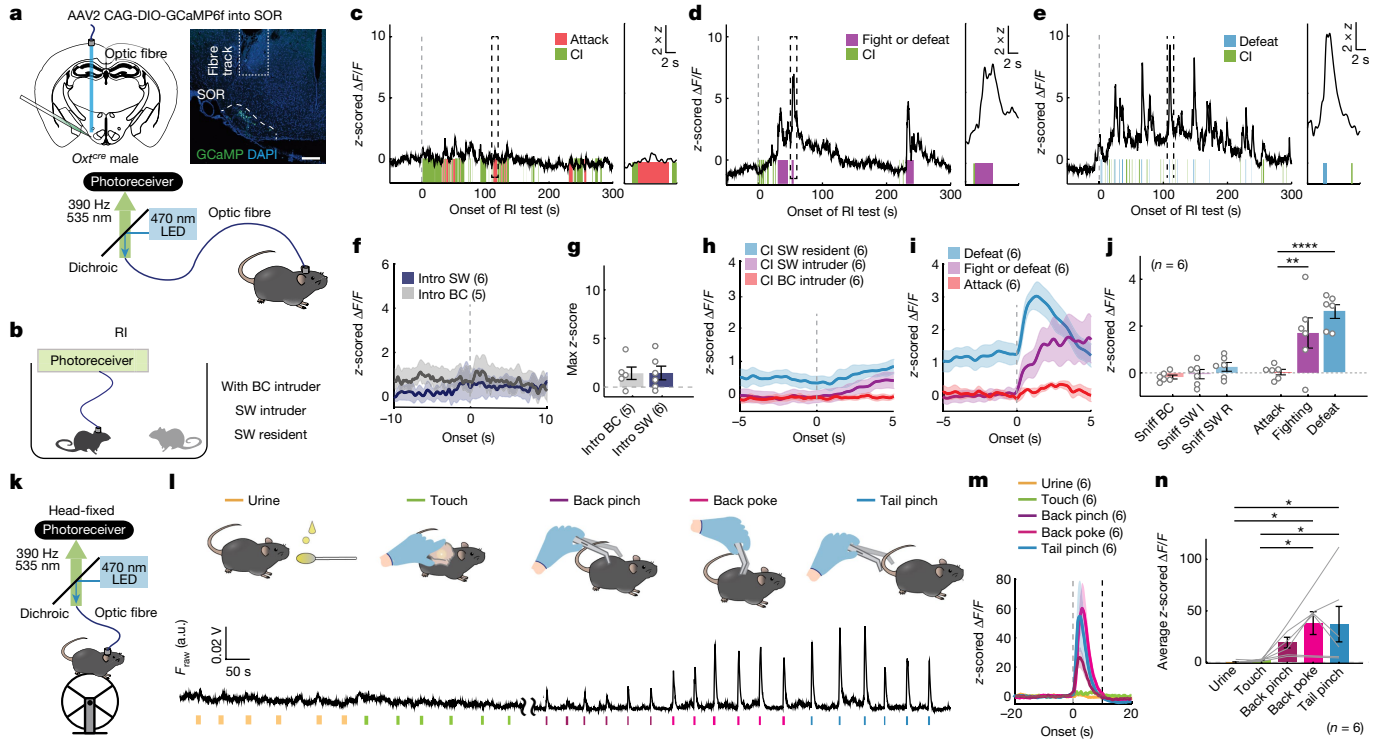


Fig. 5 | SOR^{OXT} cells are activated by noxious stimuli. **a**, Virus schematics (left) and representative histology (right). Scale bar, 200 μ m. **b**, Schematic of the three RI test conditions. **c–e**, Representative z-scored GCaMP6f traces during RI tests with a BC male intruder (**c**), a SW male intruder (**d**) or a resident SW mouse (**e**) into the HC. Graphs on the right show the enlarged boxed areas. CI, close investigation. **f**, PETHs of GCaMP6f signals aligned to initial opponent encounters. Only sessions without defeat or attack during the first 10 s of RI tests. Intro, introduction. **g**, Peak GCaMP6f response within the first 10 s of RI tests. **h, i**, PETHs of GCaMP6f signals aligned to CI (**h**) and agonistic interactions (**i**). **j**, Average z-scored responses of SOR^{OXT} cells during various social behaviours. **l**, intruder; **R**, resident. **k**, Schematics of head-fixed fibre photometry recording of SOR^{OXT} cells. **l**, Representative raw GCaMP6f traces of SOR^{OXT} cells during various stimulus presentations. Urine, presenting urine

taken from aggressor mouse. **m**, PETHs of z-scored GCaMP6f signals aligned to the onset of various stimulus presentations. Grey and black dashed lines indicate the onset and offset of stimulus presentation, respectively. **n**, Average z-scored $\Delta F/F$ during various stimulus presentations. Plots with shades and error bars represent mean \pm s.e.m. Circles and lines represent individual animals. Numbers in parentheses on the plots indicate the number of animals. Statistics: unpaired *t*-test (**g**); two-way repeated measure ANOVA with Sidak's multiple comparisons (**j**); or one-way repeated measure ANOVA with Tukey's multiple comparisons (**n**). All statistical tests are two-tailed. **P* < 0.05, ***P* < 0.01 and *****P* < 0.0001. See Supplementary Table 1 for detailed statistics. Brain illustration in **a** is adapted from the Allen Brain Reference Atlas (<https://atlas.brain-map.org>).

during an encounter with an intruder³¹ (Fig. 4l). After the light train, the postsynaptic response of aVMHvl^{OXT} cells to the PA input only increased slightly (Fig. 4n,o). By contrast, when the light pulses were delivered in the presence of TGOT, the increase in light-evoked excitatory postsynaptic potential (oEPSP) was significantly larger (Fig. 4n,o). Consequently, aVMHvl^{OXT} cells were more likely to fire action potentials after 1-ms PA terminal stimulation (Fig. 4p).

TGOT application increased aVMHvl^{OXT} cell input resistance, which raised the possibility that TGOT alone could increase oEPSP because of alternation in synaptic integration³⁴ (Fig. 4m). We measured oEPSPs after 10 min of TGOT perfusion and found no significant change in the oEPSP slope or spiking probability (Fig. 4l,q,r). We then repeatedly delivered light pulse trains to activate PA terminals and observed consistent increases in oEPSP slope and firing probability (Fig. 4q–s). These synaptic changes were maintained for at least 10 min after TGOT washoff (Fig. 4q–s). Thus, simultaneous OXTR activation and excitatory synaptic inputs to aVMHvl cells are required for synaptic potentiation, possibly through a postsynaptic voltage-dependent mechanism³⁵, although the contribution of inhibitory synapses could not be excluded.

Noxious stimuli activate SOR^{OXT} cells

To understand the in vivo response patterns of SOR^{OXT} cells, we recorded their Ca²⁺ activity using fibre photometry in male *Oxt^{cre}* mice during

pre-defeat and post-defeat MSI tests and RI tests (Fig. 5a,b and Extended Data Fig. 14a,b). SOR^{OXT} cells did not show increased activity during the initial intruder encounter, social investigation or attack (Fig. 5c–j). However, SOR^{OXT} cells were highly activated during each episode of fight and defeat, regardless of the territorial environment (Fig. 5d,e,i,j). After defeat, SOR^{OXT} cells in test mice showed no increase in response to the SW aggressor or any other conspecific mouse, which was qualitatively different from the post-defeat response patterns of aVMHvl^{OXT} cells (Extended Data Fig. 14).

Given the specific response of SOR^{OXT} cells during strenuous fight and defeat, we proposed that SOR^{OXT} cells are activated by sensory inputs associated with being attacked, for example, pain. To test this hypothesis, we recorded Ca²⁺ activity of SOR^{OXT} cells in head-fixed animals while presenting urine from an aggressor mouse, a gentle touch or poke on the back, or a pinch on the back or tail (Fig. 5k,l). SOR^{OXT} cells showed strong and consistent increases in activity during tail pinch and back poke and pinch but no response during gentle touch or urine presentation (Fig. 5l–n). SOR^{OXT} cells in female mice responded similarly to those of males (Extended Data Fig. 15). By contrast, aVMHvl^{OXT} cells did not show consistent changes in activity during the delivery of the noxious somatosensory stimuli (Extended Data Fig. 10e–g). These results suggest that SOR^{OXT} cells are activated specifically during defeat, probably due to the behaviour-associated noxious somatosensory inputs.

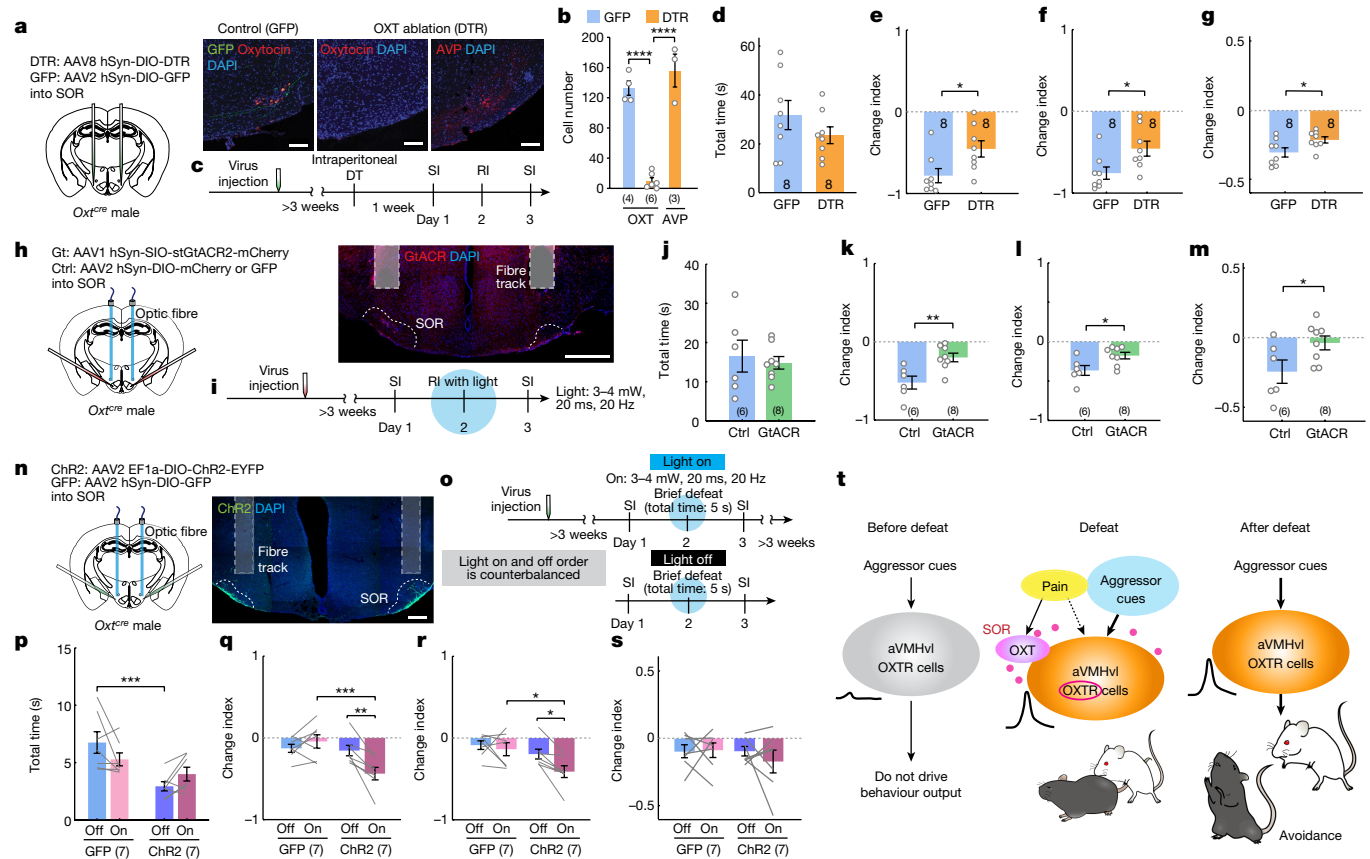


Fig. 6 | SOR^{OXT} cells are essential for social avoidance learning. **a**, Left, virus schematics. Right, Oxytocin expression in the SOR was detectable in a GFP but not in a DTR mouse. Vasopressin (AVP) expression remained in a DTR mouse. Scale bars, 100 μ m. **b**, Number of SOR OXT⁺ and AVP⁺ cells in GFP and DTR mice. **c**, Experimental timeline. **d**, Total defeated time of GFP and DTR animals during the RI test. **e–g**, Change index of aggressor investigation time percentage (**e**), time around cup percentage (**f**) and median movement velocity when far from the aggressor (**g**) during SI tests of GFP and DTR mice. **h**, Virus schematics (left) and histology (right). Scale bar, 500 μ m. **i**, Experimental timeline. **j–m**, Behavioural results of Gt and control animals during defeat (**j**) and post-defeat SI tests (investigation (**k**), time around cup (**l**) and median velocity (**m**)). **n**, Virus schematics (left) and histology (right). Scale bar, 200 μ m. **o**, Experimental timeline and illustration. **p**, Total defeat time during the RI tests. **q–s**, Change

index of aggressor investigation time percentage (**q**), time around the cup percentage (**r**) and median movement velocity when far from the aggressor (**s**) during SI tests. **t**, A model of SOR^{OXT}–aVMHvl^{OXTR} signalling-dependent social avoidance learning after defeat. Plots with error bars represent mean \pm s.e.m. Circles and lines represent individual animals. Numbers in parentheses on the plots indicate the number of animals. Statistics: one-way ANOVA with Tukey’s multiple comparisons (**b**); unpaired *t*-test (**d, f, g, j–m**); Mann–Whitney test (**e**); or two-way repeated measure ANOVA with Sidak’s multiple comparisons (**p–s**). All statistical tests are two-tailed. **P* < 0.05, ***P* < 0.01, ****P* < 0.001 and *****P* < 0.0001. See Supplementary Table 1 for detailed statistics. Brain illustrations in **a**, **h** and **n** are adapted from the Allen Brain Reference Atlas (<https://atlas.brain-map.org>).

SOR^{OXT} cells boost social avoidance learning

To understand the functional importance of SOR^{OXT} cells in defeat-induced social avoidance and fear learning, we virally expressed diphtheria toxin (DT) receptor (DTR)³⁶ to ablate SOR^{OXT} cells in *Oxtr^{cre}* male mice (DTR^{OXT} mice) (Fig. 6a). After DT injection, oxytocin staining in the SOR disappeared in DTR-expressing mice but not in mice expressing GFP in SOR^{OXT} cells (GFP^{OXT} mice), whereas vasopressin expression in DTR^{OXT} mice was intact (Fig. 6a,b). During the RI test, DTR^{OXT} and GFP^{OXT} mice were defeated for a similar amount of time by SW aggressors (Fig. 6c,d). However, during the post-defeat SI test, DTR^{OXT} mice spent more time around and investigating the constrained aggressor than GFP^{OXT} mice (Fig. 6e,f). DTR^{OXT} mice also showed slightly less reduction in movement velocity when away from the aggressor than GFP^{OXT} mice (Fig. 6g). These results provide support for a functional role of SOR^{OXT} cells in defeat-induced social avoidance and social fear.

Similar to aVMHvl *Oxtr* KO mice, mice with ablated SOR^{OXT} cells showed increased movement velocity compared with control animals, even during pre-defeat SI tests (Supplementary Note 1). To eliminate

permanent ablation-induced chronic behaviour changes and potential circuit compensation, we optogenetically inhibited SOR^{OXT} cells during RI tests using stGtACR2 (Gt^{OXT} mice); control animals were injected with GFP or mCherry virus (XFP^{OXT} mice) (Fig. 6h,i). During defeat, Gt^{OXT} or XFP^{OXT} mice were defeated for a similar duration (Fig. 6j). During the post-defeat SI test, Gt^{OXT} mice spent significantly less time investigating and around the constrained aggressor (Fig. 6k,l). Additionally, whereas XFP^{OXT} mice showed decreased movement velocity when far from the aggressor after defeat, Gt^{OXT} mice showed no change in mobility in comparison with the pre-defeat level (Fig. 6m). These results provide further support for a pivotal role of SOR^{OXT} cells in defeat-induced social avoidance and fear learning.

Last, we asked whether activating SOR^{OXT} cells could facilitate defeat-induced social avoidance. We virally expressed ChR2 or GFP in SOR^{OXT} cells in *Oxtr^{cre}* male mice (ChR2^{OXT} and GFP^{OXT} mice, respectively) and subjected the animals to subthreshold defeat (total defeat time of about 5 s) (Fig. 6n–p), which was insufficient to induce social avoidance (Fig. 6q–s). Light delivery during the brief RI test to ChR2^{OXT} mice, but not GFP^{OXT} males, caused a significant decrease in the time spent around and investigating the constrained aggressor during the

post-defeat SI test (Fig. 6q,r). However, social fear, measured as movement velocity, did not differ across groups (Fig. 6s). Thus, enhancing the activity of SOR^{OXT} cells is sufficient to facilitate social-avoidance learning after a mildly negative social experience. This effect was not due to the valence change caused by SOR^{OXT} cell activation, as Chr2^{OXT} males did not avoid or prefer the light-paired chamber in the RTTP test (Extended Data Fig. 11o,p).

Discussion

To survive in a complex social group, it is important to learn to stay away from stronger competitors. Indeed, a 10-min defeat bout is sufficient to induce multi-week avoidance of the winner¹. Our current study provided new mechanistic insight into the neural process that support this rapid change in behaviour. Before defeat, aVMHvl^{OXT} cells showed minimum responses to aggressor cues and animals did not avoid the aggressor (Fig. 6t). During defeat, pain, probably caused by biting from the aggressor, evokes strong activation of oxytocin neurons in the SOR and presumably release oxytocin, which then binds to OXTR of aVMHvl cells and facilitates the long-term potentiation of synapses that carry information about the aggressor. After defeat, when the animal re-encounters the aggressor, owing to the strengthened input that carries aggressor cues, aVMHvl^{OXT} cells are now strongly activated, which in turn drives social avoidance to ensure that the animal stays away from potentially disadvantageous conflicts (Fig. 6t and Supplementary Note 1).

Our results revealed distinct roles of aVMHvl^{OXT} cells in social avoidance and fear. Although the cells were indispensable for expressing the former, it was unnecessary for the latter. Inhibiting aVMHvl^{OXT} cells reduced defeat-induced social avoidance but did not impair social fear. However, oxytocin–OXTR signalling during defeat was essential for the emergence of both. Blocking either SOR^{OXT} cells or OXTR in the aVMHvl during defeat, but not during the post-defeat SI test, reduced social avoidance and fear. Based on the specific role of aVMHvl^{OXT} cells in social-fear learning but not expression, we propose that the aVMHvl is an input region to ‘teach’ the social-fear circuit (Supplementary Note 1). During defeat, aVMHvl input to the social-fear circuit is essential in inducing changes in this circuit. However, once the changes are complete, the social-fear circuit can operate independently of aVMHvl input (Supplementary Note 1).

Our results confirmed the crucial role of oxytocin in social behaviour plasticity³⁷ and expanded the list of regions through which oxytocin can modulate negative social responses^{38–42}. The findings that SOR^{OXT} cells are specifically activated by painful stimuli and serve as an exclusive source for aVMHvl^{OXT} cells during defeat raises the possibility that there are distinct oxytocin subsystems dedicated to promoting social learning during positive and negative social encounters. Indeed, in contrast to SOR^{OXT} cell responses, PVN^{OXT} cells are activated by positive social experiences, such as gentle social touch, non-antagonistic social interaction and maternal shepherding^{43–46}. Future studies to identify such oxytocin subsystems will be essential for harnessing the therapeutic potential of oxytocin in social-deficit disorders⁴⁷.

Online content

Any methods, additional references, Nature Portfolio reporting summaries, source data, extended data, supplementary information, acknowledgements, peer review information; details of author contributions and competing interests; and statements of data and code availability are available at <https://doi.org/10.1038/s41586-023-06958-w>.

1. Qi, C. C. et al. Interaction of basolateral amygdala, ventral hippocampus and medial prefrontal cortex regulates the consolidation and extinction of social fear. *Behav. Brain Funct.* **14**, 7 (2018).

2. Martinez, M., Calvo-Torrent, A. & Pico-Alfonso, M. A. Social defeat and subordination as models of social stress in laboratory rodents: a review. *Aggress. Behav.* **24**, 241–256 (1998).
3. Schlund, M. W. et al. Human social defeat and approach-avoidance: escalating social-evaluative threat and threat of aggression increases social avoidance. *J. Exp. Anal. Behav.* **115**, 157–184 (2021).
4. Banks, R. *ERIC Clearinghouse on Elementary and Early Childhood Education* (ERIC Development Team, 1997).
5. Huhman, K. L. et al. Conditioned defeat in male and female Syrian hamsters. *Horm. Behav.* **44**, 293–299 (2003).
6. Markham, C. M., Taylor, S. L. & Huhman, K. L. Role of amygdala and hippocampus in the neural circuit subserving conditioned defeat in Syrian hamsters. *Learn. Mem.* **17**, 109–116 (2010).
7. Day, D. E., Cooper, M. A., Markham, C. M. & Huhman, K. L. NR2B subunit of the NMDA receptor in the basolateral amygdala is necessary for the acquisition of conditioned defeat in Syrian hamsters. *Behav. Brain Res.* **217**, 55–59 (2011).
8. Markham, C. M., Luckett, C. A. & Huhman, K. L. The medial prefrontal cortex is both necessary and sufficient for the acquisition of conditioned defeat. *Neuropharmacology* **62**, 933–939 (2012).
9. Sakurai, K. et al. Capturing and manipulating activated neuronal ensembles with CANE delineates a hypothalamic social–fear circuit. *Neuron* **92**, 739–753 (2016).
10. Silva, B. A. et al. Independent hypothalamic circuits for social and predator fear. *Nat. Neurosci.* **16**, 1731–1733 (2013).
11. Wang, L. et al. Hypothalamic control of conspecific self-defense. *Cell Rep.* **26**, 1747–1758. e5 (2019).
12. Diaz, V. & Lin, D. Neural circuits for coping with social defeat. *Curr. Opin. Neurobiol.* **60**, 99–107 (2020).
13. Krzykowski, P., Penna, B. & Gross, C. T. Dynamic encoding of social threat and spatial context in the hypothalamus. *eLife* **9**, e57148 (2020).
14. Newman, S. W. The medial extended amygdala in male reproductive behavior. A node in the mammalian social behavior network. *Ann. NY Acad. Sci.* **877**, 242–257 (1999).
15. Lin, D. et al. Functional identification of an aggression locus in the mouse hypothalamus. *Nature* **470**, 221–226 (2011).
16. Toth, I. & Neumann, I. D. Animal models of social avoidance and social fear. *Cell Tissue Res.* **354**, 107–118 (2013).
17. Nasanbayan, N. et al. Oxytocin–oxytocin receptor systems facilitate social defeat posture in male mice. *Endocrinology* **159**, 763–775 (2018).
18. Lee, H. et al. Scalable control of mounting and attack by Esr1⁺ neurons in the ventromedial hypothalamus. *Nature* **509**, 627–632 (2014).
19. Hashikawa, K. et al. Esr1⁺ cells in the ventromedial hypothalamus control female aggression. *Nat. Neurosci.* **20**, 1580–1590 (2017).
20. Isosaka, T. et al. Htr2a-expressing cells in the central amygdala control the hierarchy between innate and learned fear. *Cell* **163**, 1153–1164 (2015).
21. Mahn, M. et al. High-efficiency optogenetic silencing with soma-targeted anion-conducting channelrhodopsins. *Nat. Commun.* **9**, 4125 (2018).
22. Armbruster, B. N., Li, X., Pausch, M. H., Herlitze, S. & Roth, B. L. Evolving the lock to fit the key to create a family of G protein-coupled receptors potentially activated by an inert ligand. *Proc. Natl Acad. Sci. USA* **104**, 5163–5168 (2007).
23. Thompson, K. J. et al. DREADD agonist 21 is an effective agonist for muscarinic-based DREADDs in vitro and in vivo. *ACS Pharmacol. Transl. Sci.* **1**, 61–72 (2018).
24. Liao, P. Y., Chiu, Y. M., Yu, J. H. & Chen, S. K. Mapping central projection of oxytocin neurons in unmanipulated mice using Cre and alkaline phosphatase reporter. *Front. Neuroanat.* **14**, 559402 (2020).
25. Rhodes, C. H., Morrell, J. I. & Pfaff, D. W. Immunohistochemical analysis of magnocellular elements in rat hypothalamus: distribution and numbers of cells containing neurophysin, oxytocin, and vasopressin. *J. Comp. Neurol.* **198**, 45–64 (1981).
26. Castel, M. & Morris, J. F. The neurophysin-containing innervation of the forebrain of the mouse. *Neuroscience* **24**, 937–966 (1988).
27. Ludwig, M. Dendritic release of vasopressin and oxytocin. *J. Neuroendocrinol.* **10**, 881–895 (1998).
28. Pow, D. V. & Morris, J. F. Dendrites of hypothalamic magnocellular neurons release neurohypophysial peptides by exocytosis. *Neuroscience* **32**, 435–439 (1989).
29. Kim, D.-W. *Multimodal Analysis of Cell Types in a Hypothalamic Node Controlling Social Behavior in Mice*. PhD thesis, California Institute of Technology (2020).
30. Klapeetke, N. C. et al. Independent optical excitation of distinct neural populations. *Nat. Methods* **11**, 338–346 (2014).
31. Yamaguchi, T. et al. Posterior amygdala regulates sexual and aggressive behaviors in male mice. *Nat. Neurosci.* **23**, 1111–1124 (2020).
32. Stagkourakis, S., Spigolon, G., Liu, G. & Anderson, D. J. Experience-dependent plasticity in an innate social behavior is mediated by hypothalamic LTP. *Proc. Natl Acad. Sci. USA* **117**, 25789–25799 (2020).
33. Zha, X. et al. VMHvl-projecting Vglut1⁺ neurons in the posterior amygdala gate territorial aggression. *Cell Rep.* **31**, 107517 (2020).
34. Bekkers, J. M. Changes in dendritic axial resistance alter synaptic integration in cerebellar Purkinje cells. *Biophys. J.* **100**, 1198–1206 (2011).
35. Malinow, R. & Miller, J. P. Postsynaptic hyperpolarization during conditioning reversibly blocks induction of long-term potentiation. *Nature* **320**, 529–530 (1986).
36. Saito, M. et al. Diphtheria toxin receptor-mediated conditional and targeted cell ablation in transgenic mice. *Nat. Biotechnol.* **19**, 746–750 (2001).
37. Froemke, R. C. & Young, L. J. Oxytocin, neural plasticity, and social behavior. *Annu. Rev. Neurosci.* **44**, 359–381 (2021).
38. Zoicas, I., Slatery, D. A. & Neumann, I. D. Brain oxytocin in social fear conditioning and its extinction: involvement of the lateral septum. *Neuropsychopharmacology* **39**, 3027–3035 (2014).
39. Williams, A. V. et al. Social approach and social vigilance are differentially regulated by oxytocin receptors in the nucleus accumbens. *Neuropsychopharmacology* **45**, 1423–1430 (2020).
40. Menon, R. et al. Oxytocin signaling in the lateral septum prevents social fear during lactation. *Curr. Biol.* **28**, 1066–1078.e6 (2018).

41. Guzman, Y. F. et al. Fear-enhancing effects of septal oxytocin receptors. *Nat. Neurosci.* **16**, 1185–1187 (2013).
42. Duque-Wilckens, N. et al. Extrahypothalamic oxytocin neurons drive stress-induced social vigilance and avoidance. *Proc. Natl Acad. Sci. USA* **117**, 26406–26413 (2020).
43. Carcea, I. et al. Oxytocin neurons enable social transmission of maternal behaviour. *Nature* **596**, 553–557 (2021).
44. Yu, H. et al. Social touch-like tactile stimulation activates a tachykinin 1–oxytocin pathway to promote social interactions. *Neuron* **110**, 1051–1067.e7 (2022).
45. Tang, Y. et al. Social touch promotes interfemale communication via activation of parvocellular oxytocin neurons. *Nat. Neurosci.* **23**, 1125–1137 (2020).
46. Resendez, S. L. et al. Social stimuli induce activation of oxytocin neurons within the paraventricular nucleus of the hypothalamus to promote social behavior in male mice. *J. Neurosci.* **40**, 2282–2295 (2020).
47. Erdozain, A. M. & Penagarikano, O. Oxytocin as treatment for social cognition, not there yet. *Front. Psychiatry* **10**, 930 (2020).

Publisher's note Springer Nature remains neutral with regard to jurisdictional claims in published maps and institutional affiliations.

Springer Nature or its licensor (e.g. a society or other partner) holds exclusive rights to this article under a publishing agreement with the author(s) or other rightsholder(s); author self-archiving of the accepted manuscript version of this article is solely governed by the terms of such publishing agreement and applicable law.

© The Author(s), under exclusive licence to Springer Nature Limited 2024

Methods

Mice

All procedures were approved by the New York University Langone Medical Center Institutional Animal Care and Use Committee in compliance with the National Institutes of Health Guidelines for the Care and Use of Laboratory Animals. Mice were housed under a 12-h light–dark cycle (dark cycle: 10:00–22:00 or 18:30–6:30), with food and water available ad libitum. The room temperature was maintained between 20 and 22 °C and humidity between 30 and 70%, with a daily average of approximately 45%. *Oxtr^{cre}* (strain 031303)⁴⁸, *Oxtr^{cre}* (strain 024234)⁴⁸, *Vglut2^{cre}* (strain 016963)⁴⁹ and *Oxtr^{fllox}* mice (strain 008471)⁵⁰ were purchased from the Jackson Laboratory. Ai6 (strain 007906)⁵¹ mice were from the Jackson Laboratory and crossed with *Oxtr^{cre}* and *Vglut2^{cre}* mice. Test mice were aged between 8 and 24 weeks at the time of behaviour testing or recording. Stimulus animals in the RI test were BC male mice (>9 weeks), and C57 male and female mice (>8 weeks) originally purchased from Charles River and then bred in-house. SW male and female mice (>11 weeks) were purchased from Taconic, Charles River or bred in-house. All mice were group-housed until adulthood. After surgery with fibre or cannula implantation, all test mice were single-housed. Animals were randomly assigned to control and test groups.

Viruses

The following AAVs were used in this study, with injection titres as indicated. AAV2 CAG-Flex-GCaMP6f-WPRE-SV40 (1.8×10^{12} vg per ml, UPenn, V5747S) for fibre photometry was purchased from the UPenn vector core. For functional manipulation, the following AAVs were used. Optogenetic activation: AAV2 Ef1a-DIO-hChR2(H134R)-EYFP (4.2×10^{12} vg per ml, UNC, AV4378); chemogenetic inactivation: AAV2 hSyn-DIO-hM4Di-mCherry (1.5×10^{13} vg per ml, Addgene, 44362-AAV2); optogenetic inactivation: AAV1 hSyn-SIO-stGtACR2-FusionRed (1.9×10^{13} vg per ml, Addgene, 105677-AAV1); *Oxtr* KO: AAV1 CMV-HleGFP-Cre (1.1×10^{13} vg per ml, Addgene, 105545-AAV1) or AAV2 hSyn-GFP (3.4×10^{12} vg per ml, UNC, 4876D); ablation of oxytocin cells: AAV8 hSyn-DIO-DTR (9.1×10^{13} vg per ml, Boston Children's Hospital), AAV2 hSyn-DIO-GFP (4.0×10^{12} vg per ml, UNC, 4530C) or AAV2 hSyn-DIO-mCherry (1.8×10^{13} vg per ml, Addgene, 50459-AAV2). For slice electrophysiology, the following AAVs were used: AAV2 Ef1a-DIO-hChR2(H134R)-EYFP (4.2×10^{12} vg per ml, UNC, AV4378) and AAV9 hSyn-ChrimsonR-tdTomato (2.6×10^{13} vg per ml, Addgene, 59171-AAV9).

Drugs

For chemogenetic inhibition, 1 mg kg⁻¹ agonist 21 (ref. 23) (Tocris, 5548) in saline was intraperitoneally administered. To block OXTRs in the aVMHvl, 250 nl per side of 100 µM L-368,899 hydrochloride (Tocris, 2641) in saline was injected through implanted cannulae bilaterally. To ablate SOR^{OXTR} cells, 50 µg kg⁻¹ DT in saline (Sigma-Aldrich, D0564) was administered intraperitoneally on two consecutive days (7 days before the pre-defeat SI test). A mixture of ketamine (100 mg kg⁻¹) and xylazine (10 mg kg⁻¹) in saline was administered intraperitoneally before perfusion.

Stereotaxic surgery

Mice (8–12 weeks old) were anaesthetized with 1–1.5% isoflurane and placed in a stereotaxic apparatus (Kopf Instruments Model 1900). Viruses were delivered into the targeted brain regions through glass capillaries using a nanoinjector (World Precision Instruments, Nanoliter 2010) at a speed of 20 nl min⁻¹. Around 100–120 nl AAV was injected into each targeted brain region. Stereotaxic injection coordinates were based on the Paxinos and Franklin mouse brain atlas⁵². For fibre photometry and optogenetic manipulation, a polished optical fibre (440 or 230 µm diameter, Thorlabs) was implanted 150 or 200 µm above the virus injection site either immediately after virus injection

or 2–3 weeks later. During the same surgery as optic fibre implantation, a 3D-printed head-fixation ring⁵³ was cemented onto the skull (C&B Metabond dental cement, Parkell) to allow head-fixation during fibre attachment and detachment, drug injection through the cannula and head-fixed fibre photometry recording. Mice were single-housed after optic fibre implantation. Histology was obtained from all test animals, and only animals with correct virus expression and optic fibre placement were included in the final analysis.

Common parameters for all behaviour tests

Mouse behaviours in all experiments were recorded from both the side and top of the cage using two synchronized cameras (Basler, acA640-100 gm and 120 gm) in a semi-dark room with infrared illumination. Video acquisition was achieved using StreamPix 5 (Noprix) at 25 frames per second. Manual behavioural annotations were performed on a frame-by-frame base using custom software written in Matlab (<https://pdollar.github.io/toolbox/>)¹⁵. Some videos were annotated by people who did not perform the behaviour assays in a blinded manner, and the annotations were checked and refined by an experimenter who was not blind to the group assignment of the animal. Some videos were annotated by the experimenter who performed the behaviour assays but were blinded to the animal identity or neural responses during annotation. There was high consistency (around >90%) between annotations performed by different individuals. Custom DeepLabCut⁵⁴-based models were constructed to track the body centre, head centre and nose points of the animal in top-view videos. Movement velocity was calculated as the distance of an body centre of the animal between two adjacent frames.

RI test

For inter-male RI tests in which the goal was that the test animal was defeated, we introduced the test animal into the HC cage of a sexually experienced, aggressive and single-housed SW male mouse or introduced the SW male aggressor into the HC of the test mouse (see individual experiments for details). For females, we introduced the test female into the HC of a lactating female of SW or mixed background. The RI test typically lasted for 10 min, although for several wild-type male mice in Extended Data Fig. 1, the RI test was terminated after 5 min as the aggressor was highly aggressive and continuously attacked the test animal. Across experiments, each test mouse was defeated for approximately 20 s during the RI test. Defeat was annotated when the front-end of the aggressor contacts the back of the test animal, presumably to bite, as the aggressor attacks the test mouse. Fight was annotated if the test animal successfully pushed or bit the aggressor when being attacked. For RI tests with non-aggressors, we introduced a BC non-aggressive group-housed male mouse into the HC of a male test mouse and a C57 naive female mouse into the home cage of a test female mouse. Attack was annotated when the test mouse initiated a suite of fast actions towards the non-aggressive intruder, including lunges, bites and tumbles. To analyse the behaviours, in addition to manual annotation, we also tracked the animals and calculated the percentage of time that the test animal spent immobile (body centre velocity of <1 pixel per frame) during each minute of RI tests.

SI test

For the SI test, the stimulus animals were always the same as those used in RI tests except for Extended Data Fig. 2. In the aVMHvl^{OXTR} optogenetic activation experiment, group-housed non-aggressive BC males were also used as stimulus animals. For females, on the day before the first SI test, the test animal was habituated to the empty metal wire cup (diameter of the cup bottom: 7.5 cm; height: 10.5 cm) in a clean cage for 10–15 min. There was no habituation for the SI test in males. During the SI test, the stimulus animal was placed under a cup at one end of a clean cage with bedding, and then the test animal was introduced into the cage and freely interacted with the constrained animal for 5 or 10 min.

Article

For each experiment, the SI test was performed 1 day before and 1 day after the RI test. For each experiment, the same set of aggressor mice was used for test and control groups to reduce the variability in defeat.

To analyse behaviours during the SI test, we calculated the distance of the body centre of the test animal to the cup centre for each frame and constructed histograms showing the distribution of the test animal–constrained aggressor distance. The percentage of time an animal spent around the cup was calculated as the percentage of frames when the body centre of the test animal to the distance of the cup was within 15 cm (<250 pixels), which is approximately half the length of the cage. The investigation behaviour was manually annotated as the time period when the nose point of the test animal was in close proximity to the cup. When the test animal stayed far from the constrained aggressor (distance of >300 pixels) and when its body centre and head centre velocity were <1 pixel per frame for >0.5 s, the animal was considered as immobile. We then calculated the change index for each parameter (P), including time around aggressor (%), investigation time (%) and median velocity when far from the aggressor as $(P_{\text{after}} - P_{\text{before}})/(P_{\text{after}} + P_{\text{before}})$. Where P_{before} is the value of the parameter before defeat; P_{after} is the value after defeat. The change index ranges from -1 to 1. Positive change index values indicate increases after defeat, whereas negative change index values indicate decreases after defeat. Values close to -1 or 1 indicate large changes.

MSI test

For the MSI test, the test arena (length × width × height of 56 × 46 × 41 cm) contained four wire meshed cups, one in each corner. On the habituation days (2 days), test animals freely explored the arena for around 20 min without any cups. On the test day, one cup was left empty, and the other three cups each contained a stimulus animal. The test animals were allowed to explore the arena freely for 10 min. The MSI test was performed 1 day before and 1 day after RI tests. For each male MSI test, we also introduced an aggressive SW male (16–40 weeks), a group-housed C57 male (16–24 weeks) and a BC non-aggressive group-housed male (14–24 weeks), each under a cup as stimulus animals. The same BC was encountered during the RI test, during which the test animal either attacked or investigated it but was never defeated by it. The C57 stimulus males were unfamiliar and only encountered during the MSI tests. For each female MSI test, the SW mother aggressor (16–32 weeks), a single-housed SW virgin female (10–24 weeks) and a single-housed C57 virgin female (10–24 weeks), each under a cup, were introduced as stimulus animals. The same C57 virgin mice were encountered during the RI test (only investigation). The SW virgin mice were unfamiliar and only encountered during the MSI tests.

To analyse the behaviours, we calculated the distance between the head centre of the animal and the centre of each cup. When the distance was <3 × radius of the cup (r_{cup}), the test animal was considered to be around the constrained animal. We also calculated the distance between the nose point of the animal to the centre of each cup. When the distance was <1.5 × r_{cup} , the test animal was considered investigating the constrained animal. We then calculated the percentage of time each test animal spent on investigating and around the cup during pre-defeat and post-defeat MSI tests. We also calculated the number of approaches to each stimulus during the MSI tests. When the animal moved from a far distance, and its nose reached the distance to the cup centre shorter than the cup diameter, we considered it an approaching event.

Odour–shock paired conditioning

The odour delivery chamber was custom-made by opening one odour delivery port (diameter of 6.35 mm) and one vacuum port (diameter of 6.35 mm) onto the opposite short walls of an acrylic chamber (length × width × height of 37 × 19 × 30 cm). The odours (10% pentyl acetate (Sigma-Aldrich, 109584) and (*R*)-(+)-limonene (Sigma-Aldrich, 183164)) were delivered at a rate of 2 l min⁻¹ through Tygon tubing (MFLX06422-07 and MFLX07407-75, Cole-Parmer) inserted directly into

the odour delivery port. Each odour was delivered for 3 s, 8 times, with an inter-trial interval of 60 s. There was a 10 min no-odour period between pentyl acetate and limonene presentations. A second tube was inserted into the vacuum port and connected to the building vacuum system to move air constantly. The odour delivery chamber was free of bedding or any objects.

The foot shock–odour conditioning occurred in a foot-shock chamber (ENV-307W-CT, Med Associates) that was modified for odour delivery by adding the custom odour delivery and vacuum ports. During the conditioning session, we first delivered one odour (10% pentyl acetate or limonene) at 2 l min⁻¹, 8 times for 3 s each, with 60 s intervals without any shock. Then, 10 min after completing the first odour delivery, we delivered a second odour (2 l min⁻¹, 8 times for 3 s each within 60 s intervals). The foot shock (1 mA, 1 s) was delivered between 2 and 3 s of each odour delivery trial. The odour (10% pentyl acetate or limonene) paired with the shock was randomly selected for each animal. We examined the behaviour and neural responses of male mice expressing OXTR^{GCAMP} cells in the odour delivery chamber 1 day before and 1 day after the shock–odour conditioning.

Optogenetic activation

To activate aVMHvl^{OXTR} cells, we injected 120 nl Cre-dependent ChR2 (control was GFP) expressing virus unilaterally into the aVMHvl (Bregma coordinates: anterior–posterior (AP), -1.455 mm; medial–lateral (ML), -0.65 mm; dorsal–ventral (DV), -5.70 mm) of *Oxtr^{cre}* mice and placed a 230- μ m multimode optic fibre (Thorlabs, FT200EMT) 200 μ m above injection site. On the test day, the implanted fibre was connected to a matching patch cord using a plastic sleeve (Thorlabs, ADAL1) to allow light delivery (Shanghai Dream Lasers). During the test, a non-aggressive BC male mouse or an aggressive SW male mouse was placed under a metal wire cup located at one end of a clean cage, and 20 ms, 20 Hz, 1.5–2 mW light was delivered for 60 s, followed by 0 mW sham light for 60 s, and then repeated once. In a separate group of animals, we stimulated aVMHvl^{OXTR} cells without any target in a clean cage using the same stimulation protocol (20 ms, 20 Hz, 1.5–2 mW light for 60 s, followed by 0 mW sham light for 60 s with one light-sham repeat).

To activate SOR^{OXTR} cells, we injected 120 nl Cre-dependent ChR2 (control was GFP) expressing virus bilaterally into the SOR (Bregma coordinates: AP, -1.36 mm; ML, \pm 0.90 mm; DV, -5.69 mm) of *Oxtr^{cre}* male mice and placed two 230 μ m multimode optic fibres (Thorlabs, FT200EMT) 200 μ m above the injection sites. The behaviour test started 3 weeks after the virus injection. Each ChR2 and GFP animal underwent two rounds of 3-day SI-RI-SI tests with at least 3 weeks in between. No light was delivered during SI tests. During the RI test, a SW male aggressor was introduced into the HC of the test mice until the aggressor defeated the test mouse for 3–4 times, with a total defeat duration of approximately 5 s. For one round of the SI-RI-SI test, the light (3.5–4 mW, 20 ms, 20 Hz) was delivered during the entire RI test. For the other round of the SI-RI-SI test, the test animals received no light during the RI tests. The order of light delivery during RI tests was counterbalanced across animals.

The RTPP test was performed to investigate the valence of aVMHvl^{OXTR} and SOR^{OXTR} activation. The test area contained two equal size chambers (13 cm long, 16 cm wide and 25 cm high, per chamber) made with transparent acrylic boards. During the test, the animal was allowed to freely move in the chamber for 15 min without any stimulation. Light (3.5–4 mW, 20 ms, 20 Hz) was manually delivered through the implanted optic fibre whenever the animal entered a pre-assigned chamber for 10 min. The body centre of the animal was tracked using custom tracking software (<https://pdollar.github.io/toolbox/>)¹⁵ and used to calculate the time spent in each chamber.

Optogenetic and chemogenetic inhibition

To inactivate aVMHvl^{OXTR} cells, we injected 120 nl Cre-dependent stGtACR2 (control was mCherry) virus bilaterally into the aVMHvl

(Bregma coordinates: AP, -1.455 mm; ML, ± 0.65 mm; DV, -5.70 mm) of *Oxtr^{cre}* mice and placed two 230 μ m multimode optic fibres (Thorlabs, FT200EMT) 200 μ m above the injection sites. Three weeks after the virus injection, all test animals went through 3-day SI-RI-SI tests. For each test animal, the aggressor was the same SW male mouse throughout the tests. No light was delivered during the first SI test or RI test. During the post-defeat SI test, one group of stGtACR2 and mCherry animals received light (473 nm, 3.5-4 mW, 20 ms, 20 Hz) for 5 min, and the other group received no light.

To chemogenetically inhibit aVMHvl^{OXTR} cells, we injected 100-110 nl Cre-dependent hM4Di (control was mCherry) virus bilaterally into the aVMHvl (Bregma coordinates: AP, -1.455 mm; ML, ± 0.65 mm; DV, -5.70 mm) of *Oxtr^{cre}* mice. Three weeks later, animals underwent 3-day SI-RI-SI tests with SW male aggressors. No drug was injected during the pre-defeat SI or RI tests. One hour before the post-defeat SI test, test animals were intraperitoneally injected with 250 μ l of saline or agonist 21 solutions (1 mg kg⁻¹, Tocris, 5548).

To optogenetically inactivate SOR^{OXTR} cells, we injected 120 nl Cre-dependent stGtACR2 (control was mCherry or GFP) virus bilaterally into the SOR (Bregma coordinates: AP, -1.36 mm; ML, ± 0.90 mm; DV, -5.69 mm) of *Oxtr^{cre}* mice and placed two 230- μ m multimode optic fibres (Thorlabs, FT200EMT) 200 μ m above the injection sites. Three weeks after the virus injection, all test animals underwent 3-day SI-RI-SI tests (all 10 min). For each test animal, the aggressor was the same SW male mouse throughout the tests. No light was delivered during the SI tests. During the RI test, all animals received light (473 nm, 3.5-4 mW, 20 ms, 20 Hz) for 10 min continuously.

KO of aVMHvl OXTRs

To KO OXTRs in the aVMHvl, we bilaterally injected 100 nl AAV expressing GFP-Cre (control was GFP) into the aVMHvl (Bregma coordinates: AP, -1.46 mm; ML, ± 0.65 mm; DV, -5.70 mm) of *Oxtr^{fllox/fllox}* male mice. At 3-4 weeks after the virus injection, all test animals went through the 3-day SI-RI-SI tests. During RI tests, SW aggressors were introduced into the HC of the test animals for 10 min.

OXTRA application

To block aVMHvl OXTR, we implanted bilateral cannulae (PlasticsOne, centre-to-centre distance of 1.5 mm) 0.7 mm above the aVMHvl (Bregma coordinates: AP, -1.45 mm; ML, ± 0.75 mm; DV, -5.00 mm) of wild-type C57 male mice. One week after the surgery, all animals went through the 3-day SI-RI-SI tests. To block aVMHvl OXTR during defeat, we injected 250 nl per side with 100 μ M L-368,899 hydrochloride (Tocris, 2641) into the aVMHvl through the cannula using a syringe (Hamilton, 65457-02) 20 min before the RI test when the animal was head-fixed on a running wheel. To block OXTR during the post-defeat SI test, the same drug was injected 20 min before the SI test. Control animals were injected with saline and underwent the same behaviour tests. During the waiting time after drug injection, the animal was returned to its HC. Before euthanizing the animals, 250 nl of 10 ng ml⁻¹ Dil (ThermoFisher) was injected to mark the injection site.

Ablation of OXT cells in the SOR

To ablate SOR^{OXTR} cells, we injected 120 nl AAV expressing Cre-dependent DTR (control was GFP) into the SOR (Bregma coordinates: AP, -1.36 mm; ML, ± 0.90 mm; DV, -5.69 mm) bilaterally using *Oxtr^{cre}* male mice. Three weeks later, we intraperitoneally injected each animal with 50 μ g kg⁻¹ DT (Sigma-Aldrich, D0564) per day for two consecutive days. One week after the first DT injection, all animals went through the 3-day SI-RI-SI tests.

Fibre photometry recording

We injected 120 nl AAV expressing Cre-dependent GCaMP6f into the SOR or aVMHvl unilaterally of 10-12-week old *Oxtr^{cre}* and *Oxtr^{cre}* male and female mice. The following Bregma coordinates were used: male

SOR: AP, -1.36 mm; ML, -0.90 mm; DV, -5.69 mm from the top of the skull; female SOR: AP, -1.355 mm; ML, -0.88 mm; DV, -5.68 mm from the skull surface; male aVMHvl: AP, -1.46 mm; ML, -0.65 mm; DV, -5.7 mm from the skull surface; female aVMHvl: AP, -1.455 mm, ML, -0.645 mm; DV, -5.72 mm from the skull surface. Recording started at least 3 weeks after the virus injection.

Before fibre photometry recording, a ferrule sleeve (ADAL1-5, Thorlabs) was used to connect a matching patch cord to the implanted optic fibre when the animal was head fixed. For recordings, a 390-Hz sinusoidal 470-nm blue LED light (35 mW; LED light (M470F1, Thorlabs) driven by a LED driver (LEDD1B, Thorlabs) was bandpass-filtered (passing band: 472 \pm 15 nm, Semrock, FF02-472/30-25) and delivered to the brain in to excite GCaMP6f. The emission light then passed through the same optic fibre, a bandpass filter (passing band: 534 \pm 25 nm, Semrock, FF01-535/50), detected using a Femtowatt Silicon Photoreceiver (Newport, 2151) and recorded using a RZ5 real-time processor (Tucker-Davis Technologies). The envelope of 390-Hz signals from the photoreceiver was extracted in real-time using a custom-written program (Tucker-Davis Technologies) as the readout of GCaMP6f intensity. Top-view and side-view behaviour videos were simultaneously recorded (Basler, acA640-100 gm and 120 gm) and acquired using StreamPix 5 (Noprix) at 25 frames per second. Time stamps of video frames were used to align GCaMP6f signal and behaviour videos. For the head-fixed recording of SOR^{OXTR} and aVMHvl^{OXTR} cells, urine was collected from SW male aggressors or lactating SW female mice on the same day of recording. Urine was pooled from multiple aggressors, including the mouse that defeated the test animal during the RI test. We then added 100 μ l of urine to a cotton swab using a pipette and manually presented it to the recording animal for 10 s with 50 s in between. Male urine was presented to male test mice, and female urine was presented to female animals. The gentle touch stimulus was performed on the back of test animals with a large fluffy cotton ball (five swipes from the neck to tail base for each trial). Urine exposure and gentle touch were performed six times for each animal. Back and tail pinches were applied with a pair of forceps with serrations (FST, 91100-13) at a force that did not cause visible skin damage. Back pokes were applied with the tip of a pair of fine forceps (FST, 11254-20). Twelve pinches were applied, each lasting for approximately 3 s, with 50-60 s in between. Additionally, we recorded aVMHvl^{OXTR} cell responses to unpaired and shock paired-odour in head-fixed animals 1 day after odour-pairing. In brief, 100 μ l of 10% pentyl acetate or limonene was added to a cotton swab and manually presented to the recording animals 6 times, each for 10 s with 50 s in between. Unpaired odour and paired odour were delivered sequentially with 5-min intervals in between.

We also compared aVMHvl^{OXTR} cell responses to 2MT and urine from aggressor mice in free-moving and head-fixed animals. On the day before recording, the test animal was defeated by a SW male aggressor for 10 min in the HC of the SW mouse. On the day of recording, the test animal went through a 10-min SI test with the constrained SW aggressor in a clean cage, and then 5 min later, was presented with 100 μ l 1% 2MT in PBS on a filter paper placed at one end of the clean cage for 10 min. After recording in free-moving animals, we also recorded the cell response to saline, 2MT and urine from aggressor mice in head-fixed animals. During recording, 100 μ l of saline, urine from the same SW aggressor and 1% 2MT were presented to the animals on cotton swabs, each for 6 times, 10 s per trial with 50 s between trials. There was a 5-min interval between presentations of different stimuli.

To analyse the free-moving recording data, the Matlab function msbackadj with a moving window of 20% of the total recording duration was first applied to obtain the instantaneous baseline signal. The instantaneous $\Delta F/F$ was calculated as $(F_{\text{raw}} - F_{\text{baseline}})/F_{\text{baseline}}$. The z-scored $\Delta F/F$ of the entire recording session was calculated as $(\Delta F/F - \text{mean}(\Delta F/F))/\text{s.d.}(\Delta F/F)$. The PETH of z-scored $\Delta F/F$ aligned to a given behaviour was constructed for each animal and then averaged

Article

across animals. The response during a specific behaviour for each animal was calculated by averaging the z-scored $\Delta F/F$ during all periods when the behaviour occurred.

To analyse the recording data in head-fixed animals, we constructed PETHs of the raw fluorescence signal and then calculated the averaged PETH for each animal and used the -20 to 0 s recording trace before the stimulus onset as the baseline to calculate the mean and standard deviation for z-scoring the entire PETH. The mean Ca^{2+} signal of each stimulus for each animal was calculated by averaging the z-scored PETH values from 0 s to the average duration of the stimulus presentation (approximately 10 s). We did not perform baseline correction for head-fixed recording as we noted sustained signal suppression during the 2MT presentation, which made the low-pass-based baseline correction inaccurate.

Slice electrophysiology

To prepare brain slices for patch-clamp recording, mice were anaesthetized with isoflurane, and brains were quickly removed and then immersed in ice-cold cutting solution for $1-2$ min (in mM: 110 choline chloride, 25 NaHCO_3 , 2.5 KCl , 7 MgCl_2 , 0.5 CaCl_2 , 1.25 NaH_2PO_4 , 25 glucose, 11.6 ascorbic acid and 3.1 pyruvic acid). aVMHvl coronal sections (275 μm) were cut using a Leica VT1200s vibratome, collected in oxygenated (95% O_2 and 5% CO_2) and pre-heated ($32-34$ $^\circ\text{C}$) ACSF solution (in mM: 125 NaCl , 2.5 KCl , 1.25 NaH_2PO_4 , 25 NaHCO_3 , 1 MgCl_2 , 2 CaCl_2 and 11 glucose) and incubated for 30 min. The sections were then transferred to room temperature and continuously oxygenated until use.

Current and voltage whole-cell patch-clamp recordings were performed using micropipettes filled with intracellular solution containing (in mM) 145 potassium gluconate, 2 MgCl_2 , 2 Na_2ATP , 10 HEPES, 0.2 EGTA (286 mOsm, pH 7.2) or 135 CsMeSO_3 , 10 HEPES, 1 EGTA, 3.3 QX-314 (chloride salt), 4 Mg-ATP , 0.3 Na-GTP and 8 sodium phosphocreatine (pH 7.3 adjusted with CsOH). Signals were recorded using a MultiClamp 700B amplifier (Molecular Devices) and Clampex 11.0 software (Axon Instruments), and digitized at 20 kHz with Digidata 1550B (Axon Instruments). After recording, data were analysed using Clampfit (Molecular Devices) or Matlab (Mathworks).

To characterize the physiological and synaptic properties of aVMHvl^{OXTR} cells, we identified ZsGreen⁺ cells in the aVMHvl on slices from mice expressing OXTR^{ZsGreen} using an Olympus $\times 40$ water-immersion objective with a GFP filter. For investigating intrinsic excitability, cells were recorded in current-clamp mode, and the number of action potentials was counted over 500 -ms current steps. The current steps consisted of 30 sweeps from -20 pA to 270 pA at 10 pA per step. sEPSCs and sIPSCs were recorded in the voltage-clamp mode. The membrane voltage was held at -70 mV for sEPSC recordings and at 0 mV for sIPSC recordings.

To investigate the efficacy of *Oxtr* KO, 120 nl AAV1-GFP-Cre and 120 nl AAV2-GFP were injected into the left (KO) and right (control) sides of the brain, respectively. After $3-4$ weeks, GFP⁺ cells in the aVMHvl from both KO and control sides were recorded in current-clamp mode. All cells were recorded for $3-5$ min after break-in until the RMP was stable and then perfused with TGOT (250 nM) for 10 min. Cells that had increased RMP for >4 mV after 10 min TGOT perfusion were considered OXTR⁺.

In PVN^{OXTR} and SOR^{OXTR} optogenetic activation experiments, we injected $120-140$ nl AAV2-Efla-DIO-ChR2-EYFP into either the PVN or the SOR of *Oxtr^{Cre}* male mice. After 4 weeks of virus incubation, aVMHvl cells were recorded in current-clamp mode. After the cell membrane potential was stabilized, we delivered 1 ms, 20 Hz blue light pulses (pE-300white; CoolLED) for 5 min to activate PVN^{OXTR} or SOR^{OXTR} processes. If the cell did not show a significant increase in RMP (>4 mV) after light delivery, we then perfused TGOT (250 nM) in a bath for 10 min to functionally determine OXTR expression. The cells were separated into three categories based on their response to light activation and TGOT perfusion: Light⁺, Light TGOT⁺ and Light TOGT⁻. Light⁻ and Light TGOT⁻

cells were considered as putative OXTR-expressing cells. Light TGOT⁻ cells were classified as OXTR⁻. To confirm that SOR^{OXTR} optogenetic activation induces RMP changes of aVMHvl cells through activation of OXTR, we pre-incubated brain sections in ACSF with 1 μM L-368,899 hydrochloride (Tocris, 2641) and performed the same SOR^{OXTR} stimulation protocol.

To examine the effect of oxytocin on synaptic transmission, we injected 100 nl AAV9 hSyn-ChrimsonR-tdTomato into the PA of male mice expressing OXTR^{ZsGreen} cells. After 4 weeks of virus incubation, we obtained brain slices and performed current-clamp recording of aVMHvl^{OXTR} cells. aVMHvl^{OXTR} cells are determined based on their ZsGreen expression. Before recording, the expression of ChrimsonR-tdTomato in the PA was examined using an Olympus $\times 40$ water-immersion objective with a TXRED filter. The recording only proceeded if ChrimsonR-tdTomato was correctly and robustly expressed in the PA. To probe the excitatory synaptic responses of recorded aVMHvl^{OXTR} cells, we injected a small positive or negative current to keep the cell membrane potential around -70 mV and delivered a 1 ms 605 -nm full-field light pulse every 10 s (0.1 Hz) (pE-300white; CoolLED). After 5 min of probing, we then delivered 3 trains of 20 Hz, 5 ms light pulses with 25 s per train and 5 s in between. During light pulse train delivery, the cells were not injected with any positive or negative current. After light train delivery, we again injected negative or positive current to maintain the membrane potential around -70 mV and probed the light-evoked EPSPs for 5 or 10 min, and then bath-perfused 250 nM TGOT. After 10 min of TGOT perfusion, we delivered a second set of light pulse trains and probed the light-evoked EPSPs for 5 or 10 min. In a second protocol, we probed the light-evoked EPSPs before and after perfusing TGOT (250 nM) for 10 min, and then delivered 3 trains of 25 s, 20 Hz, 5 ms light pulses, with 5 s between trains. After light stimulation, light-evoked EPSPs were probed for 5 min, and then TGOT was washed out with ACSF while the light-evoked EPSPs were continuously probed for 10 min.

Immunohistochemistry

For Fos and oxytocin staining, animals were deeply anaesthetized with a mixture of ketamine (100 mg kg^{-1}) and xylazine (10 mg kg^{-1}) and transcardially perfused with 10 ml of PBS followed by 10 ml of 4% paraformaldehyde in PBS. After perfusion, brains were collected, soaked in 30% sucrose in PBS for 24 h at 4 $^\circ\text{C}$ and then embedded with OCT compound (Fisher Healthcare). Next, 40 - μm -thick coronal brain sections were cut using a cryostat (Leica). Brain sections were washed with PBST (0.3% Triton X-100 in PBS, 10 min), blocked in 5% normal donkey serum (NDS, Jackson Immuno Research) in PBST for 30 min at room temperature and then incubated with primary antibodies in 5% NDS in PBST overnight at room temperature (about 18 h). Sections were then washed with PBST (3×10 min), incubated with secondary antibodies in 5% NDS in PBST for 4 h at room temperature, washed with PBST (2×10 min) and DAPI-mixed ($1:10,000$, Thermo Scientific) PBS solution (1×20 min). Slides were coverslipped using a mounting medium (Fluoromount, Diagnostic BioSystems) after drying.

The following primary antibodies were used: rabbit anti-oxytocin ($1:5,000$, Immunostar, 20068, lot 1607001); guinea pig anti-Fos ($1:2,000$, Synaptic Systems, 226-005, lot 2-10, 2-13); rabbit anti-vasopressin ($1:5,000$, Immunostar, 20069, lot 1004001); rabbit anti-ESR1 ($1:2,000$, Invitrogen, PA1-309, lot YA352477); and anti-GFP ($1:2,000$, Abcam, ab13970, lot GR3190550-2). The following secondary antibodies were used: Cy3-AffiniPure donkey anti-rabbit IgG ($1:500$, Jackson Immuno Research, 711-165-152, lot 124528); Cy5-AffiniPure donkey anti-rabbit IgG ($1:250$, Jackson Immuno Research, 711-175-152, lot 150312); Alexa Fluor 488-conjugated goat anti-guinea pig IgG ($1:500$, Invitrogen, A11073, lot 2160428); or Alexa Fluor 488-conjugated donkey anti-chicken IgY (IgG) ($1:500$, Jackson Immuno Research, 703-545-155, lot 116967). The $\times 10$ or $\times 20$ fluorescent images were acquired to determine the overall expression pattern in each brain region using

an Olympus VS120 Automated slide scanner and its specific software OlyVIA. The $\times 20$ fluorescent confocal images were acquired using a Zeiss LSM 800 and its specific software (Zeiss, ZEN 2.3 system) for cell counting.

In situ hybridization

To prepare the sections for in situ hybridization (ISH), 10–12-week-old C57 male mice were anaesthetized with a mixture of ketamine (100 mg kg⁻¹) and xylazine (10 mg kg⁻¹) and transcidentally perfused with 10 ml of DEPC-treated PBS (DEPC-PBS), followed by 10 ml of 4% paraformaldehyde in DEPC-PBS (from paraformaldehyde 32% solution, Electron Microscopy Sciences). After perfusion, brains were collected, soaked in 30% of sucrose in DEPC-PBS for 24 h at 4 °C and then embedded with OCT compound (Fisher Healthcare). Next, 30- μ m-thick coronal brain sections were cut using a cryostat (model CM3050S, Leica). The sections were placed on MAS-coated glass slides (MAS-03, Matsunami) and stored at -80 °C before use.

To synthesize the cDNA for the *Oxt* and *Oxtr* probes, their original templates were from mouse brain cDNA (cDNA-mmu-01, Biosettia). cDNA was amplified by PCR methods using the following oligo-DNA primers, and the products were purified with micro spin columns (MACHERY-NAGEL, 74060910). Each reverse primer also possesses T3 sequence for transcription. OXT1-forward: TGGCTTACTGGCTCTGACCT; OXT1-reverse: AATTAACCCTCACTAAAGGGAGGAAGCGCGTAAAGGTA T; OXTR1-forward: GGCGTCTGTGTCTCATAC; OXTR1-reverse: AATTAACCCTCACTAAAGGGCTCCACATCTGCACGAAGAA; OXTR 2-forward: TTCATCATGGCCATGCTCTT; OXTR2-reverse: AATTAACCCTCACTAAAGGGGGTGGCTCTCATTTCTTT; OXTR3-forward: GCTGGAGATAGGAGGCAGTG; OXTR3-reverse: AATTAACCCTCACTAAAGGGCTGTGCTACTACCAGACG.

The *Oxt* probes were approximately 400 bp in length, and the *Oxtr* probes were approximately 750 bp to 1,000 bp. ISH probes were prepared by in vitro transcription with DIG RNA labelling mix (Roche Applied Science, 11277073910) or Fluorescein RNA labelling mix (Roche Applied Science, 11685619910) and T3 polymerase (Roche Applied Science, 11031163001). The *Oxt* probe was labelled with fluorescein, and *Oxtr* probes were labelled with DIG.

Brain sections, including the VMHvl, underwent ISH at 56 °C overnight. After a series of post-hybridization washing and blocking, fluorescein-positive cells were visualized with anti-FITC antibody (PerkinElmer, NEF710001EA, 1:200 in blocking buffer) followed by TSA biotin amplification reagent (PerkinElmer, NEF749A001KT, 1:100 in 1 \times plus amplification diluent) and streptavidin Alexa488 (Invitrogen, S11223, 1:250 in blocking buffer). DIG⁺ cells were visualized using an anti-DIG antibody (Roche Applied Science, 11207733910, 1:250 in blocking buffer) and TSA Cy3 amplification reagent (PerkinElmer, NEL744001KT, 1:100 in 1 \times plus amplification diluent). Sections were counterstained with 4',6-diamino-2-phenylindole dihydrochloride (DAPI, 1:10,000 in PBS, Thermo Scientific) and mounted with a cover glass using Fluoromount (Diagnostic BioSystems, K024). The $\times 20$ fluorescent images were acquired using a slide scanner (Olympus VS120). The $\times 20$ fluorescent confocal images were acquired using a Zeiss LSM 800 (Zeiss, ZEN 2.3 system).

Quantification and statistical analysis

No statistical methods were used to predetermine sample sizes, but our sample sizes were similar to those reported in previous publications^{31,55–58}. All experiments were conducted using one to two groups of animals. The results were reproducible across groups and combined for final analysis. Statistical analyses were performed using Matlab (v.2019b, 2021b or 2023b, Mathworks) and Prism9 and Prism10 (GraphPad Software, RRID: SCR_002798). All statistical analyses were two-tailed. Parametric tests, including one sample *t*-test, paired *t*-test, unpaired *t*-test and one-way ANOVA, were used if distributions passed Kolmogorov–Smirnov (for sample sizes ≥ 5) or Shapiro–Wilk tests

(for sample sizes < 5) for normality. Otherwise, nonparametric tests, including one-sample Wilcoxon test, Wilcoxon matched-pairs signed-rank test, Mann–Whitney test and Kruskal–Wallis test were used. For comparisons across multiple groups and variables, two-way ANOVA was used without formally testing the normality of data distribution. Following two-way ANOVA, differences between groups were assessed using Sidak's multiple comparison test or Tukey's multiple comparisons test based on the recommendations in Prism. When more than two one-sample *t*-tests were performed, the *P* values were adjusted using Holm–Šidák correction. **P* < 0.05, ***P* < 0.01, ****P* < 0.001 and *****P* < 0.0001. If not indicated, *P* > 0.05. Error bars represent \pm s.e.m. For detailed statistical results, including exact *P* values, *F* values, *t* values, degrees of freedom and cohort number, see Supplementary Table 1.

Reporting summary

Further information on research design is available in the Nature Portfolio Reporting Summary linked to this article.

Data availability

Raw values associated with each figure panel can be found in the source data files. Fibre photometry recording data, behaviour annotations, tracking and raw representative histology images can be downloaded from Zenodo (<https://doi.org/10.5281/zenodo.8417540>). Behaviour videos and additional histology images are available from the corresponding authors upon reasonable request. They are not deposited to a public database owing to their large size and size limitation of online depositories. Illustrations of the coronal brain sections in Figs. 1a, 2a,g,m, 3a,h, 4j, 5a and 6a,h,n and Extended Data Figs. 4a, 5a, 6a, 9a,k, 10a, 12a, 14a and 15a were adapted from the Allen Brain Reference Atlas (<https://atlas.brain-map.org>). Source data are provided with this paper.

Code availability

Matlab codes used in this study can be downloaded from Zenodo (<https://doi.org/10.5281/zenodo.8417540>).

- Daigle, T. L. et al. A suite of transgenic driver and reporter mouse lines with enhanced brain-cell-type targeting and functionality. *Cell* **174**, 465–480.e22 (2018).
- Vong, L. et al. Leptin action on GABAergic neurons prevents obesity and reduces inhibitory tone to POMC neurons. *Neuron* **71**, 142–154 (2011).
- Lee, H. J., Caldwell, H. K., Macbeth, A. H., Tolu, S. G. & Young, W. S. 3rd A conditional knockout mouse line of the oxytocin receptor. *Endocrinology* **149**, 3256–3263 (2008).
- Madisen, L. et al. A robust and high-throughput Cre reporting and characterization system for the whole mouse brain. *Nat. Neurosci.* **13**, 133–140 (2010).
- Franklin, K. B. J. & Paxinos, G. *Paxinos and Franklin's The Mouse Brain in Stereotaxic Coordinates*. 4th edn (Academic Press, 2013).
- Osborne, J. E. & Dudman, J. T. RIVETS: a mechanical system for in vivo and in vitro electrophysiology and imaging. *PLoS ONE* **9**, e89007 (2014).
- Mathis, A. et al. DeepLabCut: markerless pose estimation of user-defined body parts with deep learning. *Nat. Neurosci.* **21**, 1281–1289 (2018).
- Yin, L. et al. VMHvl^{Cre} cells dynamically control female sexual behaviors over the reproductive cycle. *Neuron* **110**, 3000–3017.e8 (2022).
- Wong, L. C. et al. Effective modulation of male aggression through lateral septum to medial hypothalamus projection. *Curr. Biol.* **26**, 593–604 (2016).
- Falkner, A. L. et al. Hierarchical representations of aggression in a hypothalamic–midbrain circuit. *Neuron* **106**, 637–648.e6 (2020).
- Fang, Y. Y., Yamaguchi, T., Song, S. C., Tritsch, N. X. & Lin, D. A hypothalamic midbrain pathway essential for driving maternal behaviors. *Neuron* **98**, 192–207.e10 (2018).

Acknowledgements We thank R. C. Froemke, G. Buzsáki and all members from the Lin Laboratory for discussions and comments; R. Kenmochi for cartoon illustrations; and M. Karadas for helping set up the shock–odour pairing chamber. This research was supported by NIH grants R01MH101377 (D.L.), R01MH124927 (D.L.), 1R01HD092596 (D.L.), U19NS107616 (D.L., A.C.M. and R.W.T.) and 1R01NS125271 (R.W.T.), the Uehara Memorial Foundation (T.O.), a JSPS Overseas Research Fellowship (T.O.), an Osamu Hayaishi Memorial Scholarship (T.O.) and the Ichiro Kanehara Foundation (T.O.).

Author contributions D.L. conceived the project, designed experiments, analysed data, prepared figures, wrote the paper and supervised the project. T.O. co-designed experiments, performed all histology, functional manipulation and in vivo recording experiments in males, analysed data, prepared figures and co-wrote the paper. R.Y. performed all slice recording

Article

experiments, analysed data and prepared relevant figures and texts. Y.J. performed all functional manipulation and in vivo recording experiments in females and did most of the animal tracking. D.W. performed preliminary slice recordings. R.T. assisted with behaviour testing and analyses. B.D. and A.C.M. assisted with animal tracking. X.W. assisted with initial Otr KO characterization. G.Z., C.X.W. and J.-J.L. assisted with behaviour annotation. R.W.T. supervised X.W., G.Z., C.X.W. and J.-J.L. and provided critical feedback to the project.

Competing interests The authors declare no competing interests.

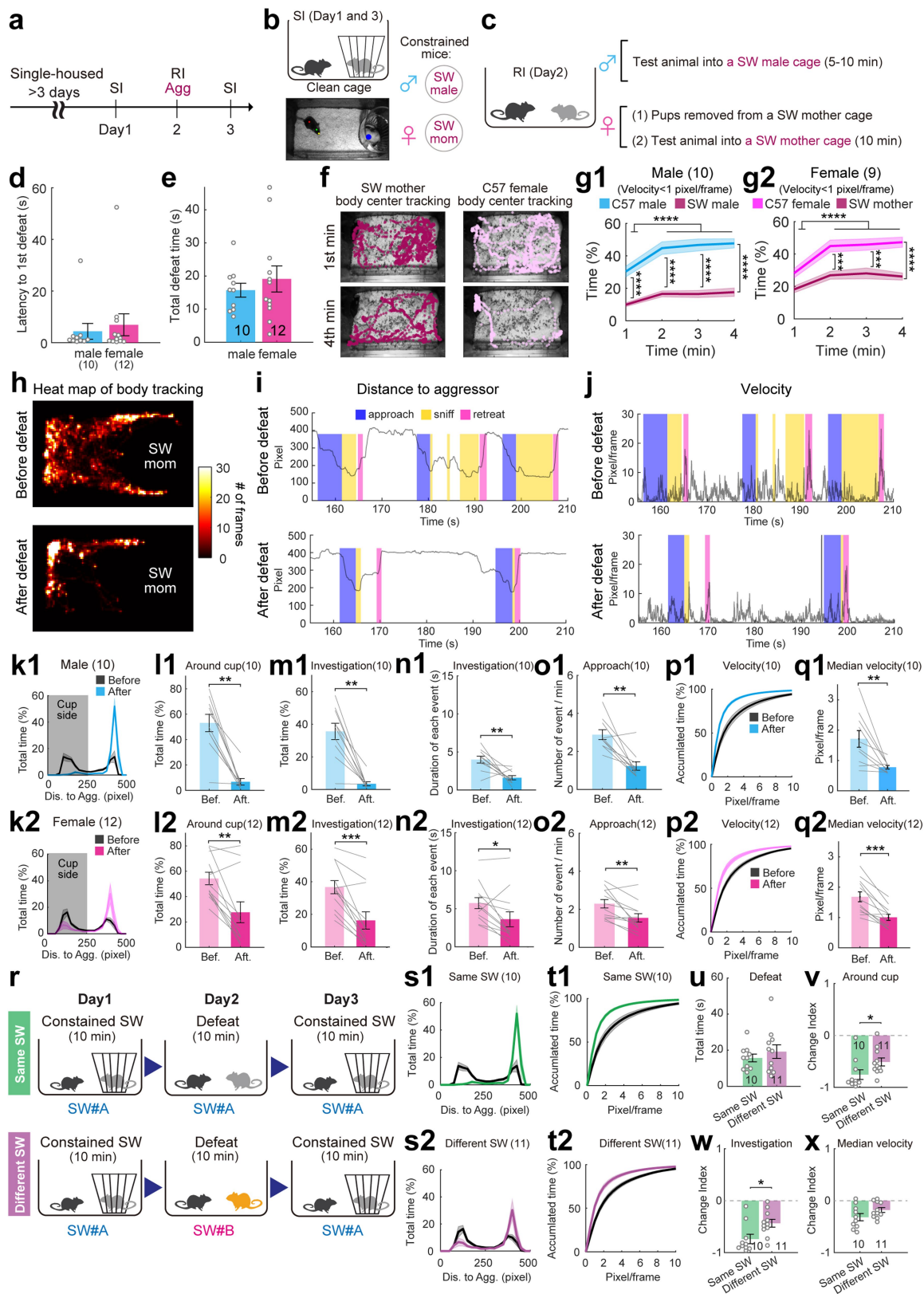
Additional information

Supplementary information The online version contains supplementary material available at <https://doi.org/10.1038/s41586-023-06958-w>.

Correspondence and requests for materials should be addressed to Takuya Osakada or Dayu Lin.

Peer review information *Nature* thanks Steven Siegelbaum, Scott Russo and the other, anonymous, reviewer(s) for their contribution to the peer review of this work. Peer reviewer reports are available.

Reprints and permissions information is available at <http://www.nature.com/reprints>.



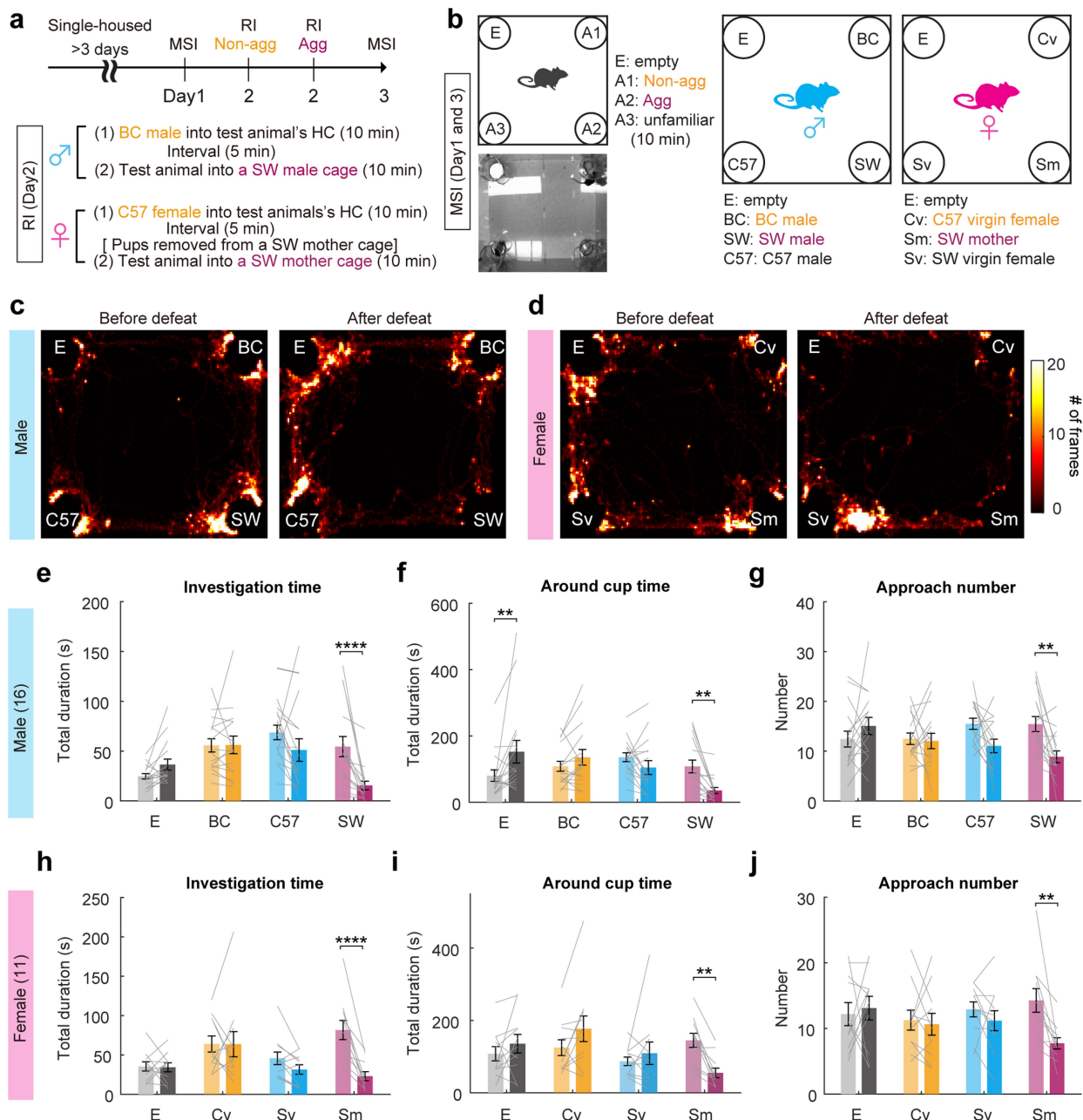
Extended Data Fig. 1 | See next page for caption.

Article

Extended Data Fig. 1 | One-day 10-min social defeat is sufficient to induce social avoidance of winner-like conspecifics. **a.** Experimental timeline.

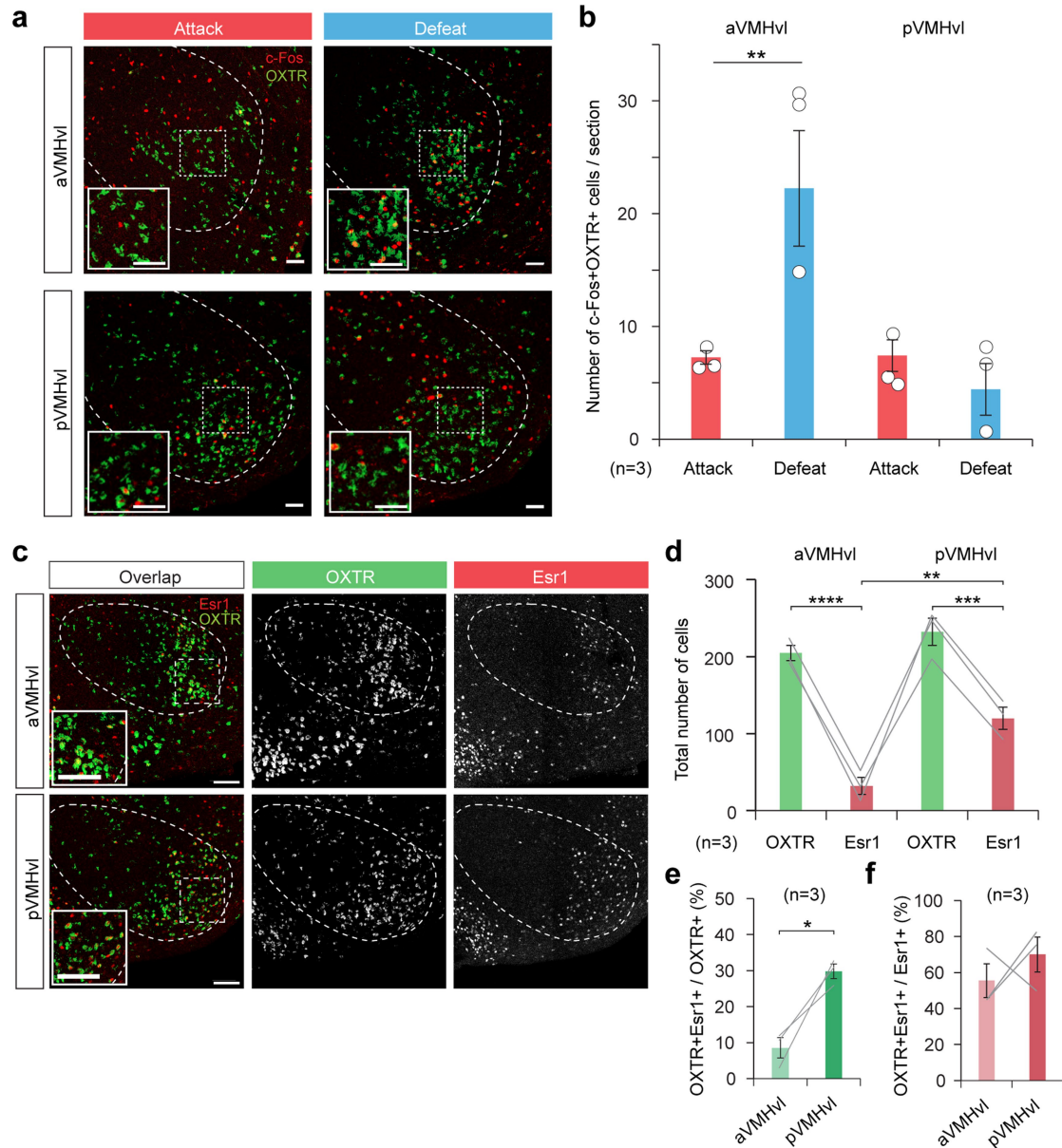
b. Cartoon illustration of the social interaction (SI) test (top) and a video frame overlaid with DLC tracking results (bottom). Red dot: body center; green dot: head center; yellow dot: nose point; blue dot: cup center. **c.** The resident-intruder (RI) test illustration and procedure. **d.** The latency to first defeat in male and female mice. **e.** The total defeat duration during the 10-min RI test in male and female mice. **f.** Video frames from SI tests overlaid with the movement trajectories of the SW mother aggressor (maroon) and C57 test female (pink) during the 1st (top) and 4th (bottom) minute of the test. **g.** The percentage of time the male (**g1**) and female (**g2**) test mice and the aggressors spent on staying stationary (velocity <1 pixel/frame) over the course of the RI tests. **h.** Heatmaps showing the body center location of a representative female mouse during pre-defeat and post-defeat SI tests. **i-j.** Representative traces showing the distance between the test animal body center to the cup center (**i**) and the movement velocity of the test animal (**j**) in pre- and post-defeat SI tests. Color shades indicate manually annotated behaviors. **k.** Distribution of the distance between the test animal's body center and cup center during the pre-defeat (gray) and post-defeat (color) SI tests for males (**k1**) and females (**k2**). Shades shown in gray represent the distance range considered as "around cup". **l.** The percentage of total time the male (**l1**) and female (**l2**) test mice spent around the aggressor cup (distance <250 pixels) during SI tests. **m.** The percentage of total time the male (**m1**) and female (**m2**) test mice spent investigating the aggressor cup during SI tests. **n.** The average duration of each investigation episode of the male (**n1**) and female (**n2**) test mice during SI tests. **o.** The cup approach frequency of the male (**o1**) and female (**o2**) test mice during SI tests. **p.** Accumulative plots showing the distribution of movement velocity when the male (**p1**) and female (**p2**) test mice are far away (distance > 300 pixels)

from the constrained aggressor during the pre-defeat (gray) and post-defeat (color) SI tests. **q.** The median velocity when the male (**q1**) and female (**q2**) test mice are far away (distance > 300 pixels) from the constrained aggressor during SI tests. **r.** Experimental design to test whether social avoidance after defeat is specific to the same aggressor. The aggressor in the RI and SI tests is the same in the AAA paradigm. Different SW aggressors are used for RI and SI tests in the ABA paradigm. **s.** Distribution of the distance between the test animal's body center and constrained aggressor during the pre- and post-defeat SI tests for AAA (**s1**) and ABA (**s2**) paradigms. **t.** Accumulative plots showing the distribution of movement velocity when the test mice are far away (distance > 300 pixels) from the constrained aggressor during the pre-defeat and post-defeat SI tests in AAA (**t1**) and ABA (**t2**) paradigms. **u.** The total defeat time during the RI tests in AAA and ABA paradigms is comparable. **v.** The change index of time spent around the constrained aggressor during the SI tests in AAA and ABA paradigms. The change index is defined as $(P_{\text{post}} - P_{\text{pre}}) / (P_{\text{post}} + P_{\text{pre}})$. P_{pre} and P_{post} are the behavior parameter values during the pre-defeat and post-defeat SI tests, respectively. **w.** The change index of investigation time of the constrained aggressor during the SI tests in AAA and ABA paradigms. **x.** The change index of the median movement velocity when the test animal is far away from the aggressor in the SI tests in AAA and ABA paradigms. Plots with shades and error bars represent mean \pm s.e.m. Circles and lines represent individual animals. Numbers on the plots indicate the number of animals. Mann-Whitney test (**d, v, w**), unpaired t-test (**e, u, x**), two-way repeated measure ANOVA with Sidak's multiple comparisons test (**g**), Wilcoxon matched-pairs signed rank test (**l1, m1, o1, l2, m2, and n2**), and paired t-test (**n1, q1, o2, and q2**). All statistical tests are two-tailed. * $p < 0.05$, ** $p < 0.01$, *** $p < 0.001$, and **** $p < 0.0001$. See Supplementary Table 1 for detailed statistics.



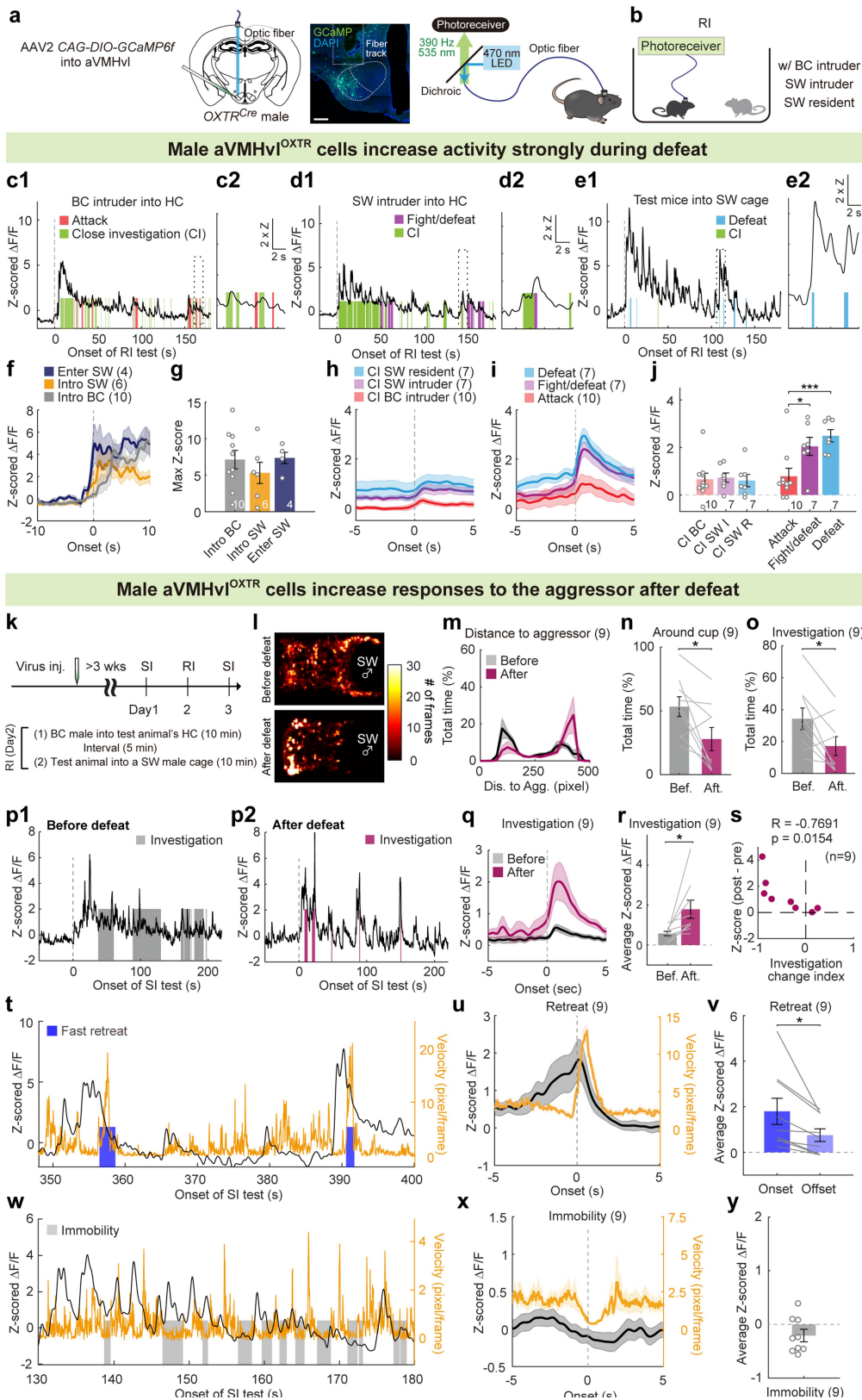
Extended Data Fig. 2 | Defeated animals do not avoid conspecifics with genetic backgrounds different from the aggressor. a. Experimental timeline. **b.** The left shows a cartoon illustration and a snapshot of the multi-animal social interaction (MSI) test. The right shows the stimulus animals used for male and female MSI tests. **c-d.** Heatmaps showing the body center location of a representative male (**c**) and a female (**d**) mouse in pre- and post-defeat MSI tests. **e-f.** Total time male test mice spent investigating (**e**) and around (**f**) each constrained animal during pre- and post-defeat MSI tests.

g. The number of approaches towards each cup during pre- and post-defeat MSI tests. **h-j.** Data from female mice. Plots follow the convention of **e-g**. Plots with error bars represent mean \pm s.e.m. Lines represent individual animals. Numbers on the plots indicate the number of animals. (**e-j**) Two-way repeated measure ANOVA with Sidak's multiple comparisons test. All statistical tests are two-tailed. ** $p < 0.01$, and **** $p < 0.0001$. See Supplementary Table 1 for detailed statistics.



Extended Data Fig. 3 | The relationship between OXTR and defeat-induced c-Fos and Esr1 in the VMHvl. **a.** Representative histological images showing c-Fos (red) and OXTR (OXTR^{ZsGreen}, green) expression in the aVMHvl (Bregma: -1.50 mm) and pVMHvl (Bregma: -1.82 mm) in OXTR^{Cre}:Ai6 (OXTR^{ZsGreen}) male mice after attack or social defeat. Insets showing enlarged views of the boxed areas. Dashed lines mark the boundary of the aVMH. Scale bars: 50 μ m. **b.** The number of c-Fos and OXTR double-positive cells after attack and defeat in the aVMHvl (Bregma: -1.34 to -1.50 mm) and pVMHvl (Bregma: -1.66 to -1.82 mm). **c.** Representative histological images showing OXTR (green) and Esr1 (red) expression in the aVMHvl (Bregma: -1.50 mm) and pVMHvl (Bregma: -1.82 mm) in OXTR^{Cre}:Ai6 (OXTR^{ZsGreen}) male mice. Insets showing enlarged views of the

boxed areas. Dashed lines mark the boundary of the VMH. Scale bars: 100 μ m. **d.** Number of OXTR and Esr1 positive cells in the aVMHvl and pVMHvl. **e.** The percentage of Esr1 and OXTR double-positive cells in OXTR positive cells in the aVMHvl and pVMHvl. **f.** The percentage of Esr1 and OXTR double-positive cells in Esr1 positive cells in the aVMHvl and pVMHvl. Plots with error bars represent mean \pm s.e.m. (**b**, **d**, **e** and **f**) n = three 40- μ m sections were counted per region per animal, 3 animals per group. Circles in **b** and lines in **d-f** represent individual animals. (**b** and **d**) Two-way repeated measure ANOVA with Sidak's multiple comparisons test. (**e**) Paired t-test. (**f**) Mann-Whitney test. All statistical tests are two-tailed. *p < 0.05, **p < 0.01, ***p < 0.001 and ****p < 0.0001. See Supplementary Table 1 for detailed statistics.



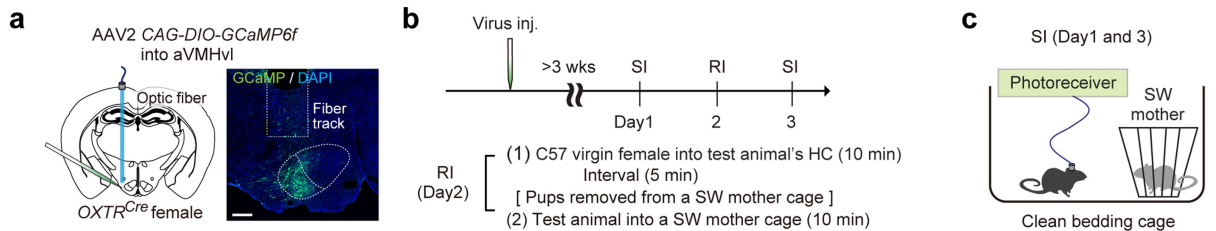
Extended Data Fig. 4 | See next page for caption.

Article

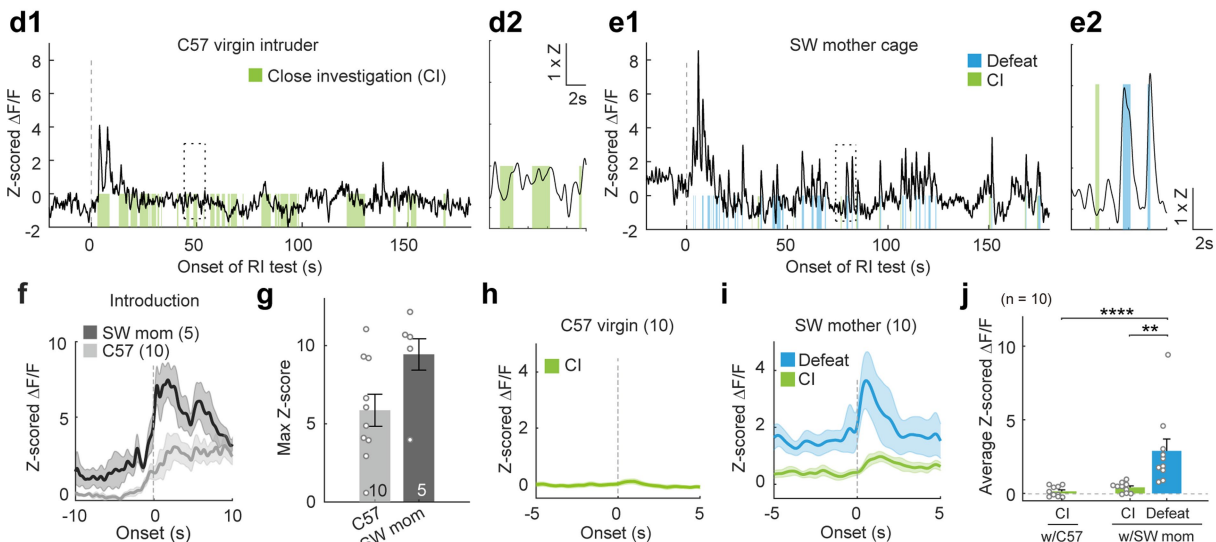
Extended Data Fig. 4 | aVMHvl^{OxTR} cells increase responses to the aggressor after defeat in male mice.

a. Schematics of virus injection and a representative histology image. Dashed line marks the aVMH. Scale bar: 200 μ m. Brain illustration is based on a reference atlas from <https://atlas.brain-map.org/>. **b.** Cartoon illustration of the RI test. **c-e.** Representative Z-scored GCaMP6f traces during RI tests with a BC male intruder (**c**), a SW male intruder (**d**), or resident SW (**e**). **c2, d2 and e2** show the enlarged boxed areas. **f.** Post-event histograms (PETHs) of GCaMP6f signal aligned to initial opponent encounters, only including sessions without defeat or attack during the first 10 s. **g.** Peak GCaMP6f response within the first 10 s of RI tests. **h-i.** PETHs of GCaMP6f signals aligned to close investigation (**h**) and agonistic interactions (**i**). **j.** Averaged Z-scored responses during various social behaviors. **k.** Experimental timeline. **l.** Heatmaps showing the body center location of a representative test male during pre- and post-defeat SI tests. **m.** Distribution of the distance between the test animal's body center and cup center during pre- and post-defeat SI tests. **n.** The percentage of total time test mice spent around the aggressor cup during pre- and post-defeat SI tests. **o.** The percentage of total time the test mice spent investigating the constrained aggressor during pre- and post-defeat SI tests. **p.** Representative Z-scored GCaMP6f traces from a recording male mouse during pre-defeat (**p1**) and post-defeat (**p2**) SI tests. Shades mark investigation events. **q.** PETHs of Z-scored GCaMP6f signals aligned to the onset of investigating aggressor during pre- and post-defeat SI tests. **r.** Average

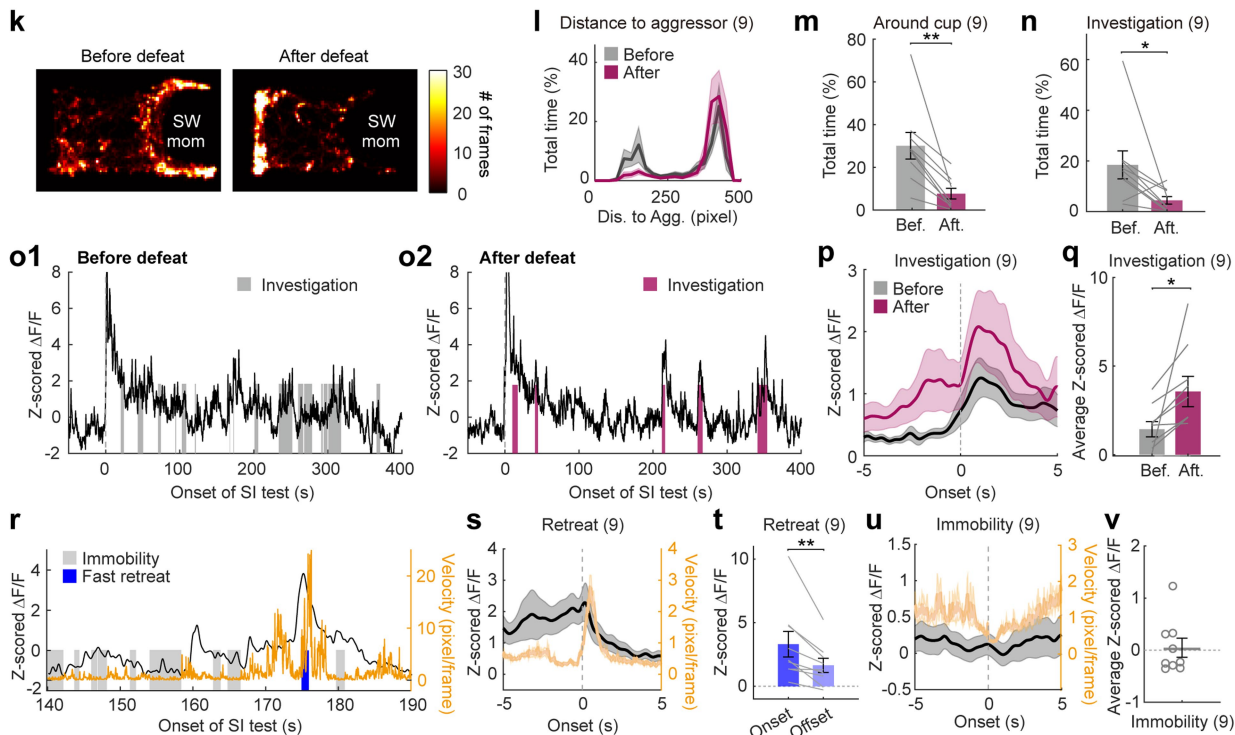
Z-scored $\Delta F/F$ of aVMHvl^{OxTR} cells during investigating aggressor in pre- and post-defeat SI tests. **s.** Scatter plot showing the correlation between investigation time change index and change in Z-scored GCaMP response to the aggressor during post-defeat SI tests from the pre-defeat level. **t.** Representative Z-scored GCaMP trace (black) overlaid with the velocity trace (orange) during the post-defeat SI test. Blue indicates the period when the test animal quickly retreated from the aggressor. **u.** PETHs of Z-scored GCaMP signal (black) and velocity (orange) aligned to the retreat onset. **v.** The retreat onset GCaMP signal is significantly higher than the retreat offset signal. **w.** Representative Z-scored GCaMP trace (black) overlaid with the velocity trace (orange) during the post-defeat SI test. Gray indicates when the test animal stayed immobile and far from the aggressor. **x.** PETHs of Z-scored GCaMP signal (black) and velocity (orange) aligned to immobility onset. Immobility trials are defined as velocity <1 pixel/frame lasting for > 0.5 s. **y.** The mean GCaMP signal during immobility. Plots with shades and error bars represent mean \pm s.e.m. Lines and circles represent individual animals. Numbers on the plots indicate the number of animals. One-way ANOVA with Tukey's multiple comparisons (**g**), Two-way repeated-measure ANOVA with Sidak's multiple comparisons (**j**), Wilcoxon matched-pairs signed rank test (**n** and **o**), paired t-test (**r, v**), one-sample t-test (**y**), and Pearson cross-correlation (**s**). All statistical tests are two-tailed. * $p < 0.05$. See Supplementary Table 1 for detailed statistics.



Female aVMHvl^{OXTR} cells are activated during social defeat



Female aVMHvl^{OXTR} cells increase responses to the aggressor after defeat

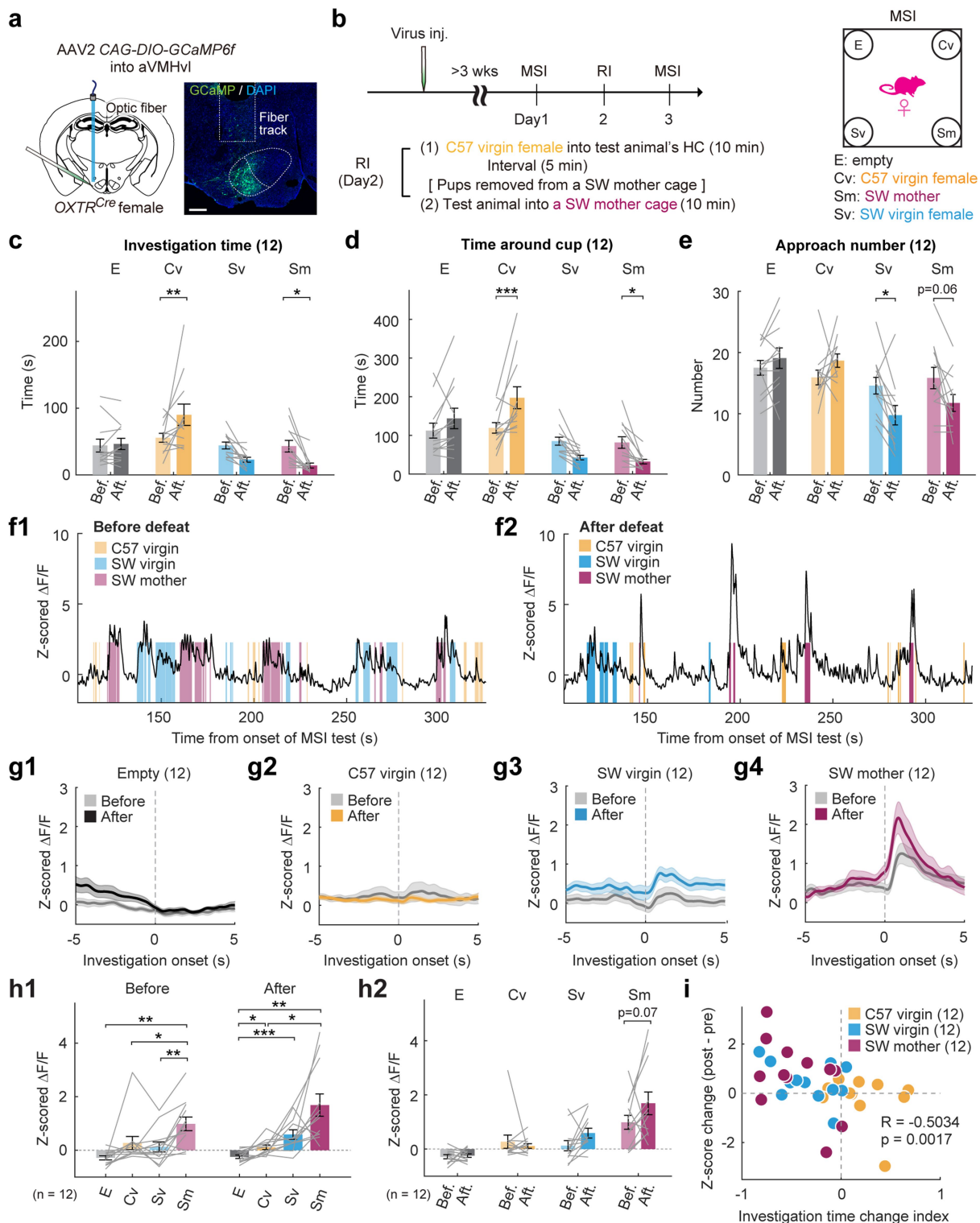


Extended Data Fig. 5 | See next page for caption.

Article

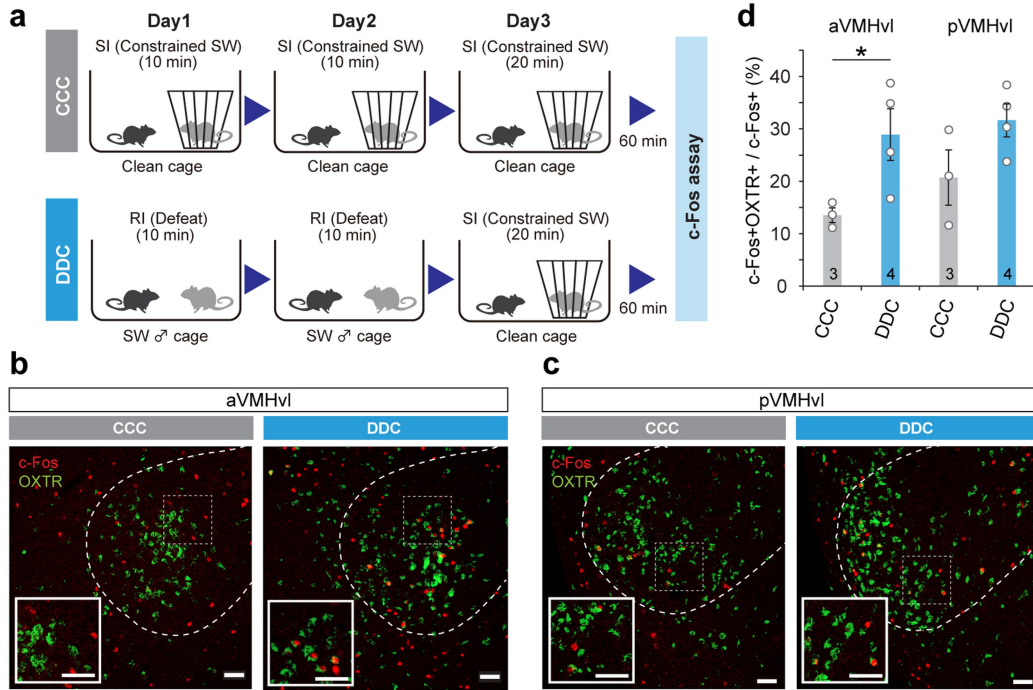
Extended Data Fig. 5 | Female aVMHv^{OXTR} cells increase responses to the aggressor after defeat. **a.** Schematics of virus injection and a representative histology image. Dashed lines mark the boundary of the aVMH. Scale bar: 200 μm . Brain illustration is based on a reference atlas from <https://atlas.brain-map.org/>. **b.** Experimental timeline. **c.** Cartoon illustration of the SI test. **d-e.** Representative Z-scored GCaMP6f traces from a recording female mouse during RI tests with a non-aggressive naïve C57 (**d**) and an aggressive lactating SW (**e**) female mouse. **d2** and **e2** show the zoomed-in view of the boxed area in **d1** and **e1**, respectively. **f.** PETHs of Z-scored GCaMP6f signals aligned to C57 intruder introduction and introduction of the test mouse to the SW lactating female's cage. Only sessions with no defeat during the first 10 s are included. **g.** The peak GCaMP6f response within the first 10 s of intruder/resident encounter. Only sessions with no defeat or attack during the first 10 s are included. **h-i.** PETHs of Z-scored GCaMP6f signals aligned to the onset of investigating C57 intruders (**h**), and investigating and being defeated by SW residents (**i**). **j.** Average Z-scored $\Delta F/F$ of aVMHv^{OXTR} cells during various social behaviors in the RI tests. **k.** Heatmaps showing the body center location of a representative test female during pre-defeat and post-defeat SI tests. **l.** Distribution of the distance between the test animal's body center and cup center during pre- and post-defeat SI tests. **m.** The percentage of the total time the test mice spent around the aggressor cup during pre- and post-defeat SI tests. **n.** The percentage of the total time the test mice spent investigating the

aggressor cup during pre- and post-defeat SI tests. **o.** Representative Z-scored GCaMP traces from a recording female during pre-defeat (**o1**) and post-defeat (**o2**) SI tests. Shades represent investigation events. **p.** PETHs of Z-scored GCaMP signals aligned to the onset of investigating the constrained aggressor during pre- and post-defeat SI tests. **q.** Average Z-scored $\Delta F/F$ of aVMHv^{OXTR} cells during investigating aggressor in pre- and post-defeat SI tests. **r.** Representative Z-scored GCaMP trace (black) overlaid with the velocity trace (orange) during the post-defeat SI test. Gray indicates the periods when the test animal stayed immobile and far from the aggressor, and blue indicates a fast retreat event. **s.** PETHs of Z-scored GCaMP signal (black) and velocity (orange) aligned to the retreat onset. **t.** The GCaMP signal at the retreat onset is significantly higher than the signal at the retreat offset. **u.** PETHs of Z-scored GCaMP signal (black) and velocity (orange) aligned to immobility onset. Immobility trials are defined as velocity $< 1 \text{ pixel/frame}$ lasting $> 0.5 \text{ s}$. **v.** The mean GCaMP signal during immobility. Plots with shades and error bars represent mean \pm s.e.m. Circles and lines represent individual animals. Numbers on the plots indicate the number of animals. Kruskal-Wallis test with Dunn's multiple comparisons test (**j**), Wilcoxon matched-pairs signed rank test (**n**), unpaired t-test (**g**), paired t-test (**m, q, t**), and one-sample t-test (**v**). All statistical tests are two-tailed. * $p < 0.05$, ** $p < 0.01$, and **** $p < 0.0001$. See Supplementary Table 1 for detailed statistics.



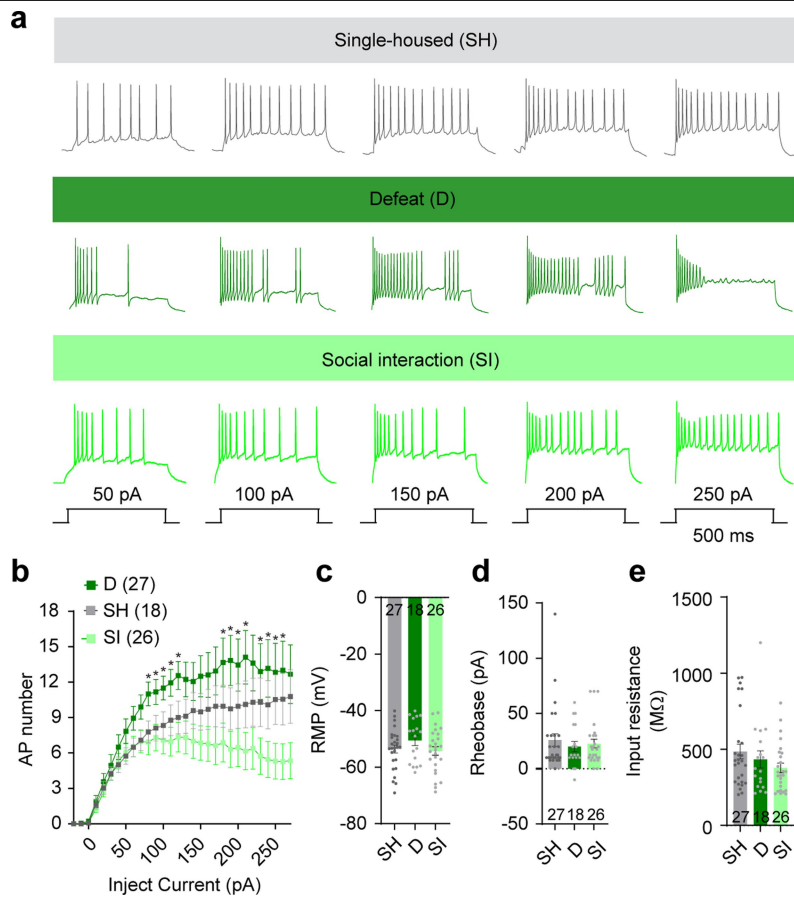
Extended Data Fig. 6 | aVMHvl^{OxTR} cells increase response to the aggressor after defeat in female mice. a. Virus injection site and a representative histology image. Scale bar: 200 μ m. Brain illustration is based on a reference atlas from <https://atlas.brain-map.org/>. **b.** Experimental timeline and cartoon illustration of the behavior assay. **c-e.** Summary plots showing the investigation time (c), time around each cup (d), and number of approach (e) during pre- and post-defeat MSI tests. E: Empty; Cv: C57 virgin female; Sv: unfamiliar SW virgin female; Sm: SW lactating female aggressor. **f.** Representative raw traces showing the Z-scored GCaMP6 signal in the pre- (**f1**) and post-defeat (**f2**) MSI tests. Shades represent investigation episodes. Empty cup investigation episodes are not marked. **g.** PETHs aligned to the investigation onset of

different stimuli in pre- and post-defeat MSI tests. **h.** The mean Z-scored GCaMP6 signal during investigation of different targets in pre- and post-defeat MSI tests. **h1** and **h2** are the same data shown in different arrangements. **i.** Scatter plots showing the correlation between change index in investigation time and change in Z-scored GCaMP responses to various social targets after defeat from the pre-defeat level. Plots with error bars and shades represent mean \pm s.e.m. Circles and lines represent individual animals. Numbers on the plots indicate the number of animals. (c, d, e, h) Two-way repeated measure ANOVA with Sidak's multiple comparisons test. (i) Pearson cross-correlation. All statistical tests are two-tailed. * $p < 0.05$, ** $p < 0.01$, and *** $p < 0.001$. See Supplementary Table 1 for detailed statistics.



Extended Data Fig. 7 | Defeat experience enhances aggressor cue-induced c-Fos in aVMHvl^{OXTR} cells during subsequent encounters. **a.** Experimental design. CCC: SI (Constrained SW)-SI (Constrained SW)-SI (Constrained SW) (top); DDC: RI (Defeat)-RI (Defeat)-SI (Constrained SW) (bottom). **b** and **c.** Representative images showing the expression of OXTR (OXTR^{ZsGreen}, green) and c-Fos (red) in the aVMHvl (**b**) and pVMHvl (**c**) in animals experienced CCC or DDC. Insets showing enlarged views of the boxed areas in the aVMHvl and

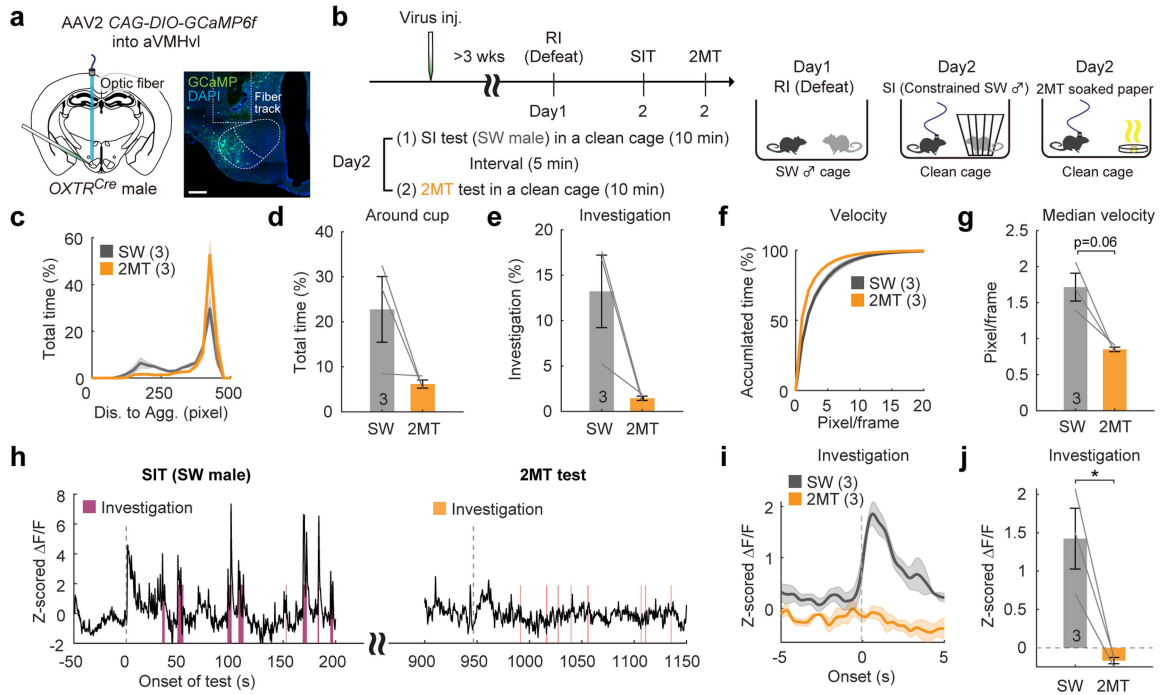
pVMHvl. Dashed lines mark the boundary of the VMH. Scale bars: 50 μ m. **d.** The percentage of CCC and DDC-induced c-Fos cells that express OXTR in the aVMHvl and pVMHvl. Numbers indicate the number of animals. Plots with error bars represent mean \pm s.e.m. Circles indicate individual animals. Two-way repeated measure ANOVA with Sidak's multiple comparisons test. All statistical tests are two-tailed. *p < 0.05. See Supplementary Table 1 for detailed statistics.



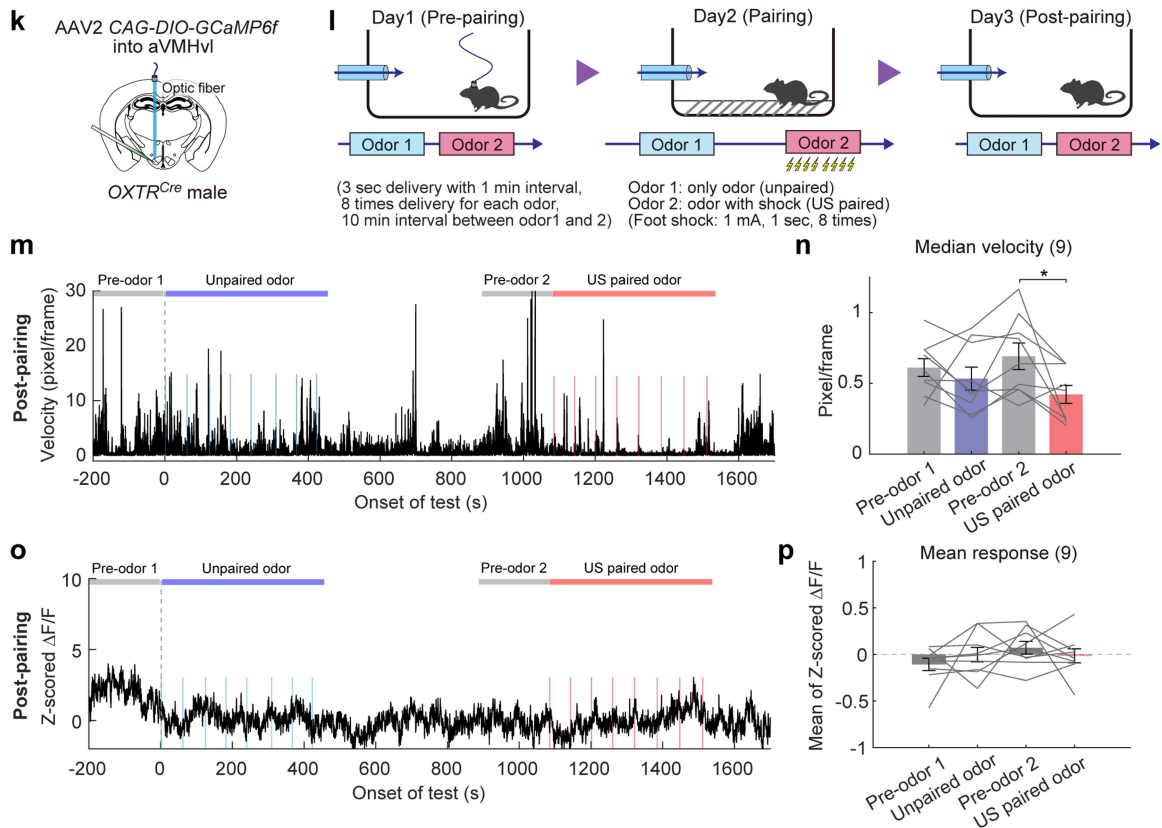
Extended Data Fig. 8 | No change in excitability of aVMHvl^{OXTR} cells one day after defeat. **a.** Representative recording traces of aVMHvl^{OXTR} cells under specific current steps, ranging from 50 pA to 250 pA, from single-housed (SH), defeated (D) and socially interacted (SI) male mice. **b.** Frequency-current (F-I) curve of aVMHvl^{OXTR} cells in SH, D, and SI groups. Two-way repeated measure ANOVA with Sidak's multiple comparison test. * $p < 0.05$ for D vs. SI comparisons. If not indicated, $p > 0.05$. **c.** Resting Membrane Potential (RMP) of aVMHvl^{OXTR}

cells in SH, D, and SI groups. **d.** Rheobase of aVMHvl^{OXTR} cells in SH, D, and SI groups. **e.** Input resistance of aVMHvl^{OXTR} cells in SH, D, and SI groups. Plots with error bars represent mean \pm s.e.m. Circles in c-e represent individual recording cells. Numbers on the plots indicate the number of cells. Cells are from 3-4 male mice per group. One-way ANOVA with Tukey's multiple comparisons test (c) and Kruskal-Wallis test with Dunn's multiple comparisons test (d-e). All statistical tests are two-tailed. See Supplementary Table 1 for detailed statistics.

aVMHvl^{OXTR} cells do not respond to predator odor



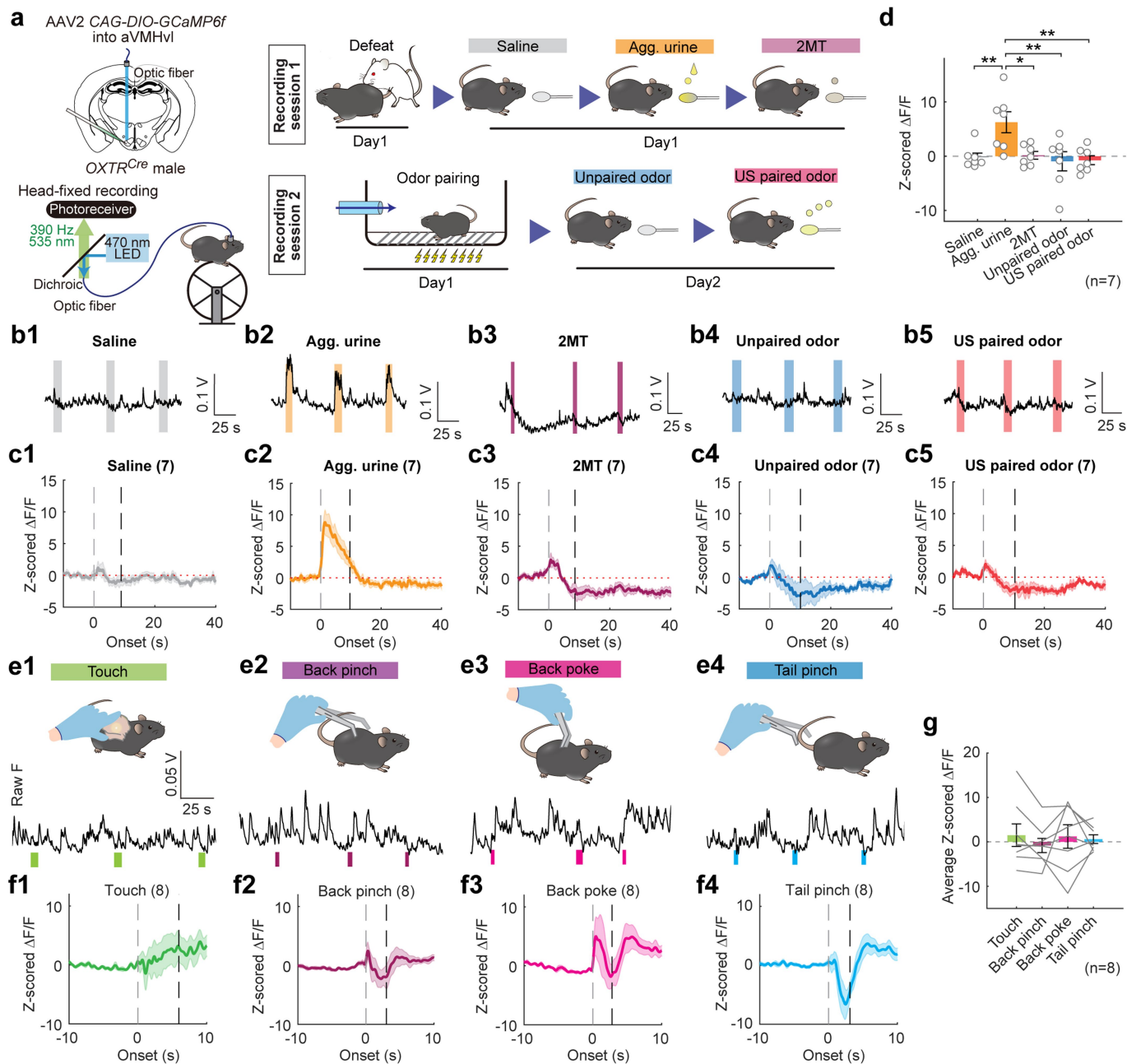
aVMHvl^{OXTR} cells do not respond to shock-paired odor



Extended Data Fig. 9 | See next page for caption.

Extended Data Fig. 9 | aVMHvl^{OXTR} cells do not respond to non-social aversive odors. Virus injection schematics and a representative histology image. Scale bar: 200 μ m. Brain illustration is based on a reference atlas from <https://atlas.brain-map.org/>. **a.** Experimental timeline for testing 2MT responses and cartoon illustration of the behavioral assay. **b.** Distribution of the distance between the test animal's body center and constrained aggressor (gray) or 2MT (orange) during the test. The test animals were defeated one day before the recording. **c.** The percentage of the total time the test mice spent around the constrained aggressor or 2MT (distance <250 pixels) during the test. Only animals that showed clear avoidance of the aggressor (< 20% of total time investigating the constrained aggressor) were included in the analysis. **d.** The percentage of the total time the test mice spent investigating the constrained aggressor or 2MT. **e.** Accumulative plots showing the distribution of movement velocity when the test mice are far away (distance > 300 pixels) from the constrained aggressor or 2MT. **f.** The median velocity of the test mice when far from the constrained aggressor or 2MT. **g.** A representative trace showing continuous Z-scored GCaMP signal during aggressor (magenta) and 2MT (orange) encounters. Shade represents investigation episodes. Dashed lines indicate the constrained aggressor and 2MT introduction. **h.** PETHs of Z-scored GCaMP signals aligned to the onset of investigating the aggressor

and 2MT. **i.** Average Z-scored $\Delta F/F$ of aVMHvl^{OXTR} cells during aggressor and 2MT investigation. **j.** Virus injection schematics. Brain illustration is based on a reference atlas from <https://atlas.brain-map.org/>. **k.** Experimental timeline for the shock-odor conditioning and testing. US-paired odor is always delivered after unpaired odor presentation. **l.** A representative trace showing the movement velocity of an animal when exposed to shock-paired and unpaired odors one day after shock-odor conditioning. Bars indicate pre-odor and odor delivery periods for calculation in **(n)**. **m.** A summary of median velocity before and during odor delivery in the post-conditioning test. **n.** A representative Z-scored GCaMP recording trace of an animal when exposed to shock-paired and unpaired odors one day after shock-odor conditioning. Bars indicate pre-odor and odor delivery periods for calculation in **(p)**. **o.** A summary of mean GCaMP response (Z-scored $\Delta F/F$) before and during odor delivery in the post-conditioning test. Plots with error bars and shades represent mean \pm s.e.m. Numbers on the plots indicate the number of animals. Lines represent individual animals. Wilcoxon matched-pairs signed rank test (**d**); Paired t-test (**e, g** and **j**); One-way ANOVA with repeated measures followed by Tukey's multiple comparisons test (**n** and **p**). All statistical tests are two-tailed. * $p < 0.05$. See Supplementary Table 1 for detailed statistics.

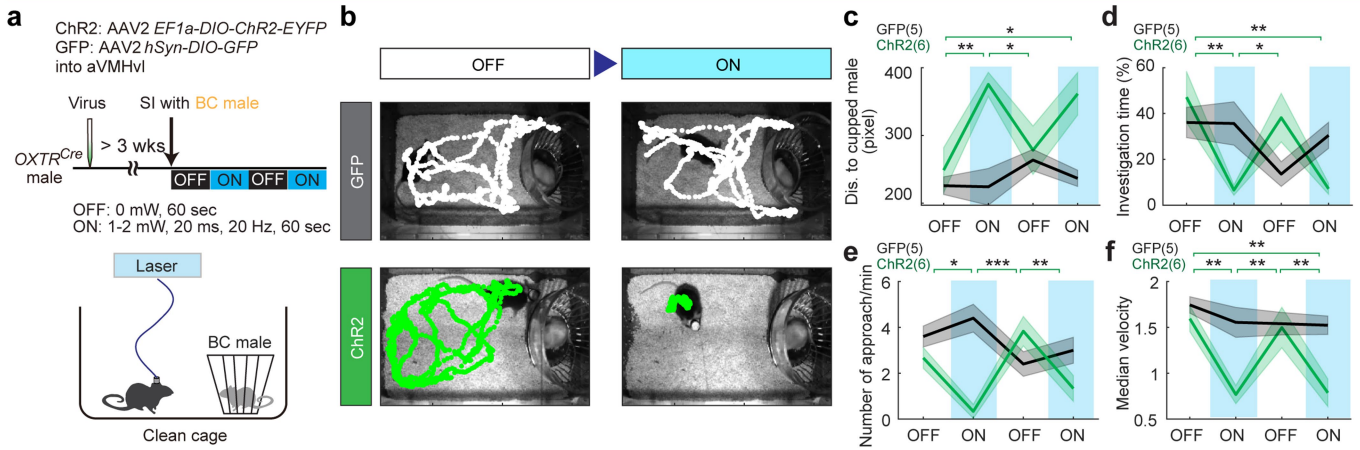


Extended Data Fig. 10 | aVMHvl^{OXTR} cells do not respond to non-social aversive cues or noxious somatosensory stimuli in head-fixed animals.

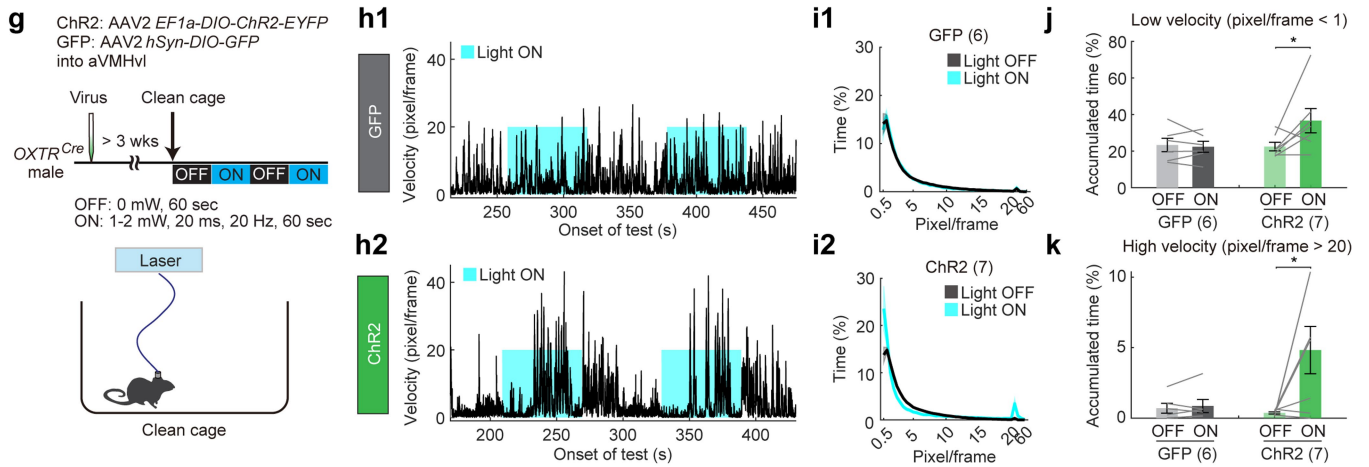
a. (left) Virus injection location and the schematics of head-fixed fiber photometry recording of aVMHvl^{OXTR} cells. Brain illustration is based on a reference atlas from <https://atlas.brain-map.org/>. (right) Experimental timelines. The responses to shock-paired and unpaired odors are recorded in one session one day after the shock-odor conditioning. The responses to saline, 2MT, and aggressor urine are recorded in a separate session one day after defeat. **b.** Representative raw GCaMP trace of aVMHvl^{OXTR} cells during delivery of saline (**b1**), aggressor urine (**b2**), 2MT (**b3**), shock-unpaired odor (**b4**) and shocked-paired odor (**b5**). All stimuli are presented on Q-tips placed approximately 1 cm in front of the mouse nose for 10 s. **c.** PETHs of Z-scored GCaMP signals aligned to the onset of various odor presentations. Red dotted horizontal lines indicate Z = 0. Gray and black vertical dashed lines indicate the onset and

average offset of stimulus presentation. **d.** Average Z-scored ΔF/F during various stimulus presentations. Circles represent individual animals. One-way ANOVA with repeated measures followed by Tukey's multiple comparisons test. *p < 0.05, and **p < 0.01. **e.** Representative raw GCaMP trace of aVMHvl^{OXTR} cells during gentle touch (**e1**), back pinch (**e2**), back poke (**e3**), and tail pinch (**e4**). All stimuli were manually delivered. **f.** PETHs of Z-scored GCaMP signals aligned to the onset of various somatosensory stimuli. Gray and black vertical dashed lines indicate the onset and average offset of stimulus presentation. **g.** Average Z-scored ΔF/F during various stimulus presentations. Lines represent individual animals. One-way ANOVA with repeated measures followed by Tukey's multiple comparisons test. Plots with error bars and shades represent mean ± s.e.m. Numbers on the plots indicate the number of animals. All statistical tests are two-tailed. See Supplementary Table 1 for detailed statistics.

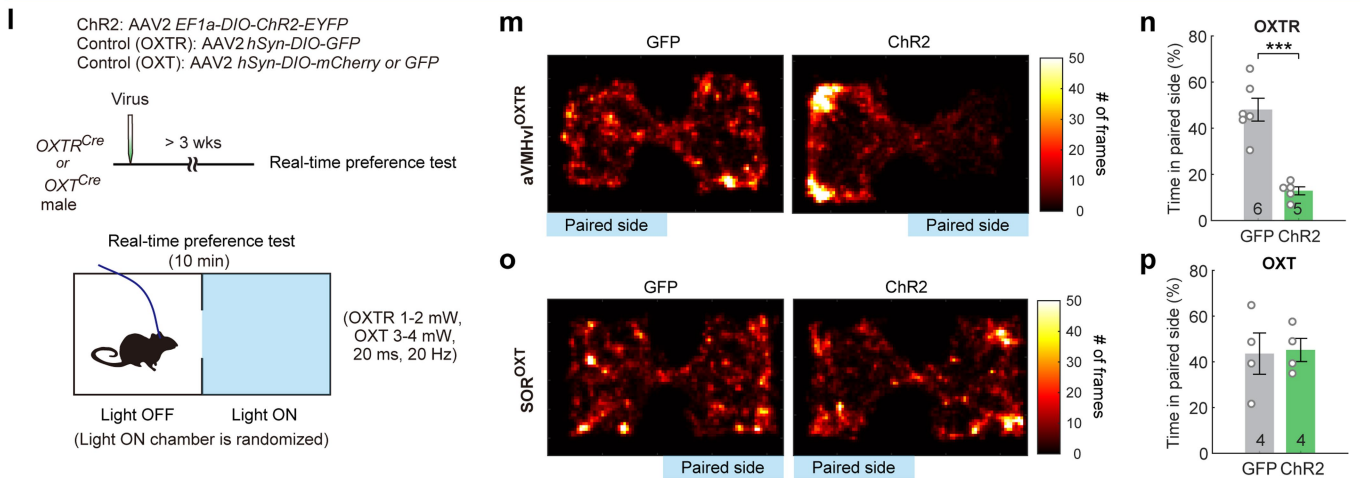
Optogenetic activation of aVMHvl^{OXTR} cells induces avoidance towards a non-aggressive male



Optogenetic activation of aVMHvl^{OXTR} cells increases flight and freeze



Optogenetic activation of aVMHvl^{OXTR} cells, but not SOR^{OXTR} cells, is aversive



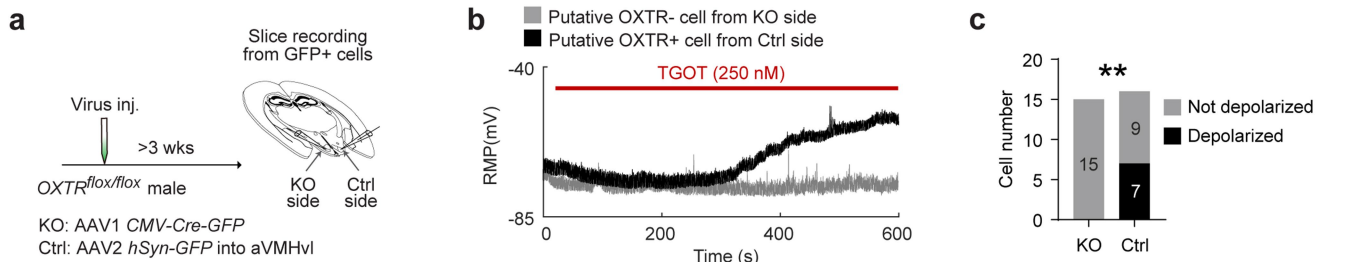
Extended Data Fig. 11 | See next page for caption.

Article

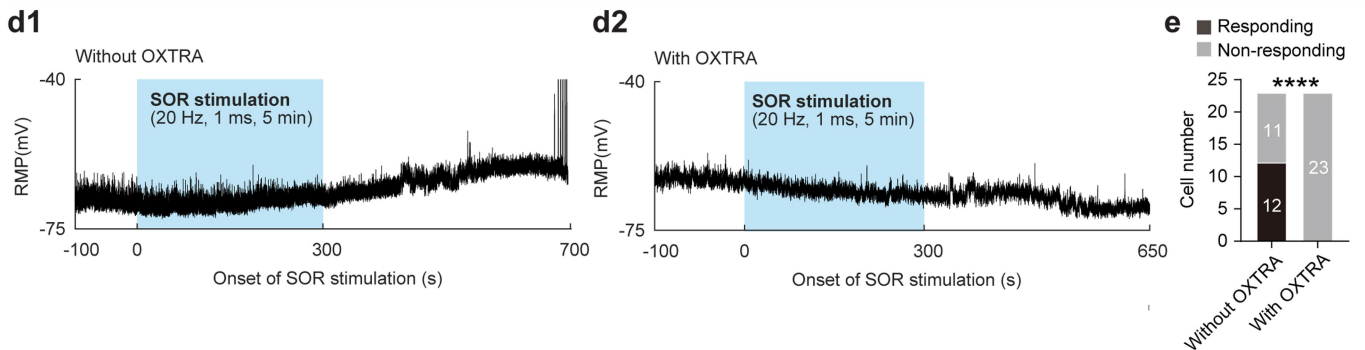
Extended Data Fig. 11 | Behavior changes induced by optogenetic activation of aVMHv1^{OXTR} and SOR^{OXTR} cells. **a.** Experimental timeline, light delivery protocol, and cartoon illustration of the behavioral assay. **b.** Video frames from SI tests overlaid with movement trajectories of a GFP (gray) and a ChR2 animal (green) during interleaved light-on (ON) and light-off (OFF) trials. **c-f.** Average distance to the constrained male (**c**), percentage of time spent investigating the constrained BC male (**d**), frequency of approaching the cup (**e**), and the median movement velocity (**f**) during light-on (blue) and light-off periods in GFP (black) and ChR2 (green) groups. Statistical results were between ON and OFF periods in ChR2 animals. All $p > 0.05$ for GFP animals. **g.** Experimental timeline, stimulation protocol, and cartoon illustration of the behavioral test. **h.** Representative traces showing the movement velocity of an GFP^{OXTR} animal (**h1**) and an ChR2^{OXTR} animal (**h2**) during the light-on (blue shade) and light-off period. **i.** Plots showing the distribution of movement velocity during the light-on and light-off periods of GFP (**i1**) and ChR2 (**i2**) animals. **j.** The percentage of

time the animals spent immobile (velocity < 1 pixel/frame). **k.** The percentage of time the animals spent flight (velocity > 20 pixels/frame). **l.** Experimental timeline and schematic illustration of the real-time place preference test. **m.** Heatmaps showing the body center distribution of representative GFP^{OXTR} and ChR2^{OXTR} animals during the 10-min RTPP tests. **n.** The percentage of time the animals spent in the light-paired chamber. Circles represent individual animals. **o.** Heatmaps showing the body center distribution of representative GFP^{OXTR} and ChR2^{OXTR} animals during the 10-min RTPP tests. **p.** The percentage of time the animals spent in the light-paired chamber. Plots with shades and error bars represent mean \pm s.e.m. Lines and circles represent individual animals. Numbers indicate the number of animals. Two-way RM ANOVA with Sidak's multiple comparisons test (**c-f, j-k**) and unpaired t-test (**n, p**). All statistical tests are two-tailed. * $p < 0.05$, ** $p < 0.01$, and *** $p < 0.001$. See Supplementary Table 1 for detailed statistics.

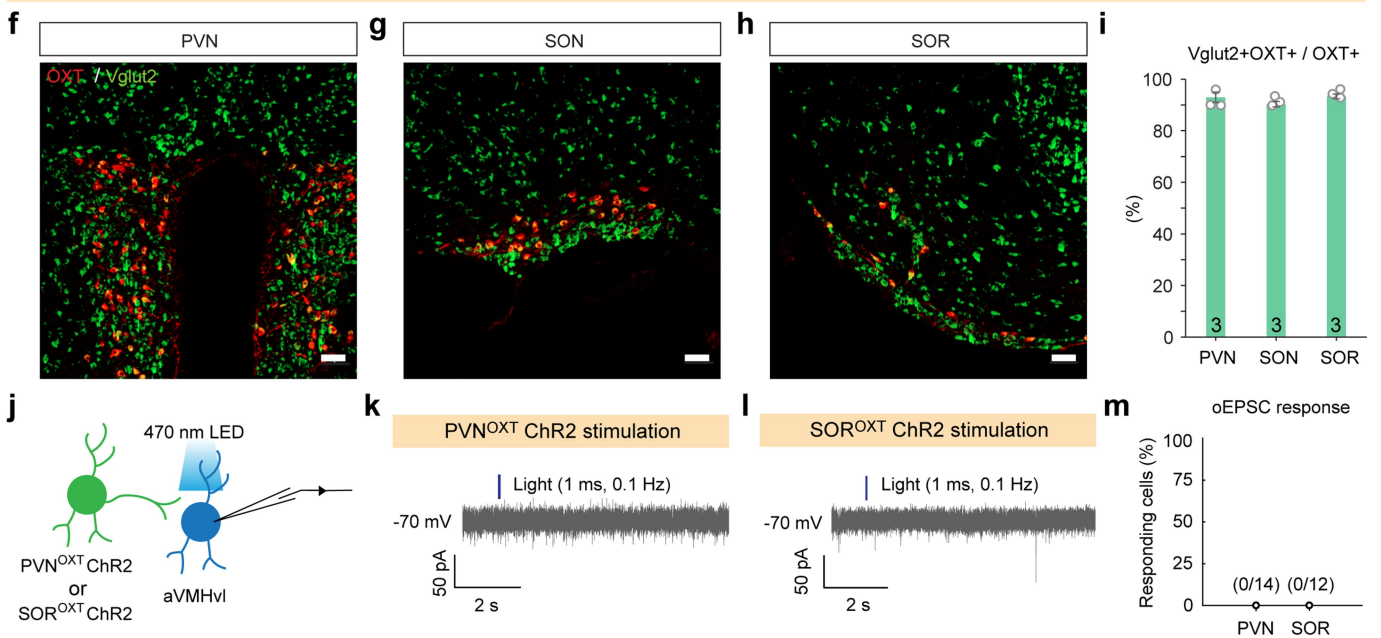
AAV-Cre can effectively knockout OXTR



OXTR antagonist blocks SOR^{OXTR} activation-induced aVMHvl cell depolarization

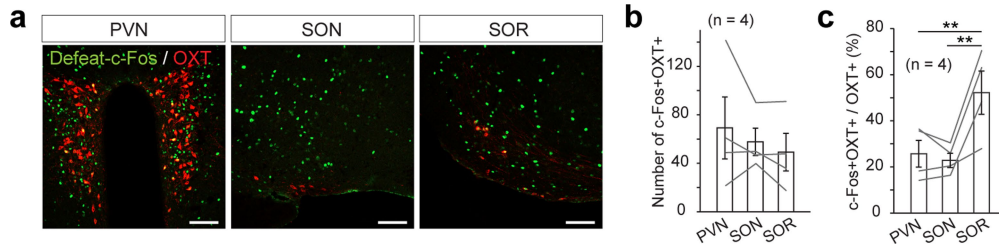


OXT cells are glutamatergic but makes no excitatory synapses with aVMHvl^{OXTR} cells



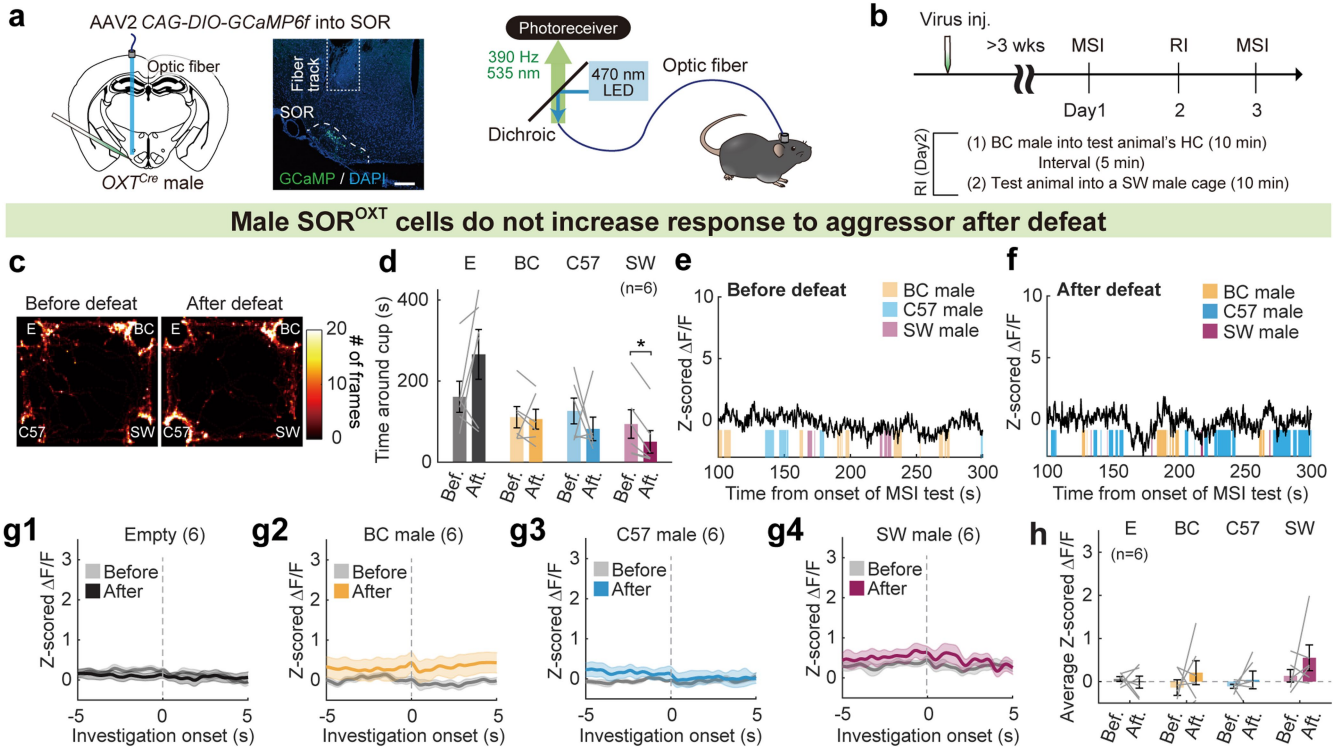
Extended Data Fig. 12 | SOR^{OXTR} affects aVMHvl cell activity by activating OXTR, not glutamatergic synaptic transmission. **a.** Strategy to evaluate OXTR knockout efficiency. **b.** Representative recording traces of GFP cells from knockout (KO) and control (Ctrl) sides under TGOT perfusion (red bar). **c.** Number of aVMHvl cells (from 4 animals) depolarized (> 4 mV) by TGOT in KO and control sides. Chi-square's test. $**p < 0.01$. **d.** Representative traces showing the membrane potential changes of two aVMHvl cells, one recorded in ACSF (**d1**) and the other in the presence of $1 \mu\text{M}$ L-368,889, a highly specific OXTR antagonist (**d2**). **e.** The number of cells depolarized ($\Delta\text{RMP} > 4$ mV) by the SOR^{OXTR} optogenetic stimulation (20 Hz, 1 ms, 5 min) and not. $n = 23$ (without OXTRA) cells from 5 animals and 23 (with OXTRA) cells from 4 animals.

Chi-square's test. $****p < 0.0001$. **f-h.** Histology images showing oxytocin (OXT, red) immunostaining and Vglut2 (green) expression in the PVN (**f**), SON (**g**), and SOR (**h**) from Vglut2^{Cre}:Ai6 male mice. Scale bars: $50 \mu\text{m}$. **i.** The percentage of OXT-positive cells that express Vglut2 in the PVN, SON, and SOR. Circles represent individual animals. Plotted as mean \pm s.e.m. $n = 3$ male mice. **j.** Slice recording schematics. **k-l.** Representative voltage clamp recording traces from aVMHvl^{OXTR} cells when a 1 ms light pulse (blue vertical bar) was delivered to activated PVN^{OXTR} (**k**) or SOR^{OXTR} (**l**) input. **m.** None of the aVMHvl^{OXTR} cells showed light-evoked EPSC during PVN^{OXTR} (0/14) cells or SOR^{OXTR} optogenetic activation (0/12 cells). See Supplementary Table 1 for detailed statistics.



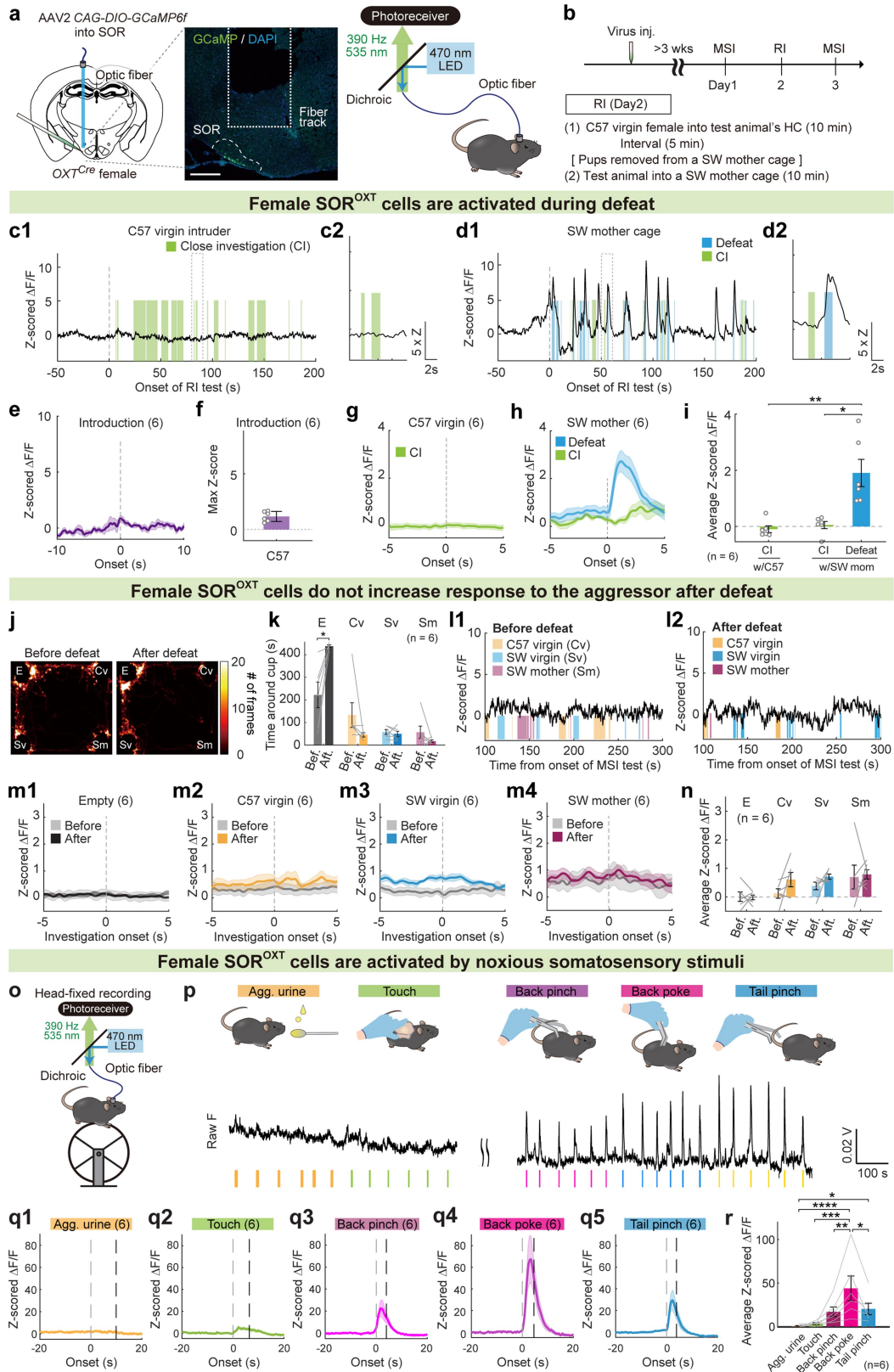
Extended Data Fig. 13 | Overlap between OXT and defeat-induced c-Fos.
a. Defeat-induced c-Fos (red) and oxytocin (OXT, green). Scale bars: 50 μ m.
b-c. Number of c-Fos+OXT+ cells (**b**) and percentage of c-Fos+ cells in OXT+ cells (**c**) in different regions. Every other brain section was counted. Plotted

as mean \pm s.e.m. Lines represent individual animals. One-way RM ANOVA with Tukey's multiple comparisons (**b-c**). All statistical tests are two-tailed. ** $p < 0.01$. See Supplementary Table 1 for detailed statistics.



Extended Data Fig. 14 | SOR^{OXT} cells do not increase responses to aggressors after defeat in male mice. **a.** Schematics of virus injection and a representative histological image for fiber photometry recording of SOR^{OXT} cells in male mice. The dashed line marks SOR. Scale bar: 200 μ m. Brain illustration is based on a reference atlas from <https://atlas.brain-map.org/>. **b.** Experimental timeline. **c.** Heatmaps showing the body center location of a recording mouse in MSI tests before and after defeat. E: empty; BC: familiar non-aggressive Balb/C male; C57: unfamiliar C57 male; and SW: SW aggressor. **d.** Time spent around each cup during MSI tests before and after defeat. **e-f.** Representative Z-scored GCaMP6f traces from a male recording mouse during pre-defeat (**e**) and

post-defeat (**f**) MSI tests. Shades represent investigation periods of different constrained stimulus animals. Periods investigating the empty cup are not marked. **g.** PETHs of Z-scored GCaMP6f signals aligned to the onset of investigation of different constrained stimuli. Gray: pre-defeat; Color: post-defeat. **h.** Average Z-scored $\Delta F/F$ of SOR^{OXT} cells during the investigation of various constrained stimuli in the pre-defeat and post-defeat MSI tests. Plots with shades and error bars represent mean \pm s.e.m. Lines represent individual animals. Numbers on the plots indicate the number of animals. Two-way repeated measure ANOVA with Sidak's multiple comparisons (**d, h**). All statistical tests were two-tailed. See Supplementary Table 1 for detailed statistics.



Extended Data Fig. 15 | See next page for caption.

Extended Data Fig. 15 | SOR^{OX}T cells in female mice are activated by noxious stimuli. **a.** Schematics of virus injection and a representative histological image for fiber photometry recording of SOR^{OX}T cells in female mice. The dashed line marks SOR. Scale bar: 200 μ m. Brain illustration is based on a reference atlas from <https://atlas.brain-map.org/>. **b.** Experimental timeline. **c-d.** Representative Z-scored GCaMP6f traces of SOR^{OX}T cells from an animal that encountered a naïve C57BL/6 female intruder (**c**) or a SW lactating female mouse in the SW cage (**d**). **c2** and **d2** show enlarged views of boxed areas in **c1** and **d1**, respectively. **e.** PETH of Z-scored GCaMP6f signal aligned to C57 female intruder introduction. As all lactating mothers attacked the test mouse within 10 s, the introduction response cannot be isolated. **f.** The peak GCaMP6f response within the first 10 s after C57 intruder introduction. **g-h.** PETHs of Z-scored GCaMP6f signals aligned to close investigation (CI) of C57BL/6 female intruders (**g**), investigating and being defeated by SW mothers (**h**). **i.** Average Z-scored $\Delta F/F$ of SOR^{OX}T cells during various social behaviors. **j.** Heatmaps showing the body center location of a recording mouse in MSI tests before and after defeat. E: empty; Cv: familiar C57BL/6 virgin female; Sv: unfamiliar virgin SW female; and Sm: SW mother. **k.** Time spent around each cup during MSI tests before and after defeat. **l.** Representative Z-scored GCaMP6f traces from a female recording mouse during pre-defeat (**l1**) and post-defeat (**l2**) MSI tests.

Shades represent investigation periods of different constrained stimulus animals. Periods investigating the empty cup are not marked. **m.** PETHs of Z-scored GCaMP6f signals aligned to the onset of investigation of different constrained stimuli. Gray: pre-defeat; Color: post-defeat. **n.** Average Z-scored $\Delta F/F$ of SOR^{OX}T cells during the investigation of various constrained stimuli in the pre-defeat and post-defeat MSI tests. **o.** Schematics of head-fixed fiber photometry recording of SOR^{OX}T cells and presented stimuli. **p.** Representative raw GCaMP6f trace of SOR^{OX}T cells during delivery of aggressor urine on a Q-tip, gentle touch, back pinch, back poke, and tail pinch. **q.** PETHs of Z-scored GCaMP6f signals aligned to the onset of aggressor urine presentation (**q1**), gentle touch (**q2**), back pinch (**q3**), back poke (**q4**), and tail pinch (**q5**). Gray and black dashed lines indicate the onset and average duration of stimulus delivery, respectively. **r.** Average Z-scored $\Delta F/F$ during various stimulus delivery. Plots with shades and error bars represent mean \pm s.e.m. Circles and lines represent individual animals. Numbers on the plots indicate the number of animals. Kruskal-Wallis test with Dunn's multiple comparisons test (**i**); Two-way repeated measure ANOVA with Sidak's multiple comparisons test (**k, n**); and One-way repeated measure ANOVA with Tukey's multiple comparisons test (**r**). All statistical tests are two-tailed. * $p < 0.05$, ** $p < 0.01$, *** $p < 0.001$ and **** $p < 0.0001$. See Supplementary Table 1 for detailed statistics.

Reporting Summary

Nature Portfolio wishes to improve the reproducibility of the work that we publish. This form provides structure for consistency and transparency in reporting. For further information on Nature Portfolio policies, see our [Editorial Policies](#) and the [Editorial Policy Checklist](#).

Statistics

For all statistical analyses, confirm that the following items are present in the figure legend, table legend, main text, or Methods section.

n/a Confirmed

- The exact sample size (n) for each experimental group/condition, given as a discrete number and unit of measurement
- A statement on whether measurements were taken from distinct samples or whether the same sample was measured repeatedly
- The statistical test(s) used AND whether they are one- or two-sided
Only common tests should be described solely by name; describe more complex techniques in the Methods section.
- A description of all covariates tested
- A description of any assumptions or corrections, such as tests of normality and adjustment for multiple comparisons
- A full description of the statistical parameters including central tendency (e.g. means) or other basic estimates (e.g. regression coefficient) AND variation (e.g. standard deviation) or associated estimates of uncertainty (e.g. confidence intervals)
- For null hypothesis testing, the test statistic (e.g. F , t , r) with confidence intervals, effect sizes, degrees of freedom and P value noted
Give P values as exact values whenever suitable.
- For Bayesian analysis, information on the choice of priors and Markov chain Monte Carlo settings
- For hierarchical and complex designs, identification of the appropriate level for tests and full reporting of outcomes
- Estimates of effect sizes (e.g. Cohen's d , Pearson's r), indicating how they were calculated

Our web collection on [statistics for biologists](#) contains articles on many of the points above.

Software and code

Policy information about [availability of computer code](#)

Data collection

Fiber photometry recording data was recorded using RZ5 real-time processor (Tucker-Davis Technologies). The envelope of 390-Hz signals from the photoreceiver were extracted in real time using a custom-written program (Tucker-Davis Technologies) as the readout of GCaMP6 intensity. Optogenetic light stimulation was controlled using a custom-written program (Tucker-Davis Technologies). Electrophysiology data were recorded with MultiClamp 700B amplifier (Molecular Devices) and Clampex 11.0 software (Axon Instruments), digitized at 20 kHz with Digidata 1550B (Axon Instruments).

Data analysis

To analyze the GCaMP recording data, custom codes written in MATLAB (version 2019b or 2021b, Mathworks) with a function “msbackadj” was used. Details are described in the method section. For behavior data analyses, custom DeepLabCut-based models (Mathis et al., Nature Neuroscience 2018, <https://pdollar.github.io/toolbox/>) were constructed to track animals’ body center, head center and nose point in top-view videos, and custom codes written in MATLAB (Mathworks) were also used and can be downloaded from 10.5281/zenodo.8417540. Electrophysiology data were analyzed using Clampfit (Molecular Devices) or MATLAB (Mathworks). The 10x or 20x fluorescent images were acquired by Olympus VS120 Automated Slide Scanner and its specific software OlyVIA (OlyVIA Ver. 2.9.1.). The 20x fluorescent confocal images were acquired by Zeiss LSM 800 and its specific software (Zeiss, ZEN 2.3 system) for cell counting. Statistical analyses were performed using MATLAB (Mathworks) and Prism9 (GraphPad Software, RRID: SCR_002798).

For manuscripts utilizing custom algorithms or software that are central to the research but not yet described in published literature, software must be made available to editors and reviewers. We strongly encourage code deposition in a community repository (e.g. GitHub). See the Nature Portfolio [guidelines for submitting code & software](#) for further information.

Data

Policy information about [availability of data](#)

All manuscripts must include a [data availability statement](#). This statement should provide the following information, where applicable:

- Accession codes, unique identifiers, or web links for publicly available datasets
- A description of any restrictions on data availability
- For clinical datasets or third party data, please ensure that the statement adheres to our [policy](#)

Raw values associated with each figure panel can be found in the source data files. Fiber photometry recording data, behavior annotations, tracking and raw representative histology images can be downloaded from 10.5281/zenodo.8417540. Behavior videos and additional histology images are available from the corresponding authors upon reasonable request. They are not deposited to public database due to their large sizes and size limitation of Online depository, e.g., Zenodo. Illustrations of coronal brain section in the manuscript were based on Allen Mouse Brain Atlas with modifications by the authors. The original reference atlas is available from <https://atlas.brain-map.org/>.

Human research participants

Policy information about [studies involving human research participants and Sex and Gender in Research](#).

Reporting on sex and gender	N/A
Population characteristics	N/A
Recruitment	N/A
Ethics oversight	N/A

Note that full information on the approval of the study protocol must also be provided in the manuscript.

Field-specific reporting

Please select the one below that is the best fit for your research. If you are not sure, read the appropriate sections before making your selection.

Life sciences Behavioural & social sciences Ecological, evolutionary & environmental sciences

For a reference copy of the document with all sections, see nature.com/documents/nr-reporting-summary-flat.pdf

Life sciences study design

All studies must disclose on these points even when the disclosure is negative.

Sample size	Sample sizes were based on comparable n-values from the literature published previously (see ref.15,19,32, 57, 58, 59, 60)
Data exclusions	For fiber photometry recording of aVMHvl OXTR-positive neurons in males, we excluded 3 mice due to misplacement of optic fibers. For fiber photometry recording of aVMHvl OXTR-positive neurons in females, we excluded 3 mice due to high avoidance (<10s investigation) before defeat. For cell ablation experiment in Fig. 6, we excluded results from two animals due to poor virus targeting. For optogenetic activation experiment in Fig. 6, we excluded on animal due to misplacement of optic fiber. For fiber photometry recording of SOR cells, only animals with good GCaMP6 baseline signal was used for the behavior testing, and there was no data exclusion after data collection. There was no data exclusion for other experiments.
Replication	All functional experiments started with a small batch of control and test animals (2-4 animals per group) and then we gradually added more animals for each group as transgenic mice became available. We made sure that control and test mice were added around the same time. For WT MSI behavior test and OXTR GCaMP recording experiments (Fig. 1k-g, Extended Data Fig. 2, and 6), data from two separate cohorts were collected approximately 2 years apart. One cohort was collected during the initial testing, one cohort was added during paper revision. The final analysis for each experiment combined all animals from different cohorts.
Randomization	Mice were randomly assigned to experimental groups (such as single-housed vs defeated in Fig1p-w, GFP vs ChR2 in Fig2a-g and Extended Data Fig8a-g, control vs KO in Fig3a-m, saline vs OXTRA in Fig3n-z, and GFP vs DTR in Fig6a-j).
Blinding	All group allocation is performed randomly during data collection. During the process of cell counting, the name of treatment was hidden from the experimenters. During the process of human annotation, most behavior videos were annotated by individuals who had no knowledge regarding the mouse treatment condition. Some videos were annotated unblindly by the experimenter who performed the behavioral tests. All human annotation was also confirmed with objective animal tracking-derived behavior analysis. All videos were double checked by one experimenter to ensure the consistency of annotation. During behavior annotation for fiber photometry experiments, the neural responses were unknown to the experimenter.

Reporting for specific materials, systems and methods

We require information from authors about some types of materials, experimental systems and methods used in many studies. Here, indicate whether each material, system or method listed is relevant to your study. If you are not sure if a list item applies to your research, read the appropriate section before selecting a response.

Materials & experimental systems

n/a	Involved in the study
<input type="checkbox"/>	<input checked="" type="checkbox"/> Antibodies
<input checked="" type="checkbox"/>	<input type="checkbox"/> Eukaryotic cell lines
<input checked="" type="checkbox"/>	<input type="checkbox"/> Palaeontology and archaeology
<input type="checkbox"/>	<input checked="" type="checkbox"/> Animals and other organisms
<input checked="" type="checkbox"/>	<input type="checkbox"/> Clinical data
<input checked="" type="checkbox"/>	<input type="checkbox"/> Dual use research of concern

Methods

n/a	Involved in the study
<input checked="" type="checkbox"/>	<input type="checkbox"/> ChIP-seq
<input checked="" type="checkbox"/>	<input type="checkbox"/> Flow cytometry
<input checked="" type="checkbox"/>	<input type="checkbox"/> MRI-based neuroimaging

Antibodies

Antibodies used

The primary antibodies used were: rabbit anti-Oxytocin (1:5000, Immunostar, #20068, Lot #1607001), guinea pig anti-c-Fos (1:2000, Synaptic Systems, 226-005, Lot #2-10, 2-13), rabbit anti-Vasopressin (1:5000, Immunostar, #20069, Lot #1004001), and chicken anti-GFP (1:2000, abcam, ab13970, lot#GR3190550-2), anti-FITC antibody from sheep (PerkinElmer, #NEF710001EA, 1:200 in blocking buffer), anti-DIG antibody from sheep (Roche Applied Science, #11207733910, 1:250 in blocking buffer), and rabbit anti-Esr1 (1:2000, Invitrogen, PA1-309, lot#: YA352477). The secondary antibodies used were: Cy3-AffiniPure donkey anti-rabbit IgG (1:500, Jackson Immuno Research, 711-165-152, lot#124528), Cy5-AffiniPure donkey anti-rabbit IgG (1:250, Jackson Immuno Research, 711-175-152, lot#150312), Alexa Fluor 488-conjugated goat anti-guinea pig IgG (1:500, Invitrogen, #A11073, lot#2160428), or Alexa Fluor 488-conjugated donkey anti-chicken IgY(IgG) (1:500, Jackson Immuno Research, 703-545-155, lot#116967).

Validation

All the antibodies used in this paper have been cited multiple times as listed on the manufacture's website or CiteAb(<https://www.citeab.com/>).

Specifically, for the primary antibodies used in this paper, rabbit anti-Oxytocin (1:5000, Immunostar, #20068, Lot #1607001) relevant citation; Takano Y et al., Heliyon 2022, Yu Y et al., Nature Communications 2022. guinea pig anti-c-Fos (1:2000, Synaptic Systems, 226-005, Lot #2-10, 2-13); Ressler RL et al., Nature Communications 2021. rabbit anti-Vasopressin (1:5000, Immunostar, #20069, Lot #1004001); Yao Y et al., Nature Communications 2021. anti-GFP (1:2000, abcam, ab13970, lot#GR3190550-2); Oswald MJ et al., Nature Communications 2022. anti-FITC antibody from sheep (PerkinElmer, #NEF710001EA, 1:200 in blocking buffer); Osakada T et al., Nature Communications 2018. anti-DIG antibody from sheep (Roche Applied Science, #11207733910, 1:250 in blocking buffer); Osakada T et al., Nature Communications 2018. rabbit anti-Esr1 (1:2000, Invitrogen, PA1-309, lot#: YA352477); Xiao S et al., eLife 2023.

Animals and other research organisms

Policy information about [studies involving animals](#); [ARRIVE guidelines](#) recommended for reporting animal research, and [Sex and Gender in Research](#)

Laboratory animals

Mice were housed under a 12-hour light-dark cycle (dark cycle; 10 a.m. to 10 p.m. or 6:30 p.m. to 6:30 a.m.), with food and water available ad libitum. Room temperature was maintained between 20–22 °C and humidity between 30–70%, with a daily average approximately 45%. OxtCre (Strain#: 031303), OXTCre (Strain#: 024234), Vglut2Cre (Strain#: 0169963), and OXTRflo mice (Strain#: 008471) were purchased from Jackson Laboratory. Ai6 (Strain#: 007906) mice were from Jackson Laboratory and crossed with OxtCre and Vglut2Cre mice. Test mice were between 8 to 24 weeks at the time of behavior testing or recording. Stimulus animals in RI test were BALB/c male (> 9 weeks), C57BL/6N male and female mice (> 8 weeks) originally purchased from Charles River and then bred in-house. Swiss Webster male and female mice (> 11 weeks) were purchased from Taconic, Charles River, or bred in house. All mice were group housed until adulthood. After surgery with fiber or cannula implantation, all test mice were single-housed. Animals were randomly assigned to control and test groups.

Wild animals

The study did not involve wild animals.

Reporting on sex

Stimulus animals in resident-intruder test were BALB/c male (>9 weeks), C57BL/6N male and female mice (>8 weeks) originally purchased from Charles River and then bred in house, and Swiss Webster male and female mice (>11 weeks) purchased from Taconic, Charles River, or bred in house. Both male and female mice from OxtCre, OXTCre, and C57BL/6N colonies were used as test animals.

Field-collected samples

The study did not involve field collected samples.

Ethics oversight

All procedures were approved by the NYULMC Institutional Animal Care and Use Committee (IACUC) in compliance with the National Institutes of Health (NIH) Guidelines for the Care and Use of Laboratory Animals.

Note that full information on the approval of the study protocol must also be provided in the manuscript.